APPLICATIONS OF FUNCTIONAL NUCLEIC ACIDS IN IMAGING, SENSING AND DRUG DELIVERY AND INVESTIGATIONS OF DNAZYME-METAL INTERACTIONS

BY

WEICHEN XU

DISSERTATION

Submitted in partial fulfillment of the requirements
for the degree of Doctor of Philosophy in Chemistry
in the Graduate College of the
University of Illinois at Urbana-Champaign, 2011

Urbana, Illinois

Doctoral Committee:

Professor Yi Lu, Chair
Professor Ryan C. Bailey
Professor R. Linn Belford
Professor Kenneth S. Suslick

Abstract

Functional nucleic acids (FNA), including nucleic acids catalysts (ribozymes and DNAzymes) and ligands (aptamers), have been discovered in nature or isolated in a laboratory through a process called *in vitro* selection. They are nucleic acids with functions similar to protein enzymes or antibodies. They have been developed into sensors with high sensitivity and selectivity; it is realized by converting the reaction catalyzed by a DNAzyme/ribozyme or the binding event of an aptamer to a fluorescent, colorimetric or electrochemical signal. While a number of studies have been reported for *in vitro* sensing using DNAzymes or aptamers, there are few reports on *in vivo* sensing or imaging. MRI is a non-invasive imaging technique; smart MRI contrast agents were synthesized for molecular imaging purposes. However, their rational design remains a challenge due to the difficulty to predict molecular interactions. Chapter 2 focuses on rational design of smart T1-weighted MRI contrast agents with high specificity based on DNAzymes and aptamers. It was realized by changing the molecular weight of the gadolinium conjugated DNA strand with the analytes, which lead to analyte-specific water proton relaxation responses and contrast changes on an MRI image. The designs are general; the high selectivity of FNA was retained.

Most FNA-based fluorescent sensors require covalent labeling of fluorophore/quencher to FNAs, which incurrs extra expenses and could interfere the function of FNAs. Chapter 3 describes a new sensor design avoiding the covalent labeling of fluorophore and quencher. The fluorescence of malachite green (MG) was regulated by the presence of adenosine. Conjugate of aptamers of MG and adenosine and a bridge strand were annealed in a solution containing MG. The MG aptamer did not bind

MG because of its hybridization to the bridge strand, resulting in low fluorescence signal of MG. The hybridization was weakened in the presence of adenosine, leading to the binding of MG to its aptamer and a fluorescence increase. The sensor has comparable detection limit (20 μM) and specificity to its labeled derivatives.

Enzymatic activity of most DNAzymes requires metal cations. The research on the metal-DNAzyme interaction is of interest and challenge to scientists because of the lack of structural information. Chapters 4 presents the research on the characterization of the interaction between a Cu^{2+}-dependent DNAzyme and Cu^{2+}. Electron paramagnetic resonance (EPR) and UV-Vis spectroscopy were used to probe the binding of Cu^{2+} to the DNAzyme; circular dichroism was used to probe the conformational change of the DNAzyme induced by Cu^{2+}. It was proposed that the conformational change by the Cu^{2+} binding is important for the activity of the DNAzyme. Chapter 5 reports the dependence of the activity of 8-17 DNAzyme on the presence of both Pb^{2+} and other metal cations including Zn^{2+}, Cd^{2+} and Mg^{2+}. It was discovered that presence of those metal cations can be cooperative or inhibitive to 8-17 activity. It is hypothesized that the 8-17 DNAzyme had multiple binding sites for metal cations based on the results.

Cisplatin is effective killing tumor cells, but with significant side effects, which can be minimized by its targeted delivery. Chapter 6 focuses on the effort to functionalize liposomes encapsulating cisplatin by an aptamer that selectively bind nucleolin, an over-expressed protein by breast cancer cells. The study proved the selective cytotoxicity to breast cancer cells of the aptamer-functionalized liposome.

Acknowledgement

First, I would like to thank Prof. Yi Lu for the opportunities to work on exciting research projects. I am grateful for his guidance, advice, support and encouragement. The attitude toward research I learned from him is one of the most valuable I obtained in the University of Illinois. I also want to thank my committee members Profs. R. Linn Belford, Ryan Bailey and Kenneth Suslick; their suggestions and advice were critical to the success of my research.

I acknowledge the following Lu group members for their help to my research projects: Dr. Juewen Liu, Dr. Hee-kyung Kim, Dr. Mehmet Yigit, Dr. Debapriya Mazumdar, Dr. Nandini Nagraj, Dr. Natasha Yeung, Dr. Zehui Cao, Mr. Tong Rong, Dr. Xuan Zhao, Dr. Dewain Garner, Dr. Kevin Nelson, Dr. Yu Xiang, Mr. Eric Null, Mr. Tian Lan and Ms. Hannah Ihms. I also hope to thank undergraduate researchers who worked with me: Adam Nguyen, Aye Lwin and Jen Wu.

Thank you to Prof. Thomas Meade for the use of relaxometer, and to Dr. Keith MacRenaris and Dr. Ying Song for the training of relaxometer. I would like to thank Dr. Shuzhou Li and Dr. Jian Zhang for the convenience when I was in Chicago. I also thank Prof. Edward Treadwell for the use of the 60 MHz NMR spectrometer. Special thanks to Prof. Brad Sutton, Dr. Boris Odintsov and Ms. Nancy Dodge for the acquisition of the MRI images at Carle Foundation Hospital Department of Radiology.

I am grateful to have friends to give me support. Thank you Debapriya Mazumdar, Nandini Nagraj, Natasha Yeung, Eric Null, Michael Motala, Kwasima Quansah, Masha Savelieff, Geng Lu, Hannah Ihms and Yingwu Lin. You make my graduate school time unforgettable.

Thank you to the secretaries – Joyce, Theresa, Connie, Beth and Sandy, for your help, comfort and support.

My family members – my parents and grandmother, bear my deepest gratitude. You are my motivation to go forward in my life.

Table of Contents

Chapter 1 Introductions of functional nucleic acids, magnetic resonance imaging (MRI) and electron paramagnetic resonance (EPR)

1.1 Functional nucleic acids

Nucleic acids were discovered and isolated 150 years ago by Johann Friedrich Miescher and Richard Altman. They were not recognized as nature-selected gene carriers until an important discovery by Erwin Chargaff in the 1950s, which inspired research into both their chemistry and biological functions. The discovery of the helical structure of nucleic acids is recognized as the beginning of molecular biology.[1]

In the intervening time since these foundational discoveries, it has been established that there are two categories of nucleic acids in nature: deoxyribonucleic acids (DNA) and ribonucleic acids (RNA). Their structures are shown in Scheme 1.1. They are biopolymers whose units contain a ribose (for RNA) or deoxyribose (for DNA), a nucleobase, and a phosphate. In nature, DNA has four bases (adenine (A), cytosine (C), thymine (T), and guanine (G)) while RNA has uracil (U) instead of thymine (structures shown in Scheme 1.1). DNA carries genetic information. Most often, RNA transfers genetic information and play important roles in protein synthesis, but it also carries genetic information in some species, such as viruses.

Scheme 1.1 Structures of nucleic acids and bases

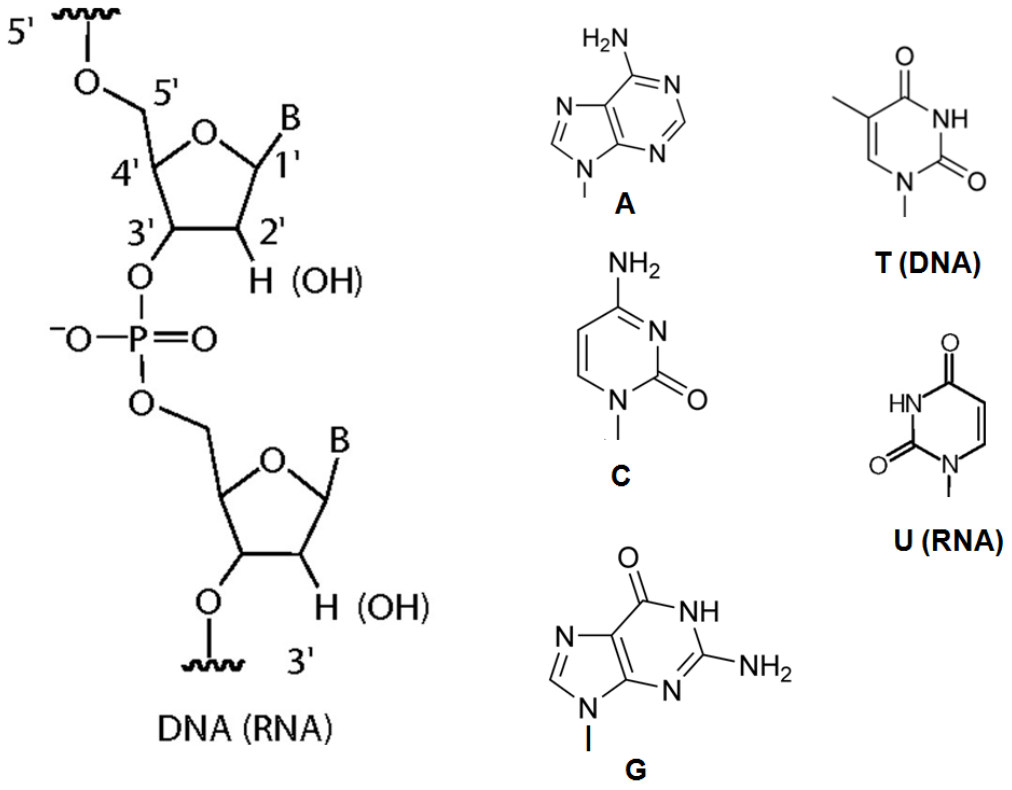

As opposed to DNA, which forms a long, helical structure, RNA assumes more diverse secondary and three dimensional structures. These more diverse structures led to the hypothesis that RNA might have functions beyond genetic information storage and transfer.[2,3] This hypothesis was validated first by the discovery of ribozymes[4-6] in the 1980s and later by the discovery of riboswitches[7-9]. Ribozymes and riboswitches are naturally-occurring or laboratory-evolved RNAs with enzymatic activity and affinity toward specific targets, respectively. They are the natural RNA analogues of protein enzymes and antibodies.

A novel technique called *in vitro* selection was developed to evolve RNA with desired functions in the laboratory, enabling researchers to obtain ribozymes or RNA aptamers which had no natural precedents.[10-17] The method could be applied to DNA, which led to the discovery of DNAzymes[18-24] and DNA aptamers.[21,25-29] DNAzyme and DNA aptamers refer to DNA molecules with catalytic activities and affinity to specific targets, respectively. Now, the term "functional nucleic acids" is used to describe the wide range of nucleic acids (ribozymes, DNAzymes, RNA aptamers, and DNA aptamers) with function beyond the traditional genetic storage and transfer roles. Functional nucleic acids have been widely applied in research, medicine, and industry.

1.1.1 *In vitro* selection

Although functional nucleic acids were originally found in nature, most functional nucleic acids have been evolved in the laboratory. The procedure to obtain functional nucleic acids is called *in vitro* selection,[30-33] or the Systematic Evolution of Ligands through Exponential Enrichment (SELEX).[34-36]

The *in vitro* selection of functional nucleic acids is similar to natural evolution. It starts with a pool of unique nucleic acids, and it is assumed that a nucleic acid with the favorable property – the winner – is included in the pool. *In vitro* selection is the systematic method used to isolate this winner.

A typical *in vitro* selection is shown in Figure 1.1. After the pool, which contains 10^{12} to 10^{14} different nucleic acid sequences, is generated, winners are separated from the rest of the pool. As the population of the winners is present at low abundance, polymerase chain reaction (PCR) is used to amplify the selected winners. This procedure

is called a round of selection. The amplified winners become the pool for the next round of selection.

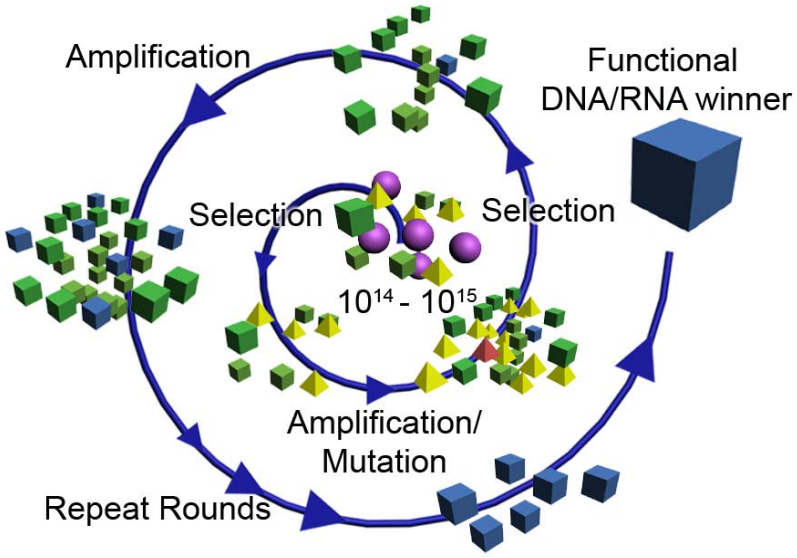

Figure 1.1 Schematic presentation of the procedure of *in vitro* selection

To obtain functional nucleic acids, 10-20 rounds of selection are often necessary.[30-33] This number of selection rounds is necessary because the winner is often not completely separated from the rest of the pool during each round of selection. Molecules without the needed properties can thus be amplified. However, the selection procedure enriches the winner population.

The procedure presented above ensures the function of the winner. However, the selected winners might additionally have unfavorable properties. For instance, a DNAzyme which performs as a nuclease was selected by Lu lab. Its enzymatic activity requires the presence of Co^{2+} as cofactor. However, the selected pool has enzymatic activity with the presence of Co^{2+} as well as Zn^{2+} and Pb^{2+}. Negative selection was

developed to enhance the selectivity of the functional nucleic acids.[37] Similar to the regular selection, the process starts with a pool, in which the winners are already enriched. The molecules with the unfavorable properties are separated from the pool and discarded. The survived molecules are amplified and/or processed to the next round of selection. It has been reported that the selectivity can be significantly enhanced through negative selection.[37]

After rounds of selection, the selected pool is then sequenced. The acquired sequences are analyzed and the sequence with the highest activity is truncated to obtain a new functional nucleic acid sequences.

1.1.2 Aptamers

The term aptamer comes from the word "aptus", which means "to fit". It refers to nucleic acids which bind targets. The first aptamers were reported independently by the Gold group[38] and the Szostak group.[30] Aptamers have been selected toward various targets, such as small metal ions, organic molecules,[10-12,26,39] peptides,[40-42] proteins,[25,43,44] and even cells.[45,46] They are the nucleic acid analogues of antibodies. However, they are superior to antibodies in terms of cost and stability. More importantly, aptamers are superior to antibodies in that they can be selected *in vitro*. Antibodies can only be generated in living organisms, and thus antibodies for certain toxins cannot be obtained. However, aptamers for these toxins would, in theory, be able to be selected *in vitro*.

Although most RNA aptamers and all DNA aptamers were obtained through *in vitro* selection, aptamers were originally discovered in nature. Riboswitches was discovered in some mRNA. They contain a sequence which binds to a specific molecule. When the riboswitch binds to its target, it undergoes a conformational change which

changes the rate at which an adjacent gene is transcribed. Thus, the gene expression in this region is regulated by the riboswitch's target molecule. Riboswitch explorations inspired research into functional nucleic acids, and today, it is the focus of many drug-based interventions.

1.1.3 Riozymes and deoxyribozymes (DNAzymes)

Ribozymes and DNAzymes are the RNA and DNA analogues of protein enzymes. The first ribozymes were discovered in the 1980s by Cech and Altman.[4-6] The Cech group discovered that introns were spliced in the absence of protein enzymes. It was proposed that a portion of the mRNA catalyzed the splicing. Altman identified that the RNA portion of an enzyme called RNase-P was essential for its enzymatic activity. Their pioneering work began the research into catalytic nucleic acids.

Ribozymes are common in biological systems. They perform important roles in gene regulation and cellular physiology. Most naturally occurring ribozymes act as nucleases, catalyzing their own hydrolysis or the hydrolysis of other RNAs. *In vitro* selection enriched the library of ribozymes.[47-50] For instance, Szostak and co-workers were the first to select an RNA molecule with ligase function.[51] *In vitro* selected ribozymes also catalyze chemical reactions beyond ligation and cleavages, such as allyl transfer, alkylation, enantiomerization, Diels-Alder, and the metallation of mesoporphyrin IX.[52] Although the reactions catalyzed by ribozymes are less diverse than those catalyzed by protein enzymes, *in vitro* selected ribozymes are uniquely important in the field of biocatalysis.

DNA has less diverse conformations than RNA because of its lack of a 2'-hydroxyl group. This could be the reason why catalytic DNA has not been discovered in

nature. However, artificial catalytic DNA molecules, known as DNAzymes, have been obtained in the laboratory. DNAzymes are capable of catalyzing many of the same reactions as ribozymes.[21,24,53-57]

1.1.4 Recent progress in the mechanistic studies of nucleic-acid-catalyzed reactions

The function of nuclease-like DNAzymes requires the presence of metal ions. For instance, the 39E DNAzyme selected in our lab (secondary structure shown in Figure 1.2) is preferentially active in the presence of UO^{2+}.[58,59] In the absence of uranyl, or in the presence of other metal ions, no activity is observed. This feature enhances the utility of the uranium sensor with high selectivity based on this DNAzyme. Because the metal ion cofactors of DNAzymes are central to their activity, much research has been carried out to characterize the interactions between DNAzymes and metal ions.

DNAzymes are most often modeled as metalloenzymes with the DNAzyme-metal complex as the catalytically active specie.[60] Michaelis-Menton models can be used to analyze a DNAzyme's kinetics.[59,61] For nuclease-like DNAzymes, the following reactions apply:

$$E\text{-}S + M \leftrightarrow ES\text{-}M$$

$$ES\text{-}M \rightarrow product + M$$

In the equations, E, S and M are the enzyme strand, the substrate strand and the metal ion co-factor, respectively.

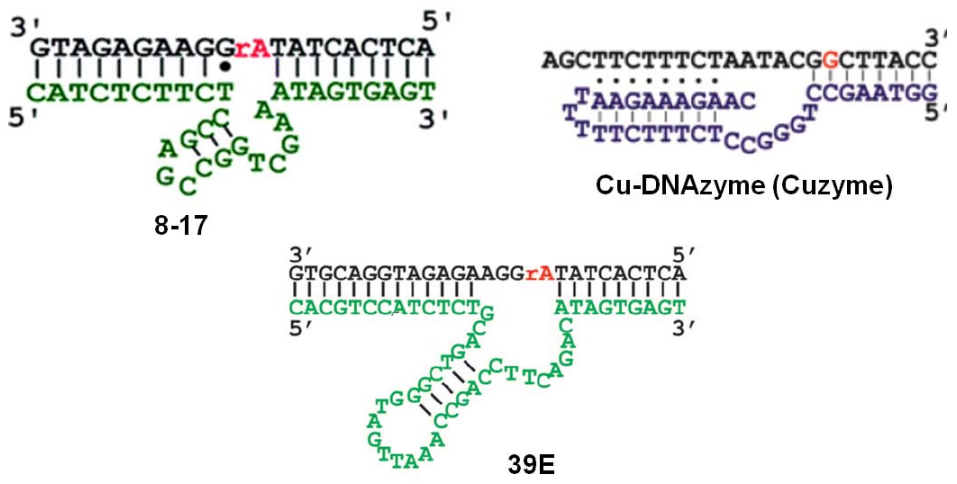

Figure 1.2 Secondary structures of several DNAzymes with nuclease activity predicted by mFold.

It is assumed that the concentration of the intermediate, the DNA-metal complex, is constant. Its dissociation constant can thus be calculated through activity assays. While a DNA-metal complex has not yet been formally observed, the Michaelis-Menton[62] model explains the activity assay well and predicts the kinetics of the reactions catalyzed by DNAzymes accurately.

Biophysical methods provide a powerful tool to characterize the metal-DNA interaction. The 8-17 DNAzyme (Figure 1.2) acts as a nuclease in the presence of Pb^{2+}, Zn^{2+}, and Mg^{2+}.[63] It can be modified with a fluorescent donor and acceptor in order to carry out biophysical studies. As a result, Förster Resonance Energy Transfer (FRET) studies[64-67] can be carried out to observe the conformational changes induced in DNAzymes by metal cations. It was discovered that the conformational change produced by Zn^{2+} or Mg^{2+} was different from that of Pb^{2+}.[64,67,68] Zn^{2+} or Mg^{2+} led to the folding of the DNAzyme, followed by the catalytic cleavage, while Pb^{2+}-induced cleavage did not involve the folding.

It has been reported that the presence of high concentrations (≥ 1 M) of monovalent metal ions such as Na^+ and Li^+ also activates DNAzymes.[69] Based on this observation, it was proposed that the folding of the DNA instead of the specific binding of the metal ions activates the DNAzymes. It was even discovered that high concentrations of monovalent metal ions or millimolar Zn^{2+} and Mg^{2+} folds the 8-17 DNAzyme into a Z-DNA conformation. Thus, it was hypothesized that the Z-DNA form is critical for 8-17's activity.[65]

The specific binding of DNAzymes to their metal ion cofactors has not been directly observed because these cofactors are colorless, prohibiting any spectroscopic characterization. Before the crystal structure of the active DNAzyme-cofactor specie is solved, it is expected that advanced spectroscopic techniques such as EPR, NMR, and EAXFS will provide insight into the DNAzyme catalysis model.

1.1.5 Functional nucleic acid-based sensors

One of the most important applications of functional nucleic acids is their ability to detect species of interest such as metal cations, organic toxins and biological pathogens.[70] Aptamers bind their targets with strong affinities, with K_ds varying from the picolmolar to the micromolar range. More importantly, the binding of aptamers to their targets is specific, which makes aptamer-based sensors selective. Also, the high affinity between aptamers and targets ensures the high sensitivities of these sensors.

DNAzymes can also be converted into biosensors.[71] As discussed above, DNAzymes require cofactors, most often metal ions, for activity. Moreover, one metal cation is the main metal cofactor for each DNAzyme. In other word, the metal-DNAzyme

interaction is typically highly specific. The specificity of the DNAzyme-basd sensors hinges on this point.

Although functional nucleic acids, especially DNA aptamers and DNAzymes, provide a platform for sensor design, the binding event of an aptamer to the target or the reaction catalyzed by a DNAzyme in the presence of its target must be transduced to a signal output.[70] So far, fluorescent, colorimetric, electrochemical, and MRI contrast agents based on functional nucleic acids have been developed and reported.

Fluorescent sensors Shortly after the initial selection of aptamers by SELEX, efforts have been made to make sensors based on aptamers. Early efforts included functionalizing aptamers with fluorophores.[72] The binding of the aptamer to the target was expected to affect the chemical surroundings of the fluorophore so that a fluorescence change could be detected. The first successful trial was reported by a group led by Ellington (Figure 1.3).[73] A fluorescent dye was incorporated between G7 and G8, and a small fluorescent change could be detected in the presence of ATP. The fluorescence signal was not observed in the presence of other nucleotides.

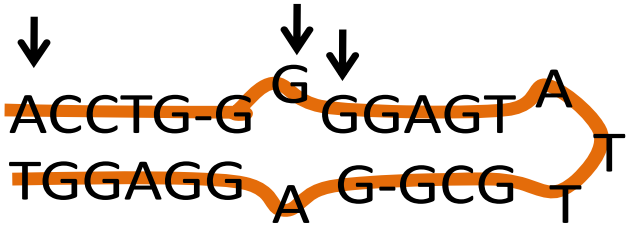

Figure 1.3 DNA aptamer that recognize ATP. The arrows point to the engineered bases for sensing.

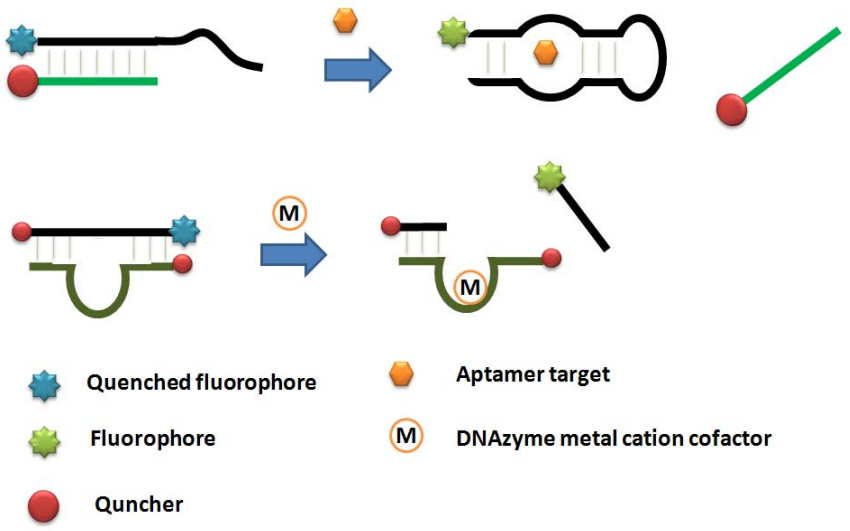

Figure 1.4 General designs for metal cation aptamer-based fluorescent sensors and DNAzyme-based sensors.

Later, Li and co-workers reported a structural switching method.[74-78] As shown in Figure 1.4, the sensor contained two strands: the aptamer strand (in black) labeled by fluorescein, and the quencher strand (in green) which was partially complementary to the aptamer strand. The two strands hybridized in solution and their fluorescence was quenched. However, the hybridization of these two strands is significantly destabilized by the presence of the analyte (adenosine, shown in orange). As a result, the quencher strand dissociated from the complex and the fluorescence was recovered. This is a general design for aptamer-based sensors and was adapted for other sensor designs.

Fluorophore/quencher pairs were also applied in DNAzyme-based florescent sensors. The first example was reported by Li *et al.* in 2000.[63] The 17E DNAzyme, which cleaves a DNA/RNA chimeric substrate strand in the presence of Pb^{2+}, was developed as a Pb^{2+} sensor.[79] As shown in Figure 1.4, the substrate strand was modified with a fluorophore and quencher while the enzyme strand was labeled with a quencher. The

hybridization of the enzyme to the substrate strand minimized the fluorescence, but the addition of the metal cation analyte activated the DNAzyme as a nuclease. As a result, the substrate was cleaved and released, leading to a recovery of the fluorescence.

Colorimetric sensors Although fluorescent sensors are sensitive and quantitative, they require a fluorometer. This makes it difficult to use these sensors onsite. In some cases, semi-quantitative, but fast and cheap detection is requested. To achieve this goal, colorimetric sensors based on functional nucleic acids were developed.[70]

Gold nanoparticles have a deep red color.[80] Generally, the smaller the nanoparticles are, the shorter their absorbance wavelength is. Thus, small gold nanoparticles (with radii around 10-20 nm) absorb light in the blue region, leading to a red color.[81-83] It was also observed that as gold nanoparticles aggregate and form clusters micrometers in size, the resulting solution assumes a blue color. DNAzyme- and aptamer-based colorimetric sensors are based on this phenomenon.

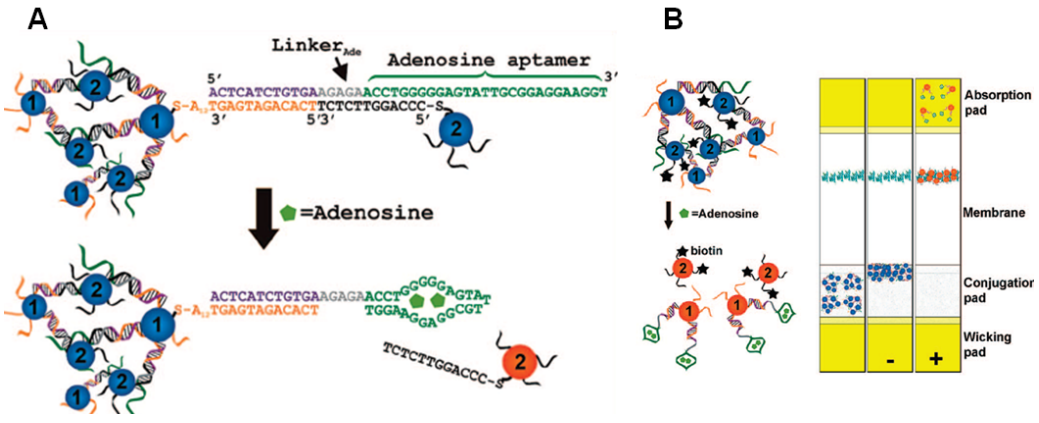

Figure 1.5 (A) Colorimetric sensor for adenosine detection based on the regulation of the assembly of gold nanoparticles by the presence of adenosine. (B) A lateral flow device for adenosine detection based on the colorimetric sensor presented in A.

As shown in Figure 1.5A, a colorimetric adenosine sensor can be assembled by covalently functionalizing nanoparticles by two different DNAs, both of which are partially complimentary to the extended adenosine aptamer strand.[84,85] When the different DNAs hybridize, the gold nanoparticles with different DNA functionalizations form aggregates, producing a faint blue solution. The addition of adenosine switches the conformation of the aptamer strand. As a result, most of the aptamer strands bind to the target and the nanoparticle aggregates disassemble. Thus, a color change from faint blue to red can be observed in the presence of the analyte. The nanoparticle aggregates can also be disassembled by metal ions if DNAzymes are used, paving the way for colorimetric metal ion devices.[86-91]

This nanoparticle-based colorimetric sensor was even converted to dip-stick device.[92,93] As shown in Figure 1.5B, the DNA-assembled gold nanoparticle aggregate is loaded at the bottom of the device. The presence of the target disassembles the aggregate. Only the dispersed nanoparticles can flow up and be captured at the top of the dipstick, so when the analyte is present in solution, a red band forms at the top of the dipstick.

Electrochemical sensors Electrochemical sensors based on functional nucleic acids have been developed. For instance, a group led by Plaxco reported the first electrochemical Pb^{2+} sensor using the 17E DNAzyme.[94,95] First, the DNAzyme was immobilized on the surface of the gold electrode. Then the substrate strand was chemically modified by methylene blue (MB) and immobilized onto the surface of the electrode through DNA hybridization. The MB molecule on the surface of the electrode was capable of electron transfer and a current could be detected when the potential

applied to the electrode was scanned. When Pb^{2+} cleaves the substrate strand, the product carrying MB was released from the electrode, resulting in a decrease in the electric signal. By correlating the change in the Pb^{2+} concentration with the decreased current signal, they successfully detected Pb^{2+} in solution.

Aptamers were also used in electrochemical sensors. The distance between the electrode and the electroactive species was regulated by the interaction of an aptamer with its analyte, leading to a detectable electrochemical signal.[95-99]

1.2 Magnetic resonance imaging (MRI)

MRI converts NMR-derived information into a meaningful image. NMR spectra provide information, such as chemical shift, J-J coupling and relaxation; relaxation time was utilized for imaging. After half a century of development, MRI is now a powerful tool in both clinical diagnosis and research. It was even more useful after the invention of MRI contrast agents.

1.2.1 Principle of MRI

Modern MRI uses the pulsed instead of the continuous wave technique. The operation procedure is described in Figure 1.6. In a magnetic field, the randomly directed (stage A) molecular magnetizations (M) align to achieve the lowest energy (stage B). An electromagnetic pulse will change the direction of the magnetization (to the x-y plate in stage C). As the pulse is very short, the magnetization tends to go back to the state with the lowest energy (relaxation, stage D). The magnetization can be decomposed into the transverse magnetization on x-y plate (M_{XY}) and longitude magnetization on z axis (M_Z). The amplitude of M_Z and M_{XY} ($|M|_{XY}$) follow the equations 1.1 and 1.2:

$$M_Z = M_{Z,0}\left(1 - e^{-\frac{t}{T_1}}\right) \quad (1.1)$$

$$|M|_{XY} = M_{XY,0}e^{-\frac{t}{T_2}} \quad (1.2)$$

T1 and T2 are the longitude and transverse relaxation time, respectively. They are the parameters that play the most important role in modern MRI technology.

MRI was performed by scanning the M_Z or M_{XY} of the NMR-active nuclei of the imaged object. The images acquired are called T1- or T2-weighted MRI images. As presented in Figure 1.6, stage D, the spot with faster relaxation (short T1), has a higher M_Z than the spot with slower relaxation. Thus, the spot with faster relaxation is brighter in a T1-weighted image than the spot with slower relaxation.

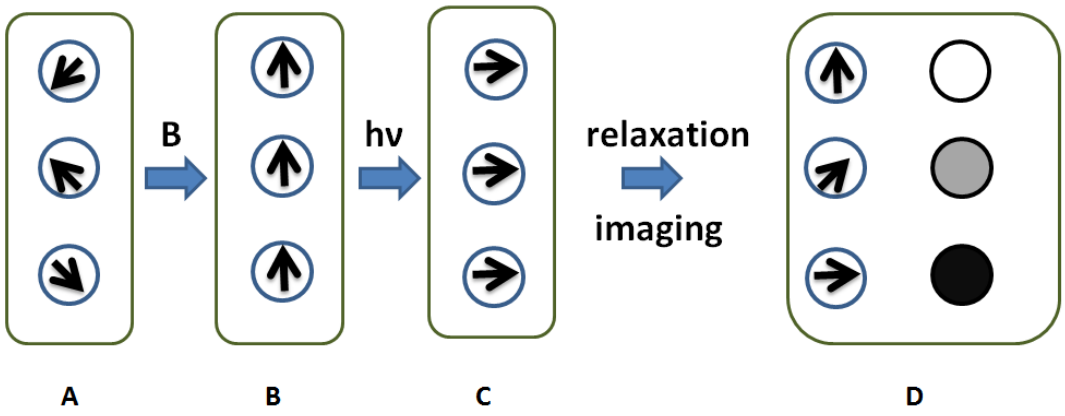

Figure 1.6 Principle of the T1-weighted MRI imaging process. The magnetization of atoms aligns with the magnetic field. They are stimulated with a microwave pulse. The magnetization goes back to the state with the lowest energy with different rate. If the magnetization on the z-axis is scanned, the contrast on the image is dependent on the relaxation rate – fast relaxation leads to bright image.

Theoretically, all the nuclei with non-zero magnetic moment are used for imaging; practically only the water proton is used for scanning. The reason for this is that water is

the most abundant specie in the human body. Moreover, hydrogen has the highest gyromagnetic ratio, which makes Hydrogen the most sensitive of all atoms.

Finally, it is important to mention encoding. It is technically not possible to apply a pulse to a very small area. Thus, the signal from one pixel from the other should be differentiated. This process is called encoding. The most straightforward method for encoding is to apply a magnetic gradient. The chemical shift of the water proton signal is related to the magnetic field. If the gradient is applied, different spots will have different magnetic fields; thus, pixels can be differentiated through chemical shifts. Besides magnetic gradient, phase encoding is more widely used in modern MRI scanners.

1.2.2 MRI contrast agents

Contrast agents were developed to shorten the imaging time and enhance the contrast of the image. MRI contrast agents are chemicals which enhance the contrast of the MRI images.[100]

It was discovered that most paramagnetic metal cations such as Fe^{3+}, Cu^{2+} and Gd^{3+} can shorten T1 of water proton.[100] Clinically Gd^{3+} compounds are used as contrast agents for T1-weighted scans because of its seven unpaired elections.

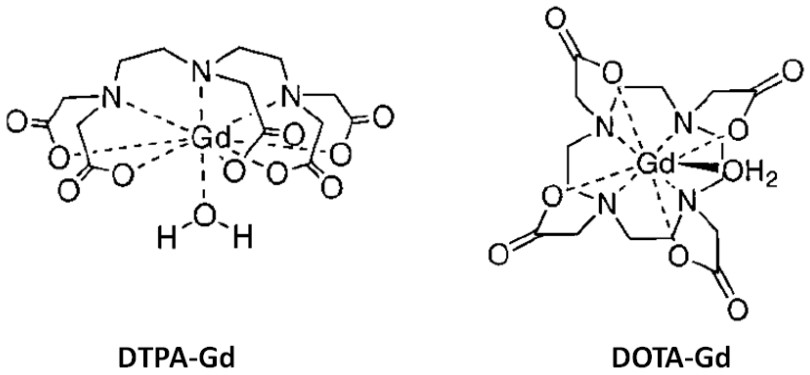

Figure 1.7 Structures of the most widely used Gd-based MRI contrast agents: DTPA-Gd and DOTA-Gd

Gd^{3+} hydrate is toxic, thus for biological applications it is necessary to complex it with a ligand that will reduce its toxicity.[101] The most common ligands used for this purpose are DTPA[102] and DOTA[103] (structures shown in Figure 1.7).[100] It has been reported that the pK_d for DTPA-Gd and DOTA-Gd are 22.46 and 25.3 respectively.[100] The strong binding between Gd^{3+} and these ligands minimizes the release of free Gd^{3+} into the body leading to the reduced toxicity.

The water proton relaxation enhancement by the Gd compound is dependent on the concentration. It is quantitatively described in Equation 1.3, in which T1 is the relaxation time of the water proton, $T1_0$ is the water proton relaxation time of pure water, [Gd] is the concentration of the gadolinium compound and r1 is defined as the compound's relaxivity.

$$\frac{1}{T1} = \frac{1}{T1_0} + r1[Gd] \quad (1.3)$$

The Relaxivity of a gadolinium compound can be quantitatively described by the Solomon-Bloembergen-Morgan theory.[100,104] The simplified model predicts Equation 1.4.

$$r1 = \frac{qP_m}{T1_m + \tau_m} \quad (1.4)$$

In Equation 1.4, P_m is the concentration of water proton, which is constant, q is the hydration number (the number of water molecules bound to each Gd cation), and τ_m is the lifetime of the bound water molecule. Finally, $T1_m$ is a fitted parameter (the bound water proton relaxation time), and is decided by factors such as the strength of the magnetic field and the size of the Gd compound.

The Solomon-Bloembergen-Morgan theory precisely predicts the performance of the Gd-based MRI contrast agents and aids the design of contrast agents with high relaxivity and smart characteristics.

1.2.3 Smart MRI contrast agents

Smart MRI contrast agents are produced by combining an MRI contrast agent with a sensor.[105] Traditional MRI contrast agents enhance MRI contrast non-specifically. However, modern medical research and clinical applications require small molecules to be imaged with non-invasive techniques. Thus, using MRI/MRI contrast agents to image the distributions of small molecules attracted the attention of researchers. The relaxivity of smart MRI contrast agents can be regulated by the presence of small molecules, leading to differential contrast on an MRI image.[105]

The Solomon-Bloembergen-Morgan theory provides a theoretical foundation for the development of the smart contrast agents. From Equation 1.4, the q and $T1_m$ are two parameters that can be regulated. q is related to the coordination of the Gd compounds, and $T1_m$ can be regulated by changing the size of the Gd compounds.

One of the earliest smart MRI contrast agents was Ca^{2+}-sensitive and invented by the Meade group.[106] They successfully designed a Gd compound that also binds Ca^{2+}. When this occurs, the binding coordination of the Gd^{3+} changes, and this translates into a relaxivity change.

Today, few smart MRI contrast agents have been developed to recognize metal ions including Ca^{2+},[106] Zn^{2+},[107,108], Cu^{2+}[109] as well as H^{+},[110] enzymes,[111] oxygen, and other species of interest.[112,113] The rational design of small contrast agents is still a challenge because their key molecular interactions are not well known or predictable.

1.3 Electron paramagnetic imaging (EPR)

1.3.1 A Brief introduction to EPR

Bleaney was the first to observe the electron resonance phenomenon.[114] The EPR phenomenon is similar to NMR, in that electrons have spin (+1/2 or -1/2), and in a magnetic field, the energy of the electrons splits (Figure 1.8). The electromagnetic radiation whose energy is the difference between the splitting energy level can be absorbed, excites the electrons from the low-energy state to the high-energy state. The wavelength of the radiation is indicated in Equation 1.5.

$$\upsilon = \frac{g_e \mu_B B_0}{h} \qquad (1.5)$$

In the equation, g_e is the g-factor, which is decided by what chemical environment the electron belongs to. μ_B is the Bohr magneton, B_0 is the magnetic field, and h is the Planck constant.

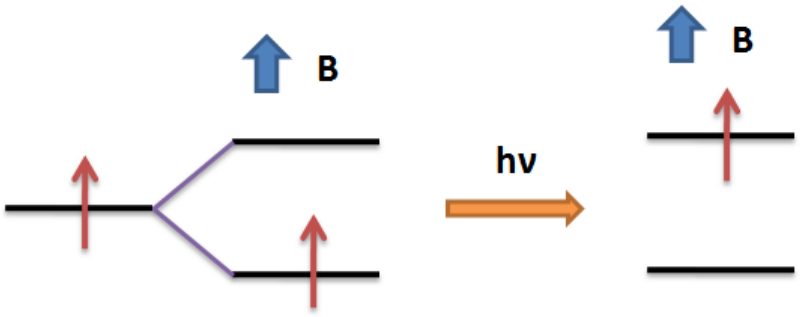

Figure 1.8 The splitting of the electron spin energy level in the magnetic field and the absorbance of the microwave radiation.

The absorbance happens only when the magnetic field (B_0) and the frequency of the radiation (υ) meet Equation 1.5. The modern EPR spectrometer uses a fixed

wavelength. The magnetic field is scanned and the absorbance of the radiation is recorded. When Equation 1.5 is met, a peak can be observed.

1.3.2 Applications of EPR in bioinorganic chemistry

EPR is not applied as widely as NMR is. The reason is that EPR requires unpaired electrons. The electrons of most organic compounds are paired, and thus do not generate a detectable EPR signal. However, EPR is a very powerful tool to detect species with unpaired electrons, such as radicals and some transition metal compounds.[115,116] As the g-factors (g_e) of unpaired electrons are sensitive to the binding ligand and binding geometry of the metal center, EPR can provide information about the interaction between metal cations and ligands.

Bioinorganic chemistry studies the interactions between metal cations and biomolecules such as protein and nucleic acids, as well as metal-related catalysis. EPR is widely used in bioinorganic chemistry because it gives information about the energy splitting caused by biomolecular ligands as well as electron configuration.

EPR in the study of metalloproteins The most common metal species found in proteins are Cu, Fe, Ni, Co, Mn, and Zn. EPR is a powerful tool to characterize proteins containing these metal cations, with the exception of Cu^{2+} and Zn^{2+}.[117-119] For instance, one of the most common metal cofactors in proteins is heme. EPR is one of the very few techniques that can distinguish a high-spin heme from a low-spin heme, since these heme's spin states are decided by the binding strength of the axial ligand. By analyzing the available data systematically, Peisach and Blumberg even presented a "truth table," which makes it possible to discern the category and orientation of the axial ligand by

simply analyzing and simulating the EPR spectra. Although it is a rough method, it does give important information about metal binding in macromolecules at an early stage of research.

EPR in the study of nucleic acid structure and dynamics EPR is not as common in nucleic acid research as in protein research. The reasons are twofold. First, nucleic acids are EPR silent. Without spin labeling, no nucleic acid signal can be detected. Second, the binding between nucleic acids and metal ions is neither specific nor strong, and this broadens the metal cations' EPR signal. However, EPR has been an important tool to study the folding and dynamics of nucleic acids.[115,116,120-122]

1.4 Research focuses

Research on the functional nucleic acids have two directions – their analytical, clinical and diagnostic applications and the characterizations of the specific interactions of the functional nucleic acids with other molecules which account for their functions. This dissertation focuses on both directions.

Functional nucleic acids have been applied in the development of fluorescent, colorimetric, electrochemical sensors and smart T2-weighted MRI contrast agents. Thus, the first part of the dissertation focuses on converting the functional nucleic acids including aptamer and DNAzyme to smart T1 weighted MRI contrast agents. It was realized by transducing the binding event of the aptamer or the reaction catalyzed by the DNAzyme to the molecular weight change of the gadolinium compounds. At clinical

MRI magnetic field (1.5 T), the molecular weight change leads to the relaxation time change of water proton and a contrast change on an MRI image.

The smart contrast agents responded to the analytes by decreased contrast (a "turn-off" signal). And the contrast agents required streptavidin, which is not cost-effective. To solve the problems, a novel structure switching system was designed, in which two aptamers are conjugated together. Although the application of this structure switching has not been applied to the smart contrast agent designs, the concept was demonstrated by a label-free sensor based on the regulation of the fluorescence of malachite green. The presence of adenosine switches the structure of the aptamer of malachite green; and the aptamer is then able to bind to malachite green in the solution. Upon the binding, a fluorescence change can be detected.

The metal cation-DNAzyme interaction was investigated in the dissertation, too. Spectroscopic techniques, such as electron paramagnetic resonance (EPR) can be used to characterize the interaction of Cu^{2+} and Cu^{2+}-dependent DNAzyme. EPR of Cu^{2+} is sensitive to the binding mode; thus the technique has been applied to probe the binding of Cu^{2+} to various ligands including proteins. UV-Vis is another technique that can be used to investigate the binding. The UV-Vis absorbance of Cu^{2+} is dependent on the d-orbital splitting induced by the binding. The binding of Cu^{2+} to the DNAzyme can thus be probed through tracking the UV-absorbance band shifting. 8-17 DNAzyme has been characterized in multiple groups by multiple techniques. However, the enzymatic activity of the DNAzyme with the presences of two metal cations has not been reported. Fluorescence assay was used to characterize the DNAzyme activity with Pb^{2+} and other metal cations.

Finally, aptamers was used to functionalize liposome encapsulating anti-cancer medicine cisplatin. The functionalized liposome showed targeted drug delivery effect to the breast cancer cells over other cells. The delivery of the drug can be diminished by applying the antisense strand of the aptamer, which is useful in the case of over-dosing.

1.5 References

(1) Crick, F. H. C. *J. Mol. Biol.* **1968**, *38*, 367-379.

(2) Woese, C. R. In *The Genetic Code*; Harper & Row: New York, 1967, p 179-195.

(3) Orgel, L. E. *J. Mol. Biol.* **1968**, *38*, 381-393.

(4) Kruger, K.; Grabowski, P. J.; Zaug, A. J.; Sands, J.; Gottschling, D. E.; Cech, T. R. *Cell* **1982**, *31*, 147-157.

(5) Guerrier-Takada, C.; Gardiner, K.; Marsh, T.; Pace, N.; Altman, S. *Cell* **1983**, *35*, 849-857.

(6) Altman, S. *Cell* **1984**, *36*, 237-239.

(7) Winkler, W. C.; Breaker, R. R. *Trends Biochem. Sci* **2005**, *59*, 487-517.

(8) Barrick, J. E.; Breaker, R. R. *Sci. Am.* **2006**, *296*, 50-57.

(9) Cochrane, J. C.; Strobel, S. A. *RNA* **2008**, *14*, 993-1002.

(10) Burgstaller, P.; Famulok, M. *Angew. Chem., Int. Ed.* **1994**, *33*, 1084-1087.

(11) Lorsch, J. R.; Szostak, J. W. *Biochemistry* **1994**, *33*, 973-982.

(12) Lauhon, C. T.; Szostak, J. W. *J. Am. Chem. Soc.* **1995**, *117*, 1246-1257.

(13) Dieckmann, T.; Suzuki, E.; Nakamura, G. K.; Feigon, J. *RNA* **1996**, *2*, 628-640.

(14) Schneider, D.; Tuerk, C.; Gold, L. *J. Mol. Biol.* **1992**, *228*, 862-869.

(15) Tuerk, C.; MacDougal-Waugh, S. *Gene* **1993**, *137*, 33-39.

(16) Conrad, R. C.; Baskerville, S.; Ellington, A. D. *Mol.Diversity* **1995**, *1*, 69-78.

(17) Gold, L.; Polisky, B.; Uhlenbeck, O.; Yarus, M. *Annu. Rev. Biochem* **1995**, *64*, 763-797.

(18) Breaker, R. R.; Joyce, G. F. *Chem. Biol.* **1994**, *1*, 223-229.

(19) Carmi, N.; Shultz, L. A.; Breaker, R. R. *Chem. Biol.* **1996**, *3*, 1039-1046.

(20) Breaker, R. R. *Nat. Biotechnol.* **1997**, *15*, 427-431.

(21) Breaker, R. R. *Curr. Opin. Chem. Biol.* **1997**, *1*, 26-31.

(22) Sen, D.; Geyer, C. R. *Curr. Opin. Chem. Biol.* **1998**, *2*, 680-687.

(23) Li, Y.; Breaker, R. R. *Curr.Opin.Struct.Biol.* **1999**, *9*, 315-323.

(24) Silverman, S. K. *Chem. Commun.* **2008**, *(30)*, 3467-3485.

(25) Bock, L. C.; Griffin, L. C.; Latham, J. A.; Vermaas, E. H.; Toole, J. J. *Nature* **1992**, *355*, 564-566.

(26) Huizenga, D. E.; Szostak, J. W. *Biochemistry* **1995**, *34*, 656-665.

(27) Kim, M.; Jeoung, Y.-H.; Lee, S. J.; Choi, I.; Pyun, K.-H.; Lee, Y. *Mol. Cells* **1995**, *5*, 555-562.

(28) Li, Y.; Geyer, C. R.; Sen, D. *Biochemistry* **1996**, *35*, 6911-6922.

(29) Majumder, P.; Gomes, K. N.; Ulrich, H. *Expert opinion on therapeutic patents* **2009**, *19*, 1603-1613.

(30) Ellington, A. D.; Szostak, J. W. *Nature* **1990**, *346*, 818-822.

(31) Berzal-Herranz, A.; Joseph, S.; Burke, J. M. *Genes Dev.* **1992**, *6*, 129-134.

(32) Griffin, L. C.; Toole, J. J.; Leung, L. L. K. *Gene* **1993**, *137*, 25-31.

(33) Szostak, J. W.; Ellington, A. D.; Gesteland, R. F.; Atkins, J. F. In *The RNA World*; Cold Spring Harbor Laboratory Press: Cold Spring Harbor, New York, 1993, p 511-533.

(34) Jayasena, S. D. *Clin. Chem.* **1999**, *45*, 1628-1650.

(35) Sen, D. *Compr. Nat. Prod. Chem.* **1999**, *7*, 615-641.

(36) Shamah, S. M.; Healy, J. M.; Cload, S. T. *Acc. Chem. Res.* **2008**, *41*, 130-138.

(37) Bruesehoff, P. J.; Li, J.; Augustine, A. J.; Lu, Y. *Combin. Chem. High Throughput Screen.* **2002**, *5*, 327-335.

(38) Tuerk, C.; Gold, L. *Science* **1990**, *249*, 505-510.

(39) Famulok, M. *J. Am. Chem. Soc.* **1994**, *116*, 1698-1706.

(40) Mendonsa, S. D.; Bowser, M. T. *J. Am. Chem. Soc.* **2005**, *127*, 9382-9383.

(41) Ogawa, A.; Tomita, N.; Kikuchi, N.; Sando, S.; Aoyama, Y. *Bioorganic & medicinal chemistry letters* **2004**, *14*, 4001-4004.

(42) Rusconi, C. P.; Scardino, E.; Layzer, J.; Pitoc, G. A.; Ortel, T. L.; Monroe, D.; Sullenger, B. A. *Nature (London, United Kingdom)* **2002**, *419*, 90-94.

(43) Giver, L.; Bartel, D. P.; Zapp, M. L.; Green, M. R.; Ellington, A. D. *Gene* **1993**, *137*, 19-24.

(44) Conrad, R. C.; Giver, L.; Tian, Y.; Ellington, A. D. *Methods Enzymol.* **1996**, *267*, 336-367.

(45) Wang, C.; Zhang, M.; Yang, G.; Zhang, D.; Ding, H.; Wang, H.; Fan, M.; Shen, B.; Shao, N. *J. Biotechnol.* **2003**, *102*, 15-22.

(46) Cerchia, L.; Duconge, F.; Pestourie, C.; Boulay, J.; Aissouni, Y.; Gombert, K.; Tavitian, B.; de, F. V.; Libri, D. *PLoS Biol.* **2005**, *3*, e123.

(47) Chapman, K. B.; Szostak, J. W. *Chem. Biol.* **1995**, *2*, 325-333.

(48) Williams, K. P.; Bartel, D. P. *Nucleic Acids Mol. Biol.* **1996**, *10*, 367-381.

(49) Vaish, N. K.; Heaton, P. A.; Eckstein, F. *Biochemistry* **1997**, *36*, 6495-6501.

(50) Piganeau, N.; Jenne, A.; Thuillier, V.; Famulok, M. *Angew. Chem., Int. Ed.* **2000**, *39*, 4369-4373.

(51) Hager, A. J.; Szostak, J. W. *Chem. Biol.* **1997**, *4*, 607-617.

(52) Carola, C.; Eckstein, F. *Curr. Opin. Chem. Biol.* **1999**, *3*, 274-283.

(53) Burgstaller, P.; Famulok, M. *Angew. Chem., Int. Ed.* **1995**, *34*, 1189-1192.

(54) Jaschke, A. *Curr. Opin. Struct. Biol.* **2001**, *11*, 321-326.

(55) Emilsson, G. M.; Breaker, R. R. *Cell. Mol. Life Sci.* **2002**, *59*, 596-607.

(56) Silverman, S. K. *Org. Biomol. Chem.* **2004**, *2*, 2701-2706.

(57) Schlosser, K.; McManus, S. A.; Li, Y. In *The Aptamer Handbook*; Klussmann, S., Ed.; Wiley-VCH Verlag GmbH & Co. KGaA: 2006, p 228-261.

(58) Liu, J.; Brown, A. K.; Meng, X.; Cropek, D. M.; Istok, J. D.; Watson, D. B.; Lu, Y. *Proc. Natl. Acad. Sci. U.S.A.* **2007**, *104*, 2056-2061.

(59) Brown, A. K.; Liu, J.; He, Y.; Lu, Y. *ChemBioChem* **2009**, *10*, 486-492.

(60) Lu, Y. *Chem. Eur. J.* **2002**, *8*, 4588-4596.

(61) Brown, A. K.; Li, J.; Pavot, C. M. B.; Lu, Y. *Biochemistry* **2003**, *42*, 7152-7161.

(62) Shih, I.; Been, M. D. *Biochemistry* **2000**, *39*, 9055-966.

(63) Li, J.; Zheng, W.; Kwon, A. H.; Lu, Y. *Nucleic Acids Res.* **2000**, *28*, 481-488.

(64) Liu, J.; Lu, Y. *J. Am. Chem. Soc.* **2002**, *124*, 15208-15216.

(65) Mazumdar, D.; Nagraj, N.; Kim, H.-K.; Meng, X.; Brown, A. K.; Sun, Q.; Li, W.; Lu, Y. *J. Am. Chem. Soc.* **2009**, *131*, 5506-5515.

(66) Kim, H. K.; Li, J.; Nagraj, N.; Lu, Y. *Chem. Eur. J.* **2008**, *232*, 8696.

(67) Kim, H.-K.; Rasnik, I.; Liu, J.; Ha, T.; Lu, Y. *Nat. Chem. Biol.* **2007**, *3*, 763-768.

(68) Liu, J.; Lu, Y. *Methods Mol. Biol.* **2006**, *335*, 275-288.

(69) Geyer, C. R.; Sen, D. *Chem. Biol.* **1997**, *4*, 579-593.

(70) Liu, J.; Cao, Z.; Lu, Y. *Chem. Rev.* **2009**, *109*, 1948-1998.

(71) Palchetti, I.; Mascini, M. *Analyst* **2008**, *133*, 846-854.

(72) Hermann, T.; Patel, D. J. *Science* **2000**, *287*, 820-825.

(73) Jhaveri, S. D.; Kirby, R.; Conrad, R.; Maglott, E. J.; Bowser, M.; Kennedy, R. T.; Glick, G.; Ellington, A. D. *J. Am. Chem. Soc.* **2000**, *122*, 2469-2473.

(74) Nutiu, R.; Li, Y. *J. Am. Chem. Soc.* **2003**, *125*, 4771-4778.

(75) Nutiu, R.; Li, Y. *Chem. Eur. J.* **2004**, *10*, 1868-1876.

(76) Nutiu, R.; Li, Y. *Angew. Chem., Int. Ed.* **2005**, *44*, 1061-1065.

(77) Nutiu, R.; Li, Y. *Methods* **2005**, *37*, 16-25.

(78) Rupcich, N.; Chiuman, W.; Nutiu, R.; Mei, S.; Flora, K. K.; Li, Y.; Brennan, J. D. *J. Am. Chem. Soc.* **2006**, *128*, 780-790.

(79) Li, J.; Lu, Y. *J. Am. Chem. Soc.* **2000**, *122*, 10466-10467.

(80) Mirkin, C. A.; Letsinger, R. L.; Mucic, R. C.; Storhoff, J. J. *Nature* **1996**, *382*, 607-609.

(81) Elghanian, R.; Storhoff, J. J.; Mucic, R. C.; Letsinger, R. L.; Mirkin, C. A. *Science* **1997**, *277*, 1078-1080.

(82) Storhoff, J. J.; Elghanian, R.; Mucic, R. C.; Mirkin, C. A.; Letsinger, R. L. *J. Am. Chem. Soc.* **1998**, *120*, 1959-1964.

(83) Storhoff, J. J.; Lazarides, A. A.; Mucic, R. C.; Mirkin, C. A.; Letsinger, R. L.; Schatz, G. C. *J. Am. Chem. Soc.* **2000**, *122*, 4640-4650.

(84) Liu, J.; Lu, Y. *Angew. Chem., Int. Ed.* **2006**, *45*, 90-94.

(85) Liu, J.; Lu, Y. *Nat. Prot.* **2006**, *1*, 246-252.

(86) Liu, J.; Lu, Y. *J. Am. Chem. Soc.* **2005**, *127*, 12677-12683.

(87) Liu, J.; Lu, Y. *Org. Biomol. Chem.* **2006**, *4*, 3435-3441.

(88) Liu, J. W.; Lu, Y. *J. Fluo.* **2004**, *14*, 343-354.

(89) Liu, J.; Lu, Y. *J. Am. Chem. Soc.* **2004**, *126*, 12298-12305.

(90) Liu, J.; Lu, Y. *Chem. Mater.* **2004**, *16*, 3231-3238.

(91) Lee, J. H.; Wang, Z.; Liu, J.; Lu, Y. *J. Am. Chem. Soc.* **2008**, *130*, 14217-14226.

(92) Liu, J.; Mazumdar, D.; Lu, Y. *Angew. Chem., Int. Ed.* **2006**, *45*, 7955-7959.

(93) Mazumdar, D.; Liu, J.; Lu, G.; Zhou, J.; Lu, Y. *Chem. Commun.* **2010**, *46*, 1416-1418.

(94) Xiao, Y.; Lai, R. Y.; Plaxco, K. W. *Nat. Prot.* **2007**, *2*, 2875-2880.

(95) Xiao, Y.; Rowe, A. A.; Plaxco, K. W. *J. Am. Chem. Soc.* **2007**, *129*, 262-263.

(96) White, R. J.; Phares, N.; Lubin, A. A.; Xiao, Y.; Plaxco, K. W. *Langmuir* **2008**, *24*, 10513-10518.

(97) Zuo, X.; Xiao, Y.; Plaxco, K. W. *J. Am. Chem. Soc.* **2009**, *131*, 6944-6945.

(98) Xiao, Y.; Lubin, A. A.; Heeger, A. J.; Plaxco, K. W. *Angew. Chem., Int. Ed.* **2005**, *44*, 5456-5459.

(99) Xiao, Y.; Piorek, B. D.; Plaxco, K. W.; Heeger, A. J. *J. Am. Chem. Soc.* **2005**, *127*, 17990-17991.

(100) Caravan, P.; Ellison, J. J.; McMurry, T. J.; Lauffer, R. B. *Chem. Rev.* **1999**, *99*, 2293-2352.

(101) Lauffer, R. B. *Chem. Rev.* **1987**, *87*, 901-927.

(102) Carr, D. H.; Brown, J.; Bydder, G. M.; Steiner, R. E.; Weinmann, H. J.; Speck, U.; Hall, A. S.; Young, I. R. *Am. J. Roentgenol.* **1984**, *143*, 215-224.

(103) Li, M.; Meares, C. F. *Bioconjugate Chem.* **1993**, *4*, 275-283.

(104) Bloembergen, N.; Morgan, L. O. *J. Chem. Phys.* **1961**, *34*, 842-850.

(105) Meade, T. J.; Taylor, A. K.; Bull, S. R. *Curr. Opin. Neurobiol.* **2003**, *13*, 597-602.

(106) Li, W.-h.; Fraser, S. E.; Meade, T. J. *J. Am. Chem. Soc.* **1999**, *121*, 1413-1414.

(107) Hanaoka, K.; Kikuchi, K.; Urano, Y.; Nagano, T. *J. Chem. Soc. Perkin Trans.* **2001**, 1840-1843.

(108) Hanaoka, K.; Kikuchi, K.; Urano, Y.; Narazaki, M.; Yokawa, T.; Sakamoto, S.; Yamaguchi, K.; Nagano, T. *Chem. Biol.* **2002**, *9*, 1027-1032.

(109) Que, E. L.; Chang, C. J. *J. Am. Chem. Soc.* **2006**, *128*, 15942-15943.

(110) Zhang, S.; Wu, K.; Sherry, A. D. *Angew. Chem., Int. Ed.* **1999**, *38*, 3192-3194.

(111) Moats, R. A.; Fraser, S. E.; Meade, T. J. *Angew. Chem., Int. Ed.* **1997**, *36*, 726-728.

(112) De Leon-Rodriguez, L. M.; Ortiz, A.; Weiner, A. L.; Zhang, S.; Kovacs, Z.; Kodadek, T.; Sherry, A. D. *J. Am. Chem. Soc.* **2002**, *124*, 3514-3515.

(113) Croisille, P.; Revel, D.; Saeed, M. *Eur Radiol* **2006**, *16*, 1951-1963.

(114) Bleaney, B. *Appl. Magn. Reson.* **1999**, *16*, 19-22.

(115) Qin, P. Z.; Dieckmann, T. *Curr. Opin. Struct. Biol.* **2004**, *14*, 350-359.

(116) Hunsicker-Wang, L.; Vogt, M.; DeRose, V. J. *Methods Enzymol.* **2009**, *468*, 335-367.

(117) Pilbrow, J. R.; Hanson, G. R. *Methods Enzymol.* **1993**, *227*, 330-53.

(118) Huttermann, J. *Electron Spin Reson.* **1996**, *15*, 59-111.

(119) Huttermann, J.; Kappl, R. *Electron Paramagn. Reson.* **1998**, *16*, 145-198.

(120) Knobloch, B.; Linert, W.; Sigel, H. *Proc. Natl. Acad. Sci. U.S.A.* **2005**, *102*, 7459-7464.

(121) Hoogstraten, C. G.; Grant, C. V.; Horton, T. E.; DeRose, V. J.; Britt, R. D. *J. Am. Chem. Soc.* **2002**, *124*, 834-842.

(122) Morrissey, S. R.; Horton, T. E.; DeRose, V. J. *J. Am. Chem. Soc.* **2000**, *122*, 3473-3481.

Chapter 2 Smart T1-weighted MRI contrast agents based on DNAzyme and aptamer for the detections uranyl cation and adenosine

2.1 Introduction

MRI contrast agents are chemicals that enhance the contrast on MRI images.[1-4] As the MRI contrast corresponds to the magnetic relaxation of water protons, MRI contrast agents decrease the longitude relaxation time (T1) of water protons. [1,2,5] Among the contrast agents, gadolinium compounds are the most widely used T1-weighted contrast agents because of the unpaired electrons of Gd (III).[1,2] Due to the toxicity of Gd^{3+}, gadolinium chelates such as gadolinium-tetraazacyclododecane-*N*,*N'*,*N''*,*N'''*-tetraacetic acid (DOTA-Gd) are usually used clinically.[6,7]

A smart contrast agent is a combination of a sensor and an MRI contrast agent, which responds to the presence of analytes by a change of the relaxivity and thus a contrast change on an MRI image.[8,9] Meade and coworkers pioneered this area by developing a contrast agent for the sensing of Ca^{2+}.[10,11] So far, the T1-weighted smart contrast agents have been developed for the recognitions of Ca^{2+},[10,11] Zn^{2+},[12,13] protons (pH),[14,15] Cu^{2+},[16] lactate[17] as well as peptides[18] and proteins[19-21] such as β-glucuronidase[22] and Gal-80.[18] Smart contrast agents have been even utilized to monitor enzymatic activity *in vivo*.[23-26] However, very few smart contrast agents are available and the rational design of smart contrast agents with high specificity remains a challenge because the design

requires the detailed information of the interaction between gadolinium compounds and the target. In this chapter, the first rational design of smart T1-weighted MRI contrast agents is presented, which are based on functional DNA. The 39E DNAzyme and adenosine aptamer were used to demonstrate the concept.

2.1.1 Adenosine aptamer and 39E DNAzyme

39E is a DNAzyme or deoxyribozyme with nuclease activity.[27,28] It is able to catalyze the hydrolysis of the substrate strand, 39S, which is a DNA/RNA chimeric strand, in the presence of the uranyl cation. The secondary structure of the 39E/39S is shown in Figure 1.2. The function of uranyl cation is unique and essential. Without the presence of uranyl, or with the presence of other metal cations, 39E is not catalytic active.

39E was also isolated through *in vitro* selection. The DNAzyme has highest activity at pH 5.5. The kinetics assay indicated a high binding affinity between UO^{2+} and the DNAzyme, with the dissociation constant to be 463 nM. 39E has been developed into fluorescent and colorimetric sensors;[27,29] the lowest detection limit was reported to be 45 pM.

The DNA aptamer for adenosine was isolated by Szostak and co-workers in 1995 by *in vitro* selection.[30] The dissociation constant was reported to be 6 μM. The adenosine aptamer has been widely used to prove the concepts of the novel designs of aptamer-based sensors.[31-38] Although the crystal structure of the aptamer has not been resolved, a great deal is known about the behavior of the adenosine aptamer.

2.1.2 Smart MRI contrast agents

As discussed above, smart MRI contrast agents are the combination of MRI contrast agent and sensor.[39,40] They have switchable relaxivity in response to the presence of the molecules of interest (analyte).

One of the earliest smart MRI contrast agents was invented in 1999 for the recognition of Ca^{2+}.[10,11] As shown in Figure 2.1A, the contrast agent is composed of two modules, DOTA-Gd and the Ca^{2+} binding module. The Ca^{2+} binding module has four carboxyl groups; without the presence of Ca^{2+}, the carboxyl groups bind to DOTA-Gd. The addition of Ca^{2+} switches the conformation of the contrast agent. As a result, the carboxyl groups bind to Ca^{2+} (Figure 2.1A). The vacancies for Gd^{3+} binding are then filled by water molecules. The hydration number is then switched from 0 to 1 and thus an increase in the relaxivity can be detected.

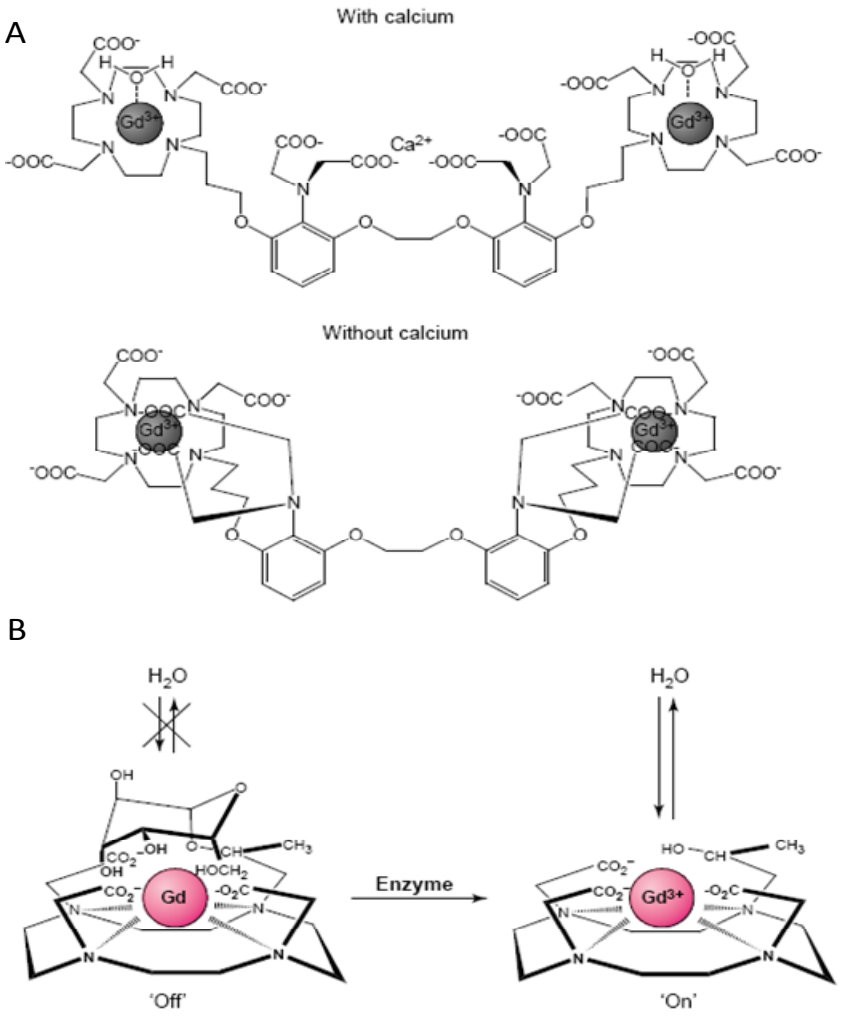

Figure 2.1 Smart MRI contrast agents for the sensing of Ca^{2+} (A) and β-galactosidase (B)

The same design can be applied to smart contrast agents for the sensing of other metal cations, such as Zn^{2+} [12,13] and Cu^{2+}.[16] The critical step of the design is to find an analyte-binding module that can introduce the conformational change. In addition, the binding event should be selective to exclude false positive response. Because of the difficulties, very few cations can be monitored by smart MRI contrast agents.

Smart MRI contrast agent can also be used to monitor the enzymatic activity.[22] Meade and co-workers synthesized a DOTA-Gd derivative for the purpose (Figure 2.1B). The water binding position was blocked by the galactopyranose residue, which was so bulky that water can not bind to Gd^{3+}. The saccharide residue can be removed by the presence of β-galactosidase (β-gal) and water can then bind to the gadolinium compound. The resulting increase of the hydration number leads to an increase of the relaxivity, and therefore the enhancement of the contrast on an MRI image.

The regulation of the hydration number is straight forward, but not the only option. The Sherry group developed a contrast agent for detection of a protein called Gal80.[18] They successfully synthesized the conjugate of DOTA-Gd and a peptide that binds Gal80 (G80BP). A relaxivity change resulted from binding of the contrast agent to the protein because of the change of the molecular weight and rotation correlation time of the gadolinium compound.

T2-weighted smart MRI contrast agents have also been reported.[41-43] Weissleder detected DNA and other bio-molecules by paramagnetic nanoparticle aggregates whose size can be regulated.[44-48] The method was generalized by Yigit, M. V. et al when an aptamer strand was used as the probe DNA.[49,50] The presence of the target disassembled the nanoparticle aggregates and induced a change of the contrast on an MRI image.

2.1.3 Rational design of the smart MRI contrast agents based on DNAzyme and DNA aptamer

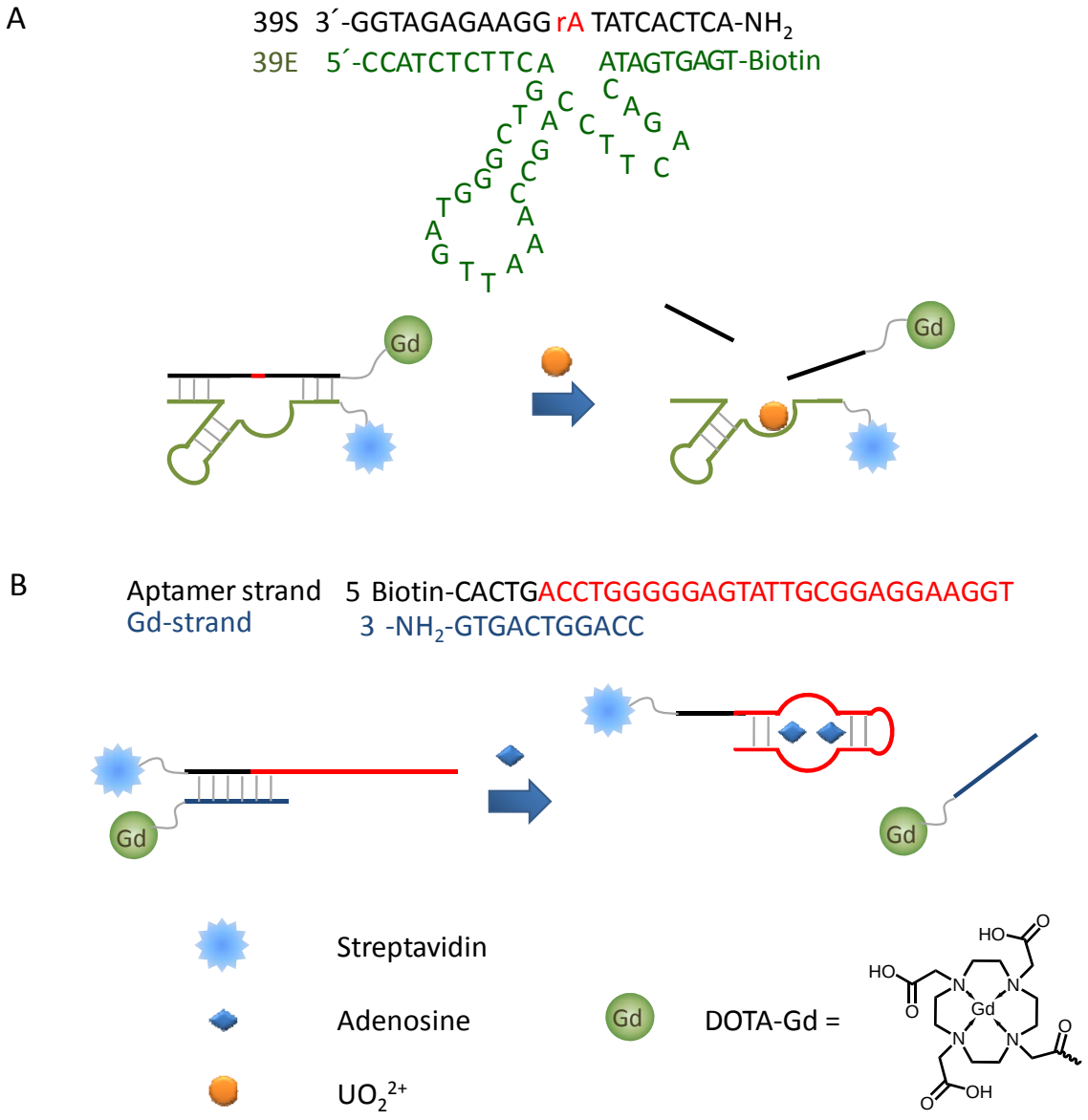

Figure 2.2 Schematic of the functional DNA-based smart MRI contrast agents for the sensing of uranyl cation (A) and adenosine (B)

It is desired to transform the cleavage of the substrate strand (39S) catalyzed by 39E with the presence of UO_2^{2+} and the binding of adenosine aptamer to the adenosine into contrast changes on MRI images. Solomon-Bloembergen-Morgan theory predicts that the relaxivity of the gadolinium compound is regulated by the rotation correlation time. Larger molecules have longer rotation correlation time. Thus, changing the size of the gadolinium compound leads to a change of its relaxivity and therefore contrast of the MRI image. The rational design of functional DNA-based smart contrast agents is then based on the change of the size or molecular weight of the gadolinium compounds upon interaction with the target.

The design of the 39E-based smart contrast agent is shown in Figure 2.2A. The enzymatic strand (in green) has a 3′-biotin modification, which is then coupled to streptavidin. DOTA-Gd was conjugated to the 5′ end of the substrate strand – 39S (in black). In solution, these two strands are hybridized and form a stable structure. With UO_2^{2+} present, 39S is cleaved; the cleaved product dissociates from the enzyme strand and streptavidin. The relaxivity of the gadolinium compound is then changed, leading to a contrast change on an MRI image.

As shown in Figure 2.2B, the contrast agent for sensing adenosine has two DNA strands – the extended aptamer strand (aptamer strand) in black and red and Gd-strand in brown which is partially complimentary to the aptamer strand. The aptamer strand (in red) is biotylated and conjugated to streptavidin. The Gd-strand is conjugated to DOTA-Gd through NHS chemistry. As these two strands are hybridized in solution, the rotation correlation time of the Gd-strand is increased (with a molecular weight of about 70 kDa). Adenosine addition results in the structure switching and dissociation of the Gd-strand. In

the process, the molecular weight of the Gd compound is decreased to about 4 kDa. The T1 of water protons will increase, resulting in contrast changes on an MRI image as a result.

2.2 Experimental

2.2.1 Materials, equipment and DNA sequences

All DNA molecules with biotin or amine modifications were purchased from Integrated DNA Technologies, Inc. (Coralville, IA). The DNA was standard desalted by the vendor and used without further purification. NHS activated DOTA was purchased from Macrocyclics, Inc. (Dallas, TX). Streptavidin and other chemicals were purchased from Sigma-Aldrich, Inc or Fisher Scientific, Inc.

T1 was measured on a Bruker Minispec mq 60 MRI contrast agent analyzer (1.5 T, Bruker), Varian NMR spectrometer (300 MHz) and 60 MHz - Varian EM360L NMR Spectrometer with Anasazi FT Upgrade. The MRI image was acquired on 1.5 GE Signa Horizon Echo Speed with 9.0 software (1.5 T, GE).

The DNA sequences of the DNA used were obtained from previous reported literatures, and listed in Table 2.1.

Table 2.1 DNA sequences used in this chapter

39E	5′-CCATCTCTTCAGTCGGGTAGTTAAACCGACCTTCAGACATAGTGAGT-biotin
39S	5′-amine-ACTCACTATrAGGAAGAGATGG
Ad-aptamer	5′-biotin-CACTGACCTGGGGGAGTATTGCGGAGGAAGGT
Gd-strand	5′-CCAGGTCAGTG-amine

2.2.2 Synthesis of the DNA-DOTA-Gd conjugates

The conjugation of DOTA-Gd is realized through NHS chemistry. The synthesis process is presented in Figure 2.3.

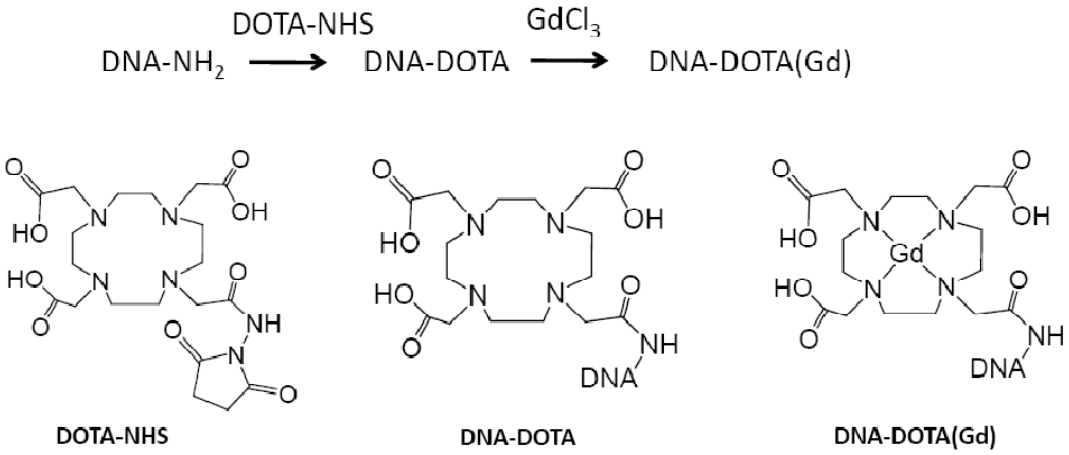

Figure 2.3 Synthesis of the DOTA-Gd conjugated DNA strands

NHS coupling of DOTA to DNA The optimized coupling conditions are described in this section. NHS activated DOTA was dissolved in acetonitrile at a concentration of 0.5 mg/μL. Modified DNA was dissolved in 50 mM carbonate buffer (pH 10) at a concentration of 25 μM. Aliquotes of the NHS-DOTA solution (4 μL) were added into 1 mL DNA solution once per hour for five hours. During the synthesis, the mixture was shaken gently at 4 °C. Shaking was continued for another 3 to 5 hours after the final addition. The product was then desalted on a C-18 cartridge (Sep-Pak, Waters) and checked by MALDI-MS. Typical yield for conjugated DNA with less than 20 bases is 85%-95%.

It is critical to keep the entire synthesis free from the metal contamination as DOTA is a strong chelator for almost all metal cations. If the contamination of metal cations, such as Zn^{2+}, Cu^{2+} and Fe^{2+} occurs, it is difficult incorporate Gd^{3+} due to both kinetic and thermodynamic issues.

Incorporation of Gd into DNA-DOTA conjugates The DOTA conjugated DNA was dissolved in 50 mM acetate buffer (pH 5.55) at a concentration of 150 μM; $GdCl_3$ solution (10 mM) was added until the concentration reached 180 μM. $GdCl_3$ and DNA-DOTA solutions should be mixed slowly and evenly to avoid the precipitation. The solution was then kept at 75 °C for 30-45 min and the final product was purified by size exclusion chromatography (PD10, GE Health Care Life Sciences). The incorporation yield was 100%.

The product cannot be purified by any reverse phase chromatography purification method as it has a strong affinity towards C18. Reverse phase HPLC and C18 affinity cartridge should be avoided for the purification.

2.2.3 T1 measurement and MRI image acquisition

Sample preparations 39E-based contrast agent was prepared by dissolving the DOTA-Gd coupled 39S and biotinylated 39E in 50 mM MES-Na (pH 5.5) buffer at a concentration of 30 μM. The solution was heated to 90 °C and cooled to ambient temperature over one hour. Streptavidin was then added into the solution at a concentration of 30 μM. Uranyl acetate (UO_2OAc_2) was added into the solution to reach various concentrations. EDTA (100 μM) was used to stop the reaction after 30 minutes. The sample was then subjected to T1 measurement.

Adenosine aptamer-based contrast agent was prepared by dissolving the DOTA-Gd coupled Gd-strand and aptamer strand in 50 mM Tris (pH 8.35), 300 mM NaCl and 5 mM $MgCl_2$ buffer at a concentration of 30 μM. The solution was heated to 90 °C and cooled to ambient temperature over one hour. Streptavidin was then added into the

solution at final concentration of 30 μM. Adenosine was added into the contrast agent solutions followed by T1 measurement.

T1 measurement on Bruker Minispec relaxometer A Bruker Minispec mq 60 MRI contrast agent analyzer (1.5 T, Bruker) was used to measure the longitude relaxation time of water protons. The temperature was kept at 37 ˚C during all T1 measurements. The parameters of the method are summarized in Table 2.2.

Table 2.2 Parameters for the T1 measurements

First Duration	Last Duration	Data points	Duration Factor	Total Analysis	Del. Sam. Win.	Sam. Win.	Expon. Order
150 ms	15 s	10	1.668	12.58 min	0.03 ms	0.03 s	1

MRI image acquisition The Gd-strand (30 μM) and aptamer strand were dissolved in 50 mM Tris (pH 8.35), 300 mM NaCl and 5 mM $MgCl_2$ buffer. The solution was heated to 90 °C and cooled to ambient temperature over one hour. Streptavidin was added into the solution at a concentration of 30 μM. Adenosine (5 mM) added into the solution as sample volume of 500 μL samples was used in the image acquisition. MRI image was

acquired at ambient temperature. The reverse and echo time were 400 ms and 14 ms, respectively.

2.3 Results and discussion

2.3.1 Synthesis of the DOTA-Gd conjugated DNA

Although in the literature it was reported that neutral solution is the optimized condition for coupling through NHS chemistry,[51,52] the incubation of amine modified DNA with the NHS ester did not lead to any reaction. The reason lies in the pK_a of the amine group. The coupling reaction takes place by the nucleophilic attack of the amine group on the nitrogen atom of the NHS ester. The active species are the amine group (-NH_2), not the protonated amine group (-NH^{3+}).

Table 2.3 pKa of alkyl amines

Name	**Molecular formula**	**pKa**
Methylamine	CH_3-NH_2	10.63
Ethylamine	C_2H_5-NH_2	10.70

Table 2.3 (cont.)

Propylamine	C_3H_7-NH_2	10.60
Butylamine	C_4H_9-NH_2	10.77
Pentanamine	C_5H_{11}-NH_2	10.59
Hexylamine	C_6H_{13}-NH_2	10.56

For the DNA coupling presented in Figure 2.3, it is important to calculate the minimum pH value when non-protonated amine group dominates. The pK_a of the amine group modified at the termini of DNA was not reported. As there is C_6H_{12} spacer between DNA and the amine group, it is reasonable to use the pKa values of the aliphatic amines. As shown in Table 2.3, they are about 10.6. Thus, it is concluded that at neutral pH, inactive protonated species dominate. Therefore pH 10 was selected for the reaction to minimize the protonated amine species.

It is noted that the yield of the coupling of DOTA to DNA is sequence dependent. The yield reached 90% with a sequence length less than 20 bases; it decreased dramatically when the DNA is longer. For example, the coupling reaction of 17E, which has 34 bases, had yield lower than 10%. This phenomenon is ascribed to the fact that bases on the DNA strands can catalyze the hydrolysis of the NHS-ester. It has been reported that the NHS coupling reaction not only happened to aliphatic amines, but also

amine on the DNA bases.[53] However, the conjugate on nucleobases is not stable, which leads to a spontaneous hydrolysis reaction. Therefore, DNA performs as a catalyst which accelerates the hydrolysis of the NHS ester, resulting in the decrease of the effective concentration of the active NHS ester.

The traditional method for Gd incorporation, during which $Gd(OH)_3$ and DOTA are kept at high temperature, was shown to be an inappropriate choice. The $Gd(OH)_3$ solid can adsorb DNA molecules due to electrostatic interaction. Another difficulty of the incorporation is that Gd^{3+} binds to the phosphate backbone of DNA, leading to the precipitation of DNA molecules.

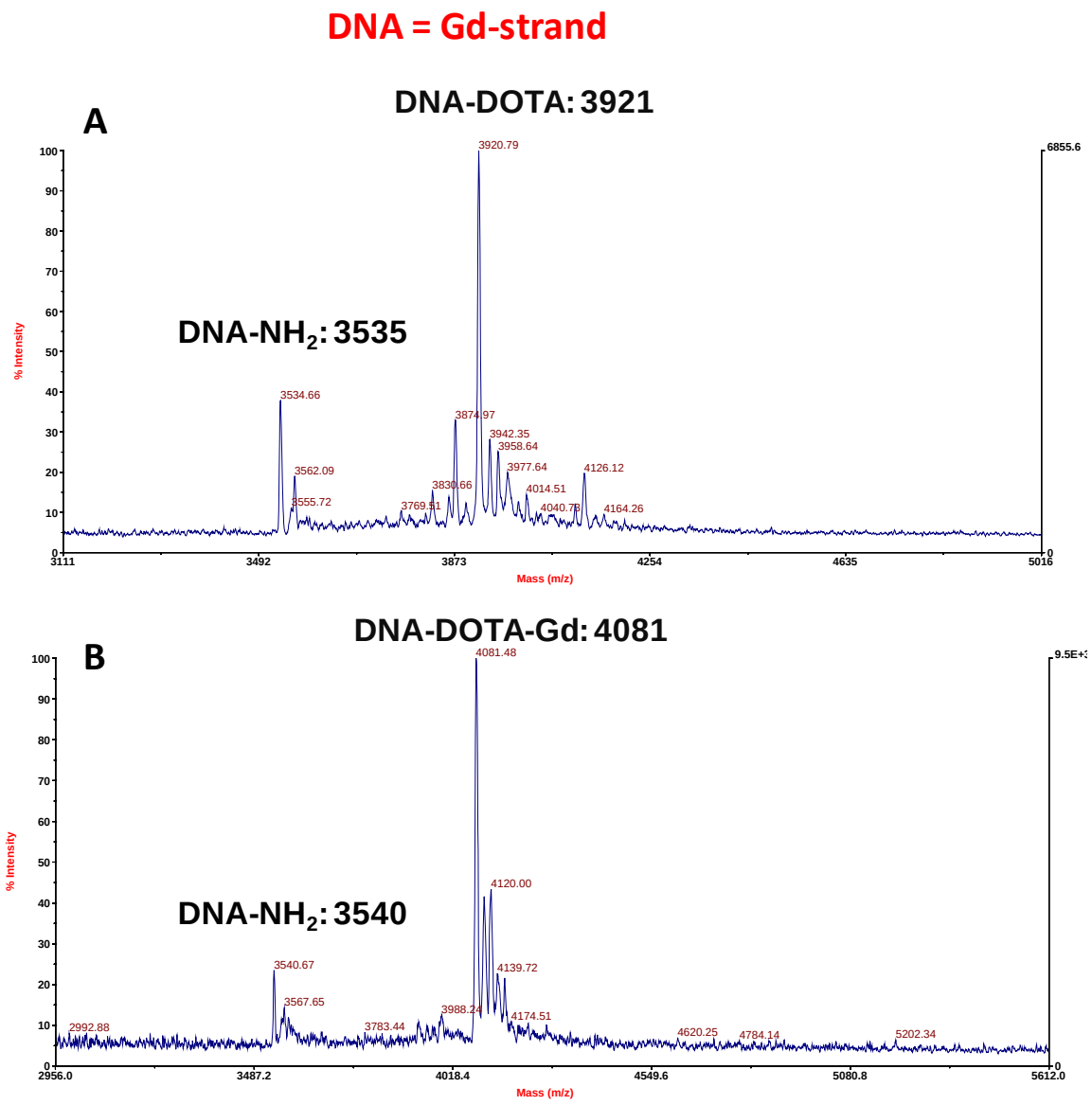

Figure 2.4 MS of the product after the coupling of DOTA (A) and the incorporation of Gd^{3+} (B)

To avoid the precipitation, the buffer should contain a ligand that binds Gd^{3+}. The affinity between buffer and Gd^{3+} should be lower than the affinity between $Gd^{3+}$and DOTA to ensure incorporation. It was found that acetate buffer, pH 5.5, was the appropriate media. Heating to 75 ˚C was used to facilitate the reaction.

The mass spectrum of the product of the first step is shown in Figure 2.4A. There are two major peaks. The peak at 3534.7 is assigned unreacted Gd-strand and the peak at 3920.8 is assigned to the DOTA coupled Gd-strand. The molecular weight difference of the two species (381.1) is consistent with the addition of DOTA.

Figure 2.4B shows the MS of the DNA sample after the incorporation of gadolinium to the DOTA conjugated Gd-strand. The peak of 3540 is ascribed to unconjugated Gd-strand and the major peak with m/z of 4081 is ascribed to the DNA strand with DOTA-Gd conjugation. The difference of the molecular weight (540.81) is consistent with what is calculated (540).

2.3.2 Activity of 39E under experimental conditions

To our knowledge, the activity of 39E has not been reported at the high concentration (30 μM). Streptavidin binds to uranyl non-specifically, which might lead to the decrease of the activity. To test the activity of 39E under current experimental conditions, 30 μM 39E and carboxyfluorecein labeled 39S was incubated with various concentrations of uranyl cation for 30 min. The reaction was quenched upon the addition of 8M urea and 100 mM EDTA and the product was analyzed by denaturing gel electrophoresis. The results are presented in Figure 2.5.

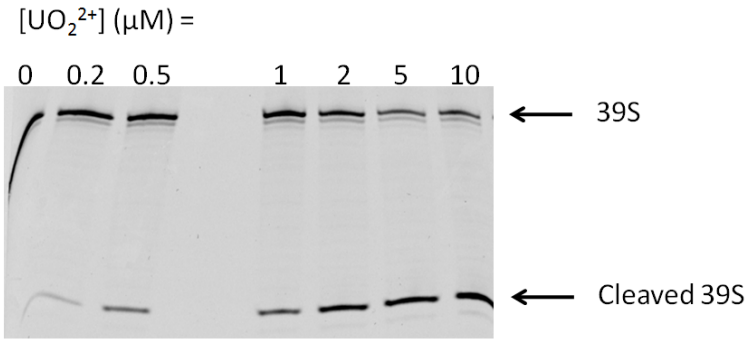

Figure 2.5 Activity assay of 30 μM 39E DNAzyme with the presence of 30 μM streptavidin

In the presence of 0.5 μM uranyl, around 20% 39S was cleaved. With 10 μM uranyl the cleavage percentage is about 65%. Compared to literature, the activity of 39E is significantly decreased by the presence of streptavidin.[28] Though the high concentration of DNA increased the absolute value of the reaction rate, the cleavage percentage is decreased.

2.3.3 T1 Response of the 39E-based contrast agent

The idea to regulate the longitude relaxation time of the water proton through regulating the size of the contrast agent was applied to the 39E DNAzyme. The smart MRI contrast agent for the sensing of uranyl cation was dissolved in 50 mM MES-Na buffer with a concentration of 30 μM. Metal cations (2 μM) were added into the solution and T1 was measured after overnight incubation.

Concentration-dependent T1 response towards the uranyl cation As shown in Figure 2.6, it was observed that T1 increased from 1.5 s to almost 2 s. The T1 change

reached saturation at 2 μM uranyl cation. However, the linearity between T1 and the concentration of the uranyl cation was poor, but the quantification of the uranyl concentration is still possible.

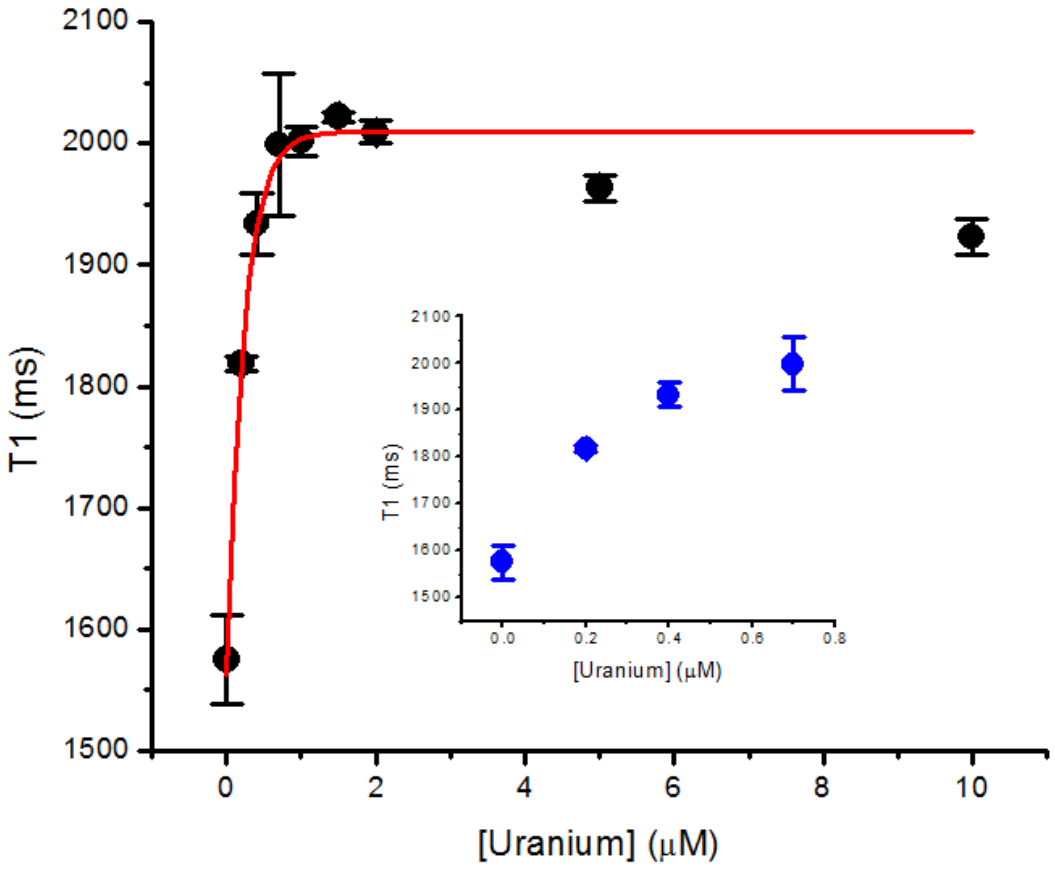

Figure 2.6 T1 response of the 39E-based contrast agent to the uranyl cation at various concentrations

T1 change with the presence of metal cations The T1 responses to 10 μM various metal ions, including UO_2^{2+}, Cd^{2+}, Hg^{2+}, Pb^{2+} and Zn^{2+}, are presented in Figure 2.7. As indicated in the figure, only the addition of UO_2^{2+} introduced 0.35 s increase for T1. The cleavage of 39S happened when uranyl cation was present and was detected by T1

measurement. Without the uranyl cation, or with other metal cations, no significant T1 change was observed.

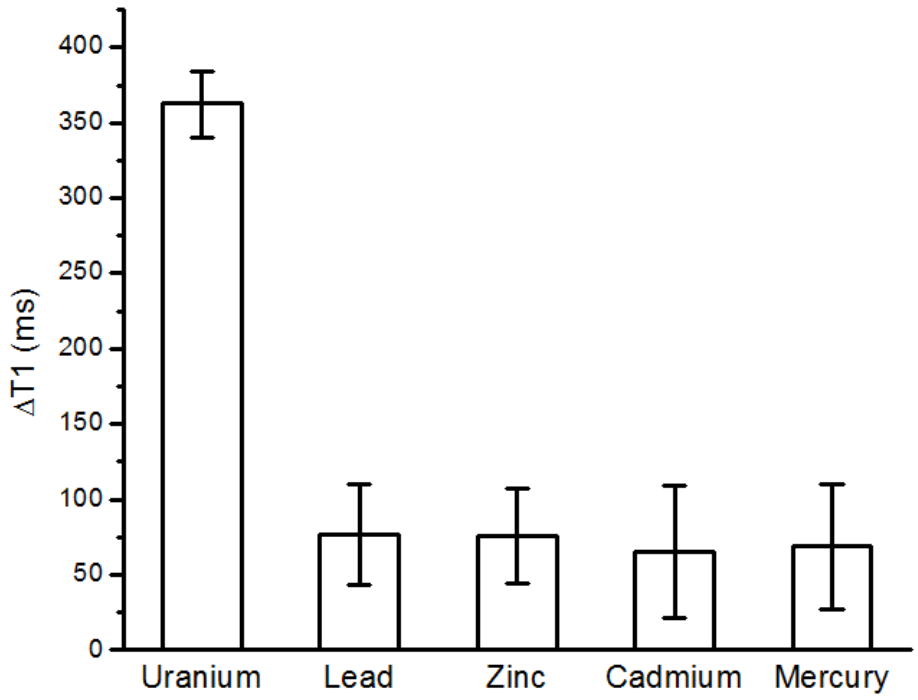

Figure 2.7 The T1 responses of the 39E-based smart MRI contrast agents towards various divalent cations

2.3.4 T1 Response of the adenosine aptamer-based contrast agent

To confirm the adenosine sensing process shown in Figure 2.2, 30 μM of both DNA strands (including the biotinylated aptamer strand and DOTA-Gd conjugated Gd-strand) were dissolved in buffer with 30 μM streptavidin. Adenosine was added to the solution to reach various concentrations. T1 measurement was carried on after more than 30 min.

T1 responses with various concentrations of adenosine As shown in Figure 2.8, it was found that T1 increased from 1.43 s to 1.59 s when 0.5 mM adenosine was present. With an increase of adenosine concentration, T1 increased to 1.87 s when the concentration of adenosine was 5 mM. Adenosine concentration higher than 5 mM was not measured due to the poor solubility of adenosine. With 5 mM adenosine, around 35% decrease of relaxivity was observed.

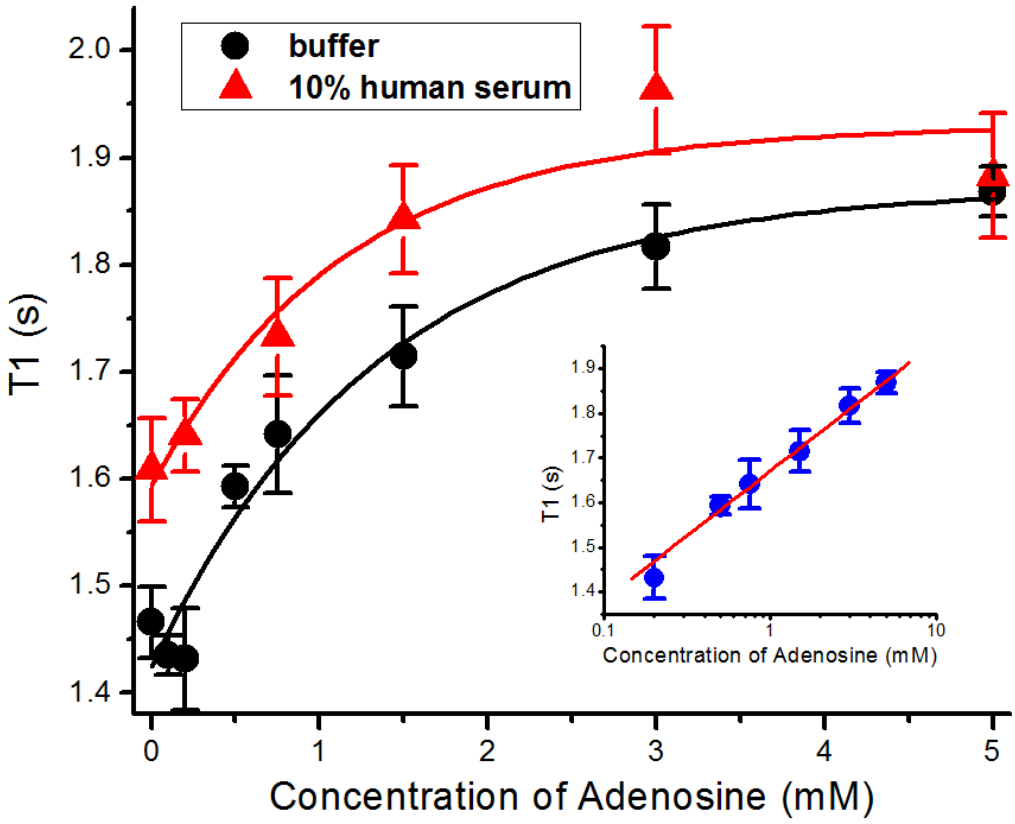

Figure 2.8 T1 response of the smart MRI contrast agent based on the adenosine aptamer in buffer (black) and 10% human serum (red). The inset presents the T1 response versus logarithm of the concentrations in buffer.

We also observed a linear relationship between T1 and the logarithm of adenosine concentration (inset of Figure 2.8). This linearity makes the semi-quantitative detection of adenosine feasible.

In order to obtain the theoretical maximum signal increase, we dissolved 30 μM DOTA-Gd coupled Gd-strand and 30 μM streptavidin in buffer. Without the presence of the biotinylated aptamer strand, DOTA-Gd was not associated with streptavidin. It simulated the case when the Gd-strand was completely dissociated. T1 of the solution was 2.18 s. Not surprisingly, T1 response to adenosine did not exceed the limit, which indicated that the T1 response was from the structure switching.

The concentration of streptavidin was varied. Without streptavidin, less than 0.1 s T1 increase was observed even with 5 mM adenosine (Figure 2.9A). The presence of 10 μM streptavidin significantly enhanced T1 response to adenosine. The T1 response to 5 mM adneosine reached maximum upon the presence of 20 μM or 30 μM streptavidin. This might be due to multiple biotin binding sites on streptavidin resulting in binding of multiple DNA strands. Streptavidin is necessary for the contrast agent to function. This is evidence that the T1 response observed is due to behavior of the system as displayed in Figure 2.2.

Performance of the contrast agent responses in human serum To test the performance of the contrast agent in human serum, the T1 response was measured in 10% human serum with various concentrations of adenosine. The results are plotted in Figure 2.8 (red trace).

It was observed that T1 increased from 1.61 s when adenosine was absent to 1.96 s with 3 mM adenosine. The contrast agent still responded to the presence of adenosine, even with human serum. However, it is worth noting that the contrast agent in human serum has a longer T1. This is probably because of the interaction of Gd compounds to the proteins in serum, such as albumin with a result of decreased hydration number. However, it did not affect the sensing *in vivo*.

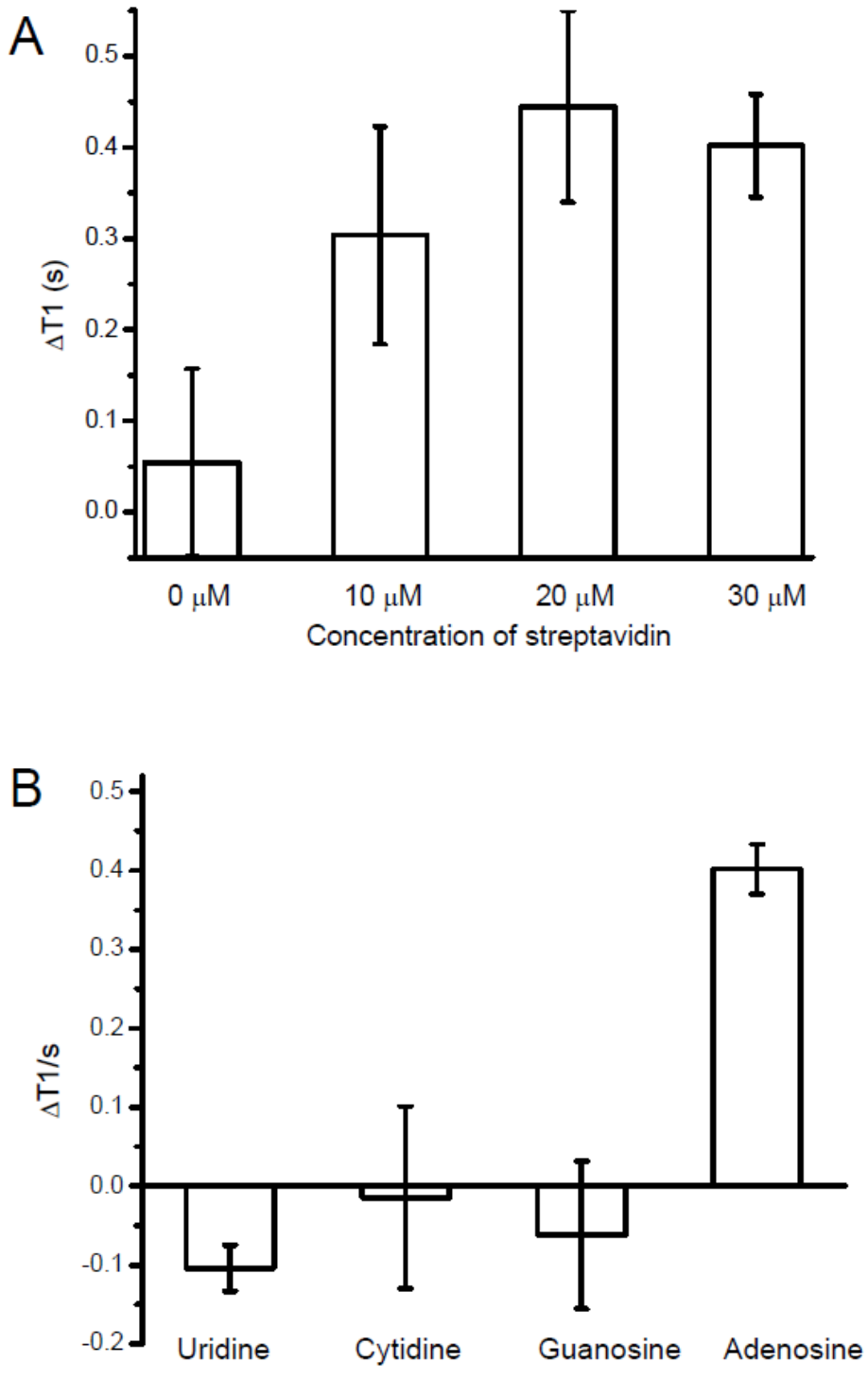

Figure 2.9 (A) Streptavidin dependence the performance of the contrast agent, without which no T1 response can be observed. (B) Selectivity of the smart MRI contrast agent.

Selectivity of the contrast agent The T1 response of water protons induced by nucleosides other than adenosine was measured. The results are presented in Figure 2.9B. Different from adenosine, cytidine, guanosine or uridine did not increase T1. This is because the adenosine aptamer is specific; the Gd-strand was not released and almost no T1 change was observed. It was noted that the contrast agent had a slight negative T1 response, ascribed to the viscosity change of the solution. Pyrimidine or purine at concentrations of 5 mM thickens the solution, leading to a longer rotation correlation time and drop of T1. The selectivity of the adenosine aptamer was inherited by the MRI contrast agent herein, which makes the differentiation of adenosine from other molecules with similar structure possible.

2.3.5 *In vitro* MRI image change induced by adenosine

An MRI image was acquired on a clinical MRI scanner. The image is shown in Figure 2.10. The left and middle samples are the contrast agent before and after addition of adenosine, respectively. As the T1 of the system increased after addition of adenosine, the sample showed a 25% contrast decrease with the presence of adenosine. The right sample contained only streptavidin and Gd-strand to simulate 100% released Gd-strand. As expected, the contrast of the left sample is brighter than the middle and right ones. The image shows that although T1 increased around 30% with the presence of adenosine, the contrast agents can give a significant contrast change on an MRI image.

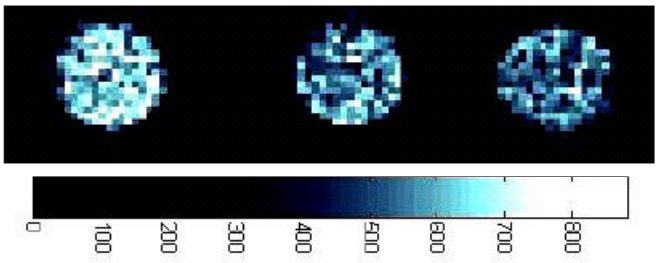

Figure 2.10 in vitro MRI images of the adenosine aptamer-based contrast agent without (left) and with (middle) the presence of 5 mM adenosine. The right sample is the positive control to simulate 100% release of the Gd-strand.

2.4 Conclusion, perspectives and future direction

In conclusion, we designed and realized a smart T1-weighted MRI contrast agent based on DNAzyme and DNA aptamer. The 39E DNAzyme and adenosine aptamer were utilized in the contrast agent designs. The 39E DNAzyme-based contrast agent changed T1 only in the presence of uranyl cations. The adenosine aptamer-based contrast agent provided T1 increase in response to more than 0.5 mM adenosine. The T1 response was also observed in human serum. Both contrast agents have outstanding selectivity. The MRI image was acquired *in vitro* and a contrast change was observed with adenosine. The design of the contrast agent can be applied to other DNA or RNA aptamers and it opens a door to design smart MRI contrast agents rationally. However, the contrast agent is a "turn-off" sensor, which causes potential problems for *in vivo* application; the work presented is a first-step in this area.

It is worthwhile to point out the direction of the research of the MRI contrast agents presented herein. First of all, streptavidin is expensive and not present *in vivo*. To decrease the cost, other proteins with high abundance is preferred. Thus, the next

generation of the contrast agents should avoid streptavidin. Proteins abundant in human body, such as albumin, should be used instead. Besides, the turn-on contrast response to the analytes is preferred because it excludes artifacts. Thus, research on turning on the contrast upon the presence of the analytes should be focused.

2.5 References

(1) Caravan, P.; Ellison, J. J.; McMurry, T. J.; Lauffer, R. B. *Chem. Rev.* **1999**, *99*, 2293-2352.

(2) Kumar, K.; Tweedle, M. F. *Pure Appl. Chem.* **1993**, *65*, 515-520.

(3) Zhang, Z.; Nair, S. A.; McMurry, T. J. *Curr. Med. Chem.* **2005**, *12*, 751-778.

(4) Carr, D. H.; Brown, J.; Bydder, G. M.; Steiner, R. E.; Weinmann, H. J.; Speck, U.; Hall, A. S.; Young, I. R. *Am. J. Roentgenol.* **1984**, *143*, 215-224.

(5) Shapiro, M. G.; Atanasijevic, T.; Faas, H.; Westmeyer, G. G.; Jasanoff, A. *Magn. Reson. Imaging* **2006**, *24*, 449-462.

(6) Li, M.; Meares, C. F. *Bioconjugate Chem.* **1993**, *4*, 275-283.

(7) Gries, H. *Top. Curr. Chem.* **2002**, *221*, 1-24.

(8) Allen, M. J.; Meade, T. J. *Met. Ions Biol. Syst.* **2004**, *42*, 1-38.

(9) Meade, T. J.; Taylor, A. K.; Bull, S. R. *Curr. Opin. Neurobiol.* **2003**, *13*, 597-602.

(10) Li, W.-h.; Fraser, S. E.; Meade, T. J. *J. Am. Chem. Soc.* **1999**, *121*, 1413-1414.

(11) Li, W.-h.; Parigi, G.; Fragai, M.; Luchinat, C.; Meade, T. J. *Inorg. Chem.* **2002**, *41*, 4018-4024.

(12) Hanaoka, K.; Kikuchi, K.; Urano, Y.; Nagano, T. *J. Chem. Soc. Perkin Trans.* **2001**, 1840-1843.

(13) Hanaoka, K.; Kikuchi, K.; Urano, Y.; Narazaki, M.; Yokawa, T.; Sakamoto, S.; Yamaguchi, K.; Nagano, T. *Chem. Biol.* **2002**, *9*, 1027-1032.

(14) Raghunand, N.; Howison, C.; Sherry, A. D.; Zhang, S.; Gillies, R. J. *Magn. Reson. Med.* **2003**, *49*, 249-257.

(15) Zhang, S.; Wu, K.; Sherry, A. D. *Angew. Chem., Int. Ed.* **1999**, *38*, 3192-3194.

(16) Que, E. L.; Chang, C. J. *J. Am. Chem. Soc.* **2006**, *128*, 15942-15943.

(17) Aime, S.; Delli Castelli, D.; Fedeli, F.; Terreno, E. *J. Am. Chem. Soc.* **2002**, *124*, 9364-9365.

(18) De Leon-Rodriguez, L. M.; Ortiz, A.; Weiner, A. L.; Zhang, S.; Kovacs, Z.; Kodadek, T.; Sherry, A. D. *J. Am. Chem. Soc.* **2002**, *124*, 3514-3515.

(19) Nivorozhkin, A. L.; Kolodziej, A. F.; Caravan, P.; Greenfield, M. T.; Lauffer, R. B.; McMurry, T. J. *Angew. Chem., Int. Ed.* **2001**, *40*, 2903-2906.

(20) Caravan, P.; Cloutier, N. J.; Greenfield, M. T.; McDermid, S. A.; Dunham, S. U.; Bulte, J. W. M.; Amedio, J. C., Jr.; Looby, R. J.; Supkowski, R. M.; Horrocks, W. D., Jr.; McMurry, T. J.; Lauffer, R. B. *J. Am. Chem. Soc.* **2002**, *124*, 3152-3162.

(21) Bull, S. R.; Guler, M. O.; Bras, R. E.; Venkatasubramanian, P. N.; Stupp, S. I.; Meade, T. J. *Bioconjugate Chem.* **2005**, *16*, 1343-1348.

(22) Louie, A. Y.; Meade, T. J. *New Technologies for Life Sciences: A Trends Guide* **2000**, 7-11.

(23) Allen, M. J.; MacRenaris, K. W.; Venkatasubramanian, P. N.; Meade, T. J. *Chem. Biol.* **2004**, *11*, 301-307.

(24) Gilad, A. A.; McMahon, M. T.; Walczak, P.; Jr, P. T. W.; Raman, V.; Laarhoven, H. W. M. v.; Skoglund, C. M.; Bulte, J. W. M.; Peter, C. M. v. Z. *Nat. Biotechnol.* **2007**, *25*, 217-219.

(25) Croisille, P.; Revel, D.; Saeed, M. *Eur Radiol* **2006**, *16*, 1951-1963.

(26) Allen, M. J.; Meade, T. J. *J. Biol. Inorg. Chem.* **2003**, *8*, 746-750.

(27) Liu, J.; Brown, A. K.; Meng, X.; Cropek, D. M.; Istok, J. D.; Watson, D. B.; Lu, Y. *Proc. Natl. Acad. Sci. U.S.A.* **2007**, *104*, 2056-2061.

(28) Brown, A. K.; Liu, J.; He, Y.; Lu, Y. *ChemBioChem* **2009**, *10*, 486-492.

(29) Lee, J. H.; Wang, Z.; Liu, J.; Lu, Y. *J. Am. Chem. Soc.* **2008**, *130*, 14217-14226.

(30) Huizenga, D. E.; Szostak, J. W. *Biochemistry* **1995**, *34*, 656-665.

(31) Nutiu, R.; Li, Y. *J. Am. Chem. Soc.* **2003**, *125*, 4771-4778.

(32) Liu, J.; Lu, Y. *Angew. Chem., Int. Ed.* **2006**, *45*, 90-94.

(33) Xiang, Y.; Tong, A.; Lu, Y. *J. Am. Chem. Soc.* **2009**, *131*, 15352-15357.

(34) Xu, W.; Lu, Y. *Anal. Chem.* **2009**.

(35) Nutiu, R.; Li, Y. *Chem. Eur. J.* **2004**, *10*, 1868-1876.

(36) Nutiu, R.; Mei, S.; Liu, Z.; Li, Y. *Pure Appl. Chem.* **2004**, *76*, 1547-1561.

(37) Nutiu, R.; Yu, J. M. Y.; Li, Y. *ChemBioChem* **2004**, *5*, 1139-1144.

(38) Nutiu, R.; Li, Y. *Angew. Chem., Int. Ed.* **2005**, *44*, 1061-1065.

(39) Sosnovik, D. E.; Weissleder, R. *Curr. Opin. Biotechnol.* **2007**, *18*, 4-10.

(40) Lowe, M. P. *Curr. Pharm. Biotechnol.* **2004**, *5*, 519-528.

(41) Josephson, L.; Lewis, J.; Jacobs, P.; Hahn, P. F.; Stark, D. D. *Magn. Reson. Imaging* **1988**, *6*, 647-653.

(42) Shen, T.; Weissleder, R.; Papisov, M.; Bogdanov, A., Jr.; Brady, T. J. *Magn. Reson. Med.* **1993**, *29*, 599-604.

(43) Moore, A.; Marecos, E.; Bogdanov, A., Jr.; Weissleder, R. *Radiology* **2000**, *214*, 568-574.

(44) Hoegemann, D.; Ntziachristos, V.; Josephson, L.; Weissleder, R. *Bioconjugate Chem.* **2002**, *13*, 116-121.

(45) Perez, J. M.; Josephson, L.; Weissleder, R. *ChemBioChem* **2004**, *5*, 261-264.

(46) Zhao, M.; Josephson, L.; Tang, Y.; Weissleder, R. *Angew. Chem., Int. Ed.* **2003**, *42*, 1375-1378.

(47) Harisinghani, M. G.; Barentsz, J.; Hahn, P. F.; Deserno, W. M.; Tabatabaei, S.; van de Kaa, C. H.; de la, R. J.; Weissleder, R. *New Eng. J. Med.* **2003**, *348*, 2491-2499.

(48) Perez, J. M.; O'Loughin, T.; Simeone, F. J.; Weissleder, R.; Josephson, L. *J. Am. Chem. Soc.* **2002**, *124*, 2856-2857.

(49) Yigit, M. V.; Mazumdar, D.; Kim, H. K.; Lee, J. H.; Odintsov, B.; Lu, Y. *ChemBioChem* **2007**, *8*, 1675-1678.

(50) Yigit, M. V.; Mazumdar, D.; Lu, Y. *Bioconjugate Chem.* **2008**, *19*, 412-417.

(51) Lewis, M. R.; Raubitschek, A.; Shively, J. E. *Bioconjugate Chem.* **1994**, *5*, 565-576.

(52) Lewis, M. R.; Kao, J. Y.; Anderson, A. L.; Shively, J. E.; Raubitschek, A. *Bioconjugate Chem.* **2001**, *12*, 320-324.

(53) Anjaneyulu, P. S. R.; Staros, J. V. *Int. J. Peptide Protein Res.* **1987**, *30*, 117-124.

Chapter 3 Label-free aptamer-based fluorescent sensor by lighting up the fluorescence of malachite green

In this chapter, a novel aptamer based-fluorescent sensor is presented. Different from previously reported designs, the DNA is not labeled with fluorophore and quencher in this work. This work is the basis for a published manuscript Xu, W.; Lu, Y. *Anal. Chem.* 2010, **82**, 574-578

3.1 Introduction

3.1.1 Malachite green and its aptamer

Malachite green (MG) is a widely used dye in industry. The structure of the compound is presented in Figure 3.1. Because of its intense green color, MG has been used to dye silk, leather and paper. MG is considered a Class II Health Hazard as it can intercalate into the DNA duplex and introduce mutations in the DNA, leading to generation of tumors. Therefore, the use of this dye is strictly monitored and regulated.

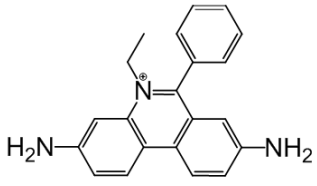

Figure 3.1 Structure of malachite green

Although MG has an intense color, with an extinction coefficient as high as 10^5 $M^{-1}cm^{-1}$ at 621 nm, it is not fluorescent. The deep color indicates that the molecule is able to absorb photons. However, the energy from the photons is not transferred to fluorescent emission. Instead, it is converted to heat because of the flexible σ-bonds.[1,2] The quantum yield of MG was reported to be lower than 10^{-4}.[3]

In 1998, a RNA ligand (RNA aptamer) for malachite green was evolved by Grate et al.[4,5] using SELEX.[6-15] Their initial motivation was to fuse the MG binding site in cellular mRNA. The RNA-MG complex was then hydrolyzed selectively at the binding sites upon exposure to laser. Structural studies were then carried out to characterize the interaction between MG and its RNA ligand.[16,17] An NMR study showed that MG was intercalated between a Watson-Crick base pair and a base quadruple. Both the stacking of aromatic rings and electrostatic interactions accounted for the binding affinity. The binding pocket is small and free vibration is restricted. The study indicated that the fluorescence of MG can be affected upon binding to its RNA aptamer.

3.1.2 Light-up fluorescent sensor using MG

As discussed above, MG is nearly non-fluorescent because of its flexible structure. Thus, if the structure is more rigid, it can be fluorescent – it can absorb photons because of its deep color and the energy relaxation is limited; photon emission then becomes the only option for energy release. The aptamer of MG was evidenced to make the MG molecule more rigid, thus, Tsien and co-workers systematically studied the fluorescence of triphenylmethane dyes, including MG, upon binding to their aptamers.[3] It was discovered that the nearly non-fluorescent dyes became fluorescent. MG has an over 2000-fold increase in quantum yield (from less than 0.0001 to 0.19). It was hypothesized

that the binding of the dye to its target limited its ability to vibrate and rotate at its previously flexible bonds. Thus, as the dye absorbed energy from excitation photons, it emitted it as fluorescence.

The research opened a door for the design of fluorophore/quencher label-free sensors based on functional nucleic acids. The traditional fluorescent sensors regulate the distances between fluorophore and quencher so that the fluorescence can be changed in response to the analytes. These sensors require fluorophore/quencher labeling, which is costly and difficult to store and transport. Moreover, the quencher cannot completely remove the fluorescence of the fluorophore, leading to a relatively high background. If the binding of MG to its aptamer can be regulated by the presence of the analyte, a fluorescence change can then be monitored and the system can be applied as a sensor. Because the fluorescence is from MG, which is not fluorescent naturally, the background is expected to be lower than the labeled rivals. Avoiding fluorescent labeling significantly reduces the cost and difficulties in storage and transportation of the sensor.

3.1.3 MG aptamer-based sensor development

Aptamers have been converted into sensors with high sensitivity and selectivity.[8,18-26] The fluorescent sensors[27-35] are especially interesting because of the feasibility of quantification. However, most fluorescent aptamer-based sensors require fluorophore/quencher labeling, which is not convenient and cost effective as discussed above. Thus, we investigated methods to avoid the covalent labeling of fluorophore using MG and its aptamer as the platform.

Label-free sensors were developed even before the MG aptamer was selected. It was realized by the fluorescence change of the fluorescent dyes upon intercalating into

double strand DNA. Although fluorophore labeling was avoided, most sensors have decreased fluorescent signal upon binding to the analytes. The sensitivity is thus significantly worsened compared to their labeled rivals.[28,36-40]

The first successful trial using MG to realize turn-on sensing was reported by Stojanovic and co-workers.[41,42] They conjugated the MG aptamers and analytes through an engineered "communication module." The aptamer's stem loop (shown in blue in Figure 3.2A) is critical for its affinity for MG, but when the aptamer binds its analyte its conformation changes. As shown in Figure 3.2B, the binding of the analyte (shown as a star) converts the dynamic, flexible structure of the aptamer into a rigid structure. The bases at the 3' and 5' termini hybridize in the presence of the analyte. The researchers combined the two aptamers shown in Figures 3.2A and 3.2B to produce the single structure shown in Figure 3.2C (the blue stems shown in Figures 3.2A and 3.2B are identical and serve as the connection point, or the "communication module"). As shown in Figure 3.2C, the blue stem in the combined structure will not hybridize in the absence of the analyte. Thus, the MG affinity is inhibited. Even with MG (shown as a grey circle) present in solution, no binding occurs and the MG remains non-fluorescent. When the analyte is added, the structure changes its conformation: the blue stem hybridizes, and its affinity for the MG aptamer (in red) is restored. Thus MG binds to its aptamer and increases in fluorescence. In their studies, three targets, adenosine triphosphate (ATP), theophylline, and flavin mononucleotide (FMN) as well as their aptamers were investigated. For the ATP sensor, a 4-5 fold maximum fluorescence increase was observed. An over 10-fold fluorescence increase was realized for the FMN sensor.

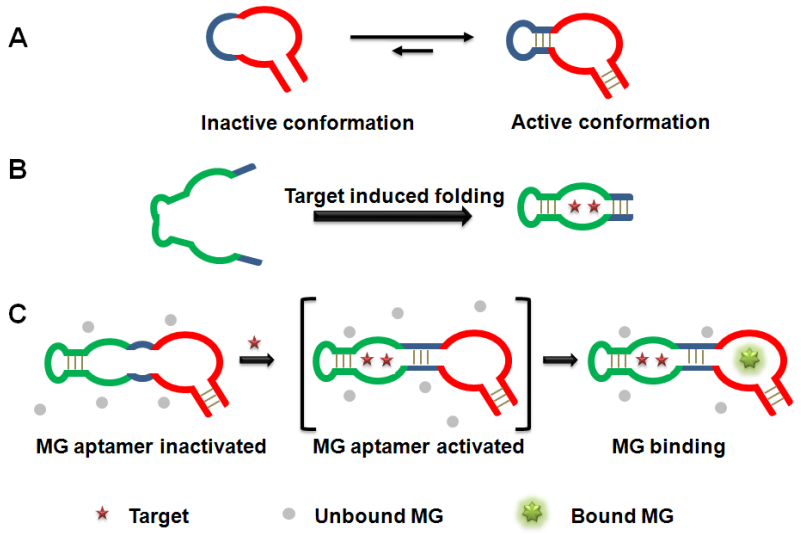

Figure 3.2 (A) The binding affinity of the aptamer is conformation-sensitive; (B) Binding-induced conformational change of the aptamer; (C) Label-free sensor based on MG aptamer

The MG system was also utilized for DNA detection. Kolpashchikov pioneered this area by his work on nucleic acid recognition.[43] As shown in Figure 3.3A, the MG aptamer is split into two subunits. Because the subunits interacted only weakly, they remained separate in solution. Thus, MG was free in solution and had low fluorescence. They designed the sensor by extending the subunits of the MG aptamer (shown in blue in Figure 3.3B). It now performed as a probe for the target DNA, since the target DNA provided extra affinity between the two subunits. Therefore, the two subunits hybridized together when MG and DNA was present. Meanwhile, as MG bound to the aptamer, its fluorescence increased. This system can detect single nucleotide mismatches, a gold-standard for nucleic acid detection methods. Every single mismatch was tried, and 41 out of 42 mutations can be discriminated with an acceptable discrimination factor.

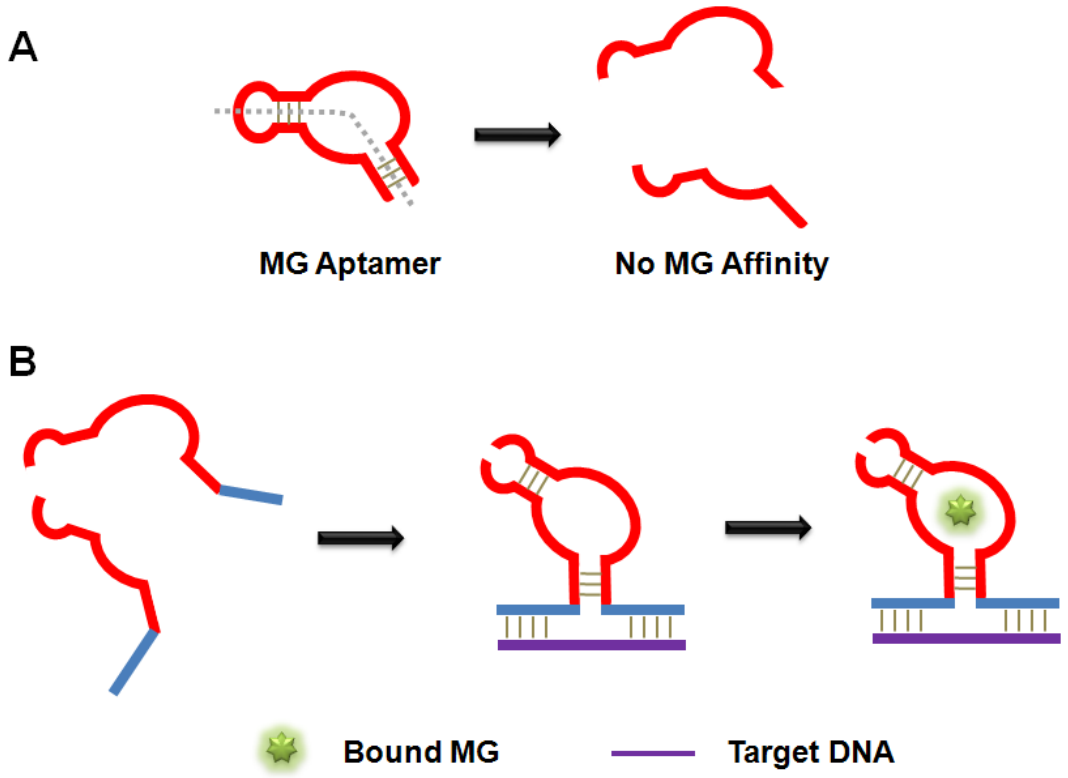

Figure 3.3 (A) Splitting of the MG aptamer and (B) DNA sensing based on MG aptamer

The generalization of this methodology is still challenging. First, the communication module is the shared stem between the MG aptamer and the analyte aptamer. This stem does not necessarily exist for all aptamers. Second, structural information is important and even essential in the design. The engineering of the communication module is based on the knowledge of the conformation of the aptamer. Finally, the authors pointed out that optimizing the communication module was a trial-and-error process that was time-and-money-consuming.

3.2 Generalized sensor design

The design of the label-free aptamer fluorescent sensor is shown in Figure 3.4.[44] The sensor contains two nucleic acid strands. One is a chimeric conjugate of the adenosine DNA aptamer[45] sequence (in blue) and MG RNA aptamer sequence (in red), called the "aptamer strand" in this chapter. The other is a DNA strand, called the "bridging strand" (in brown), that contain sequences complimentary to both the adenosine and MG aptamers. The sequence of the bridging strand is designed so that the aptamer and bridging strands form a stable complex in buffer at room temperature to prevent the MG aptamer strand from binding MG in the solution if there is no adenosine present. Under this condition, the MG remains free in solution and almost non-fluorescent. In the presence of adenosine, however, the aptamer strand binds adenosine, leaving much less number of complimentary base pairs between the aptamer strand and bridging strand, which is less stable at room temperature, resulting in release of the bridging strand from the aptamer strand. As a consequence, the fluorescence of the MG is recovered.

The sequence of the bridging strand is critical. However, there are some clues for the selection of the sequence. Firstly, the bridge strand inhibits the affinity of the MG aptamer to ensure low background when adenosine is not present. Secondly, the affinity of the adenosine aptamer to adenosine is not significantly affected by the bridging strand. Thus, the affinities should rank in the following order: bridge-MG aptamer > MG-MG aptamer; adenosine-adenosine aptamer > bridge-adenosine aptamer. The affinities of the aptamers are pre-determined by the nature of the aptamers; the sequence of the bridging

strand should make the affinities between the two strands meet the conditions presented above.

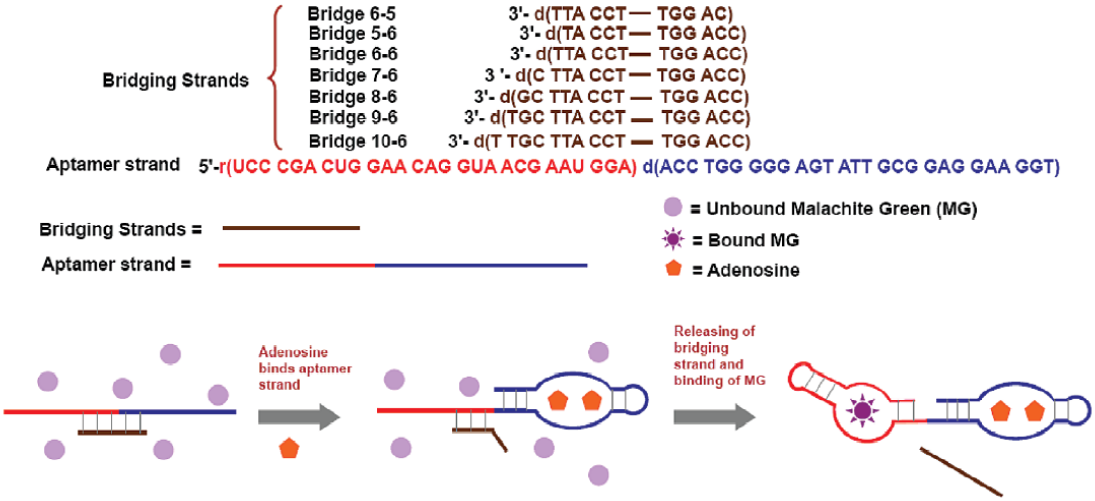

Figure 3.4 Scheme showing the regulation of the fluorescence of malachite green by adenosine. Without adenosine, the affinity of the aptamer strand (in red and blue) is inhibited by the bridging strand (in brown). With adenosine, the bridging strand separates from the aptamer strand, which then binds malachite green, leading to an enhancement of fluorescence.

3.3 Experimental

3.3.1 Materials and DNA sequences

Materials Nucleic acids were purchased from Integrated DNA Technologies, Inc. (Coralville, IA) with standard desalting. No further purification was performed. Malachite green and all other chemicals were purchased from Sigma-Aldrich. Buffers were prepared in Millipore water.

Nucleic acids sequences The sequences of the nucleic acids in the research are presented in Figure 3.4. The bridging strands are named as Bridge M-N. M is the number

of the complimentary bases between the bridging strand and the MG aptamer; N is the number of the complimentary bases between the bridging strand and the adenosine aptamer. The length of the bridging strand is (M+N).

3.3.2 Sensor preparations

The sensor solution was prepared by dissolving the nucleic acid strands and malachite green in buffer. The solution was then heated to 80 ºC and cooled down to room temperature in about one hour to ensure that the system folds into the structure described in Figure 3.4.

Because of the poor solubility of adenosine, the highest concentration of the stock solution that could be prepared was 50 mM. Thus, during the sensor preparation step, the dilution effect by the addition of adenosine was considered. In a typical procedure at the optimized conditions, 1.11 μM aptamer strand, 1.56 μM Bridge 9-6 and 0.67 μM MG were dissolved in 22 mM Tris buffer containing 5.56 mM NaCl, 155.6 mM KCl and 5.56 mM $MgCl_2$. After heating and cooling the solution as described above, 0.45 mL of the prepared solution was mixed with 0.05 mL of 10-times adenosine stock solution. After 30 min, the fluorescence of the sample was measured and recorded.

3.3.3 Fluorescence measurement

Fluorescence experiments were carried out on a Fluromax-2 fluorimeter (HORIBA Jobin Yvon inc., Edison, NJ). Emission acquisition mode was used. The excitation wavelength was 615 nm. The fluorescence at 650 nm was recorded. F/F_0 was plotted as sensor signal. F is the fluorescence of MG after the addition of adenosine. During optimization procedure, F_0 is the fluorescence of MG before addition of adenosine stock solution. For the sensor calibration curve acquisition, F_0 is the fluorescence of the sensor solution with

addition of 0 mM adenosine (water). All the measurements were performed for 3 times and the standard deviation was plotted as the error bar.

3.4 Results and discussions

3.4.1 MG affinity to the extended aptamer strand

MG was incubated with or without the aptamer strand in the buffer (20 mM Tris (pH 7.4), 145 mM NaCl and 5 mM $MgCl_2$). The fluorescence of MG was measured in both conditions and presented in Figure 3.5. The purpose of the comparison is to ensure that the fluorescence enhancement by MG is not affected by the conjugation of the adenosine aptamer and that the selected buffer, which is a compromise of the selection buffers for both aptamers, is effective for the MG aptamer. An over 1000 fold fluorescence increase was observed, which indicated that the affinity of the MG aptamer was not affected significantly; it is reasonable to conclude that the affinity of the adenosine aptamer was not affected either.

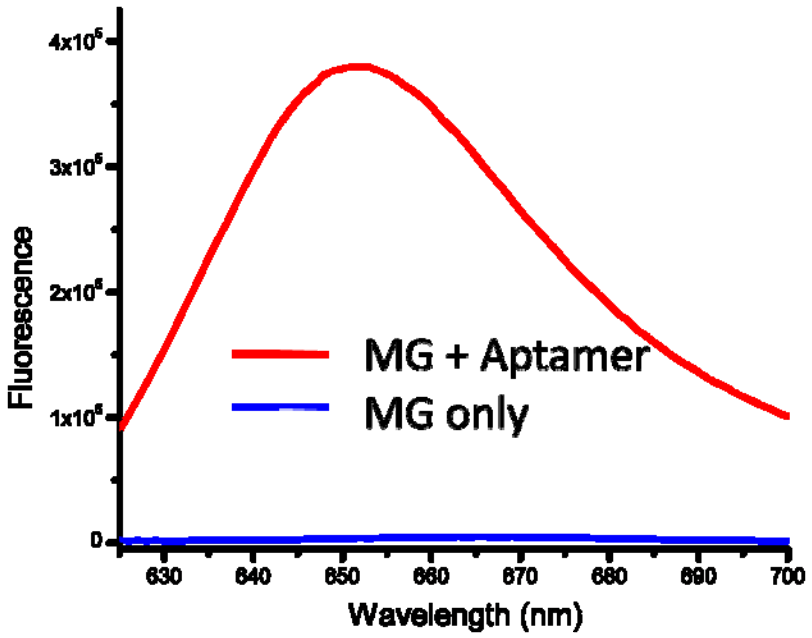

Figure 3.5 The conjugate of aptamers of adenosine and MG has high affinity to MG in the selected buffer

It is noted that the fluorescence increase was not as high as what was reported. This can be due to the conjugation of two aptamer sequences. However, with the decrease of the aptamer affinity, we still observed a thousand fold fluorescence increase, which is the up-limit of the signal-to-noise ratio for the future sensor. This upper-limit is already high than most labeled system; the quencher can only quench around 90% of the fluorescence from a fluorophore.

3.4.2 Optimization of the bridging strand

As mentioned above, the adenosine aptamer has been used to prove the concept of the structure switching sensors multiple times. Therefore, a significant amount of data is available about the properties of this aptamer. For example, when the first seven bases at

the 5□ terminus hybridize with the antisense strand, the affinity of the adenosine aptamer is not significantly decreased. This provides valuable information for the sequence design of the bridging strand.

In the present study, 6 base pairs at the adenosine aptamer end were selected to ensure the binding affinity between the aptamer strand and adenosine. It has been reported that 6 base pairs are effective in an adenosine aptamer structure switching.[46]

The MG aptamer was less investigated than the adenosine aptamer; thus more attention was focused on the optimization of the number M (M was defined in section 3.3.1). The bridge strand should prevent the MG aptamer from binding MG in the absence of adenosine to ensure a low background. At the same time, once adenosine binds to adenosine aptamer and starts structure switching, the hybridization between the MG aptamer part and the bridging DNA should not be stable at room temperature to ensure the release of it and binding of the aptamer strand to MG. We investigated the bridging strand that contains 6 bases that are complementary to adenosine aptamer and various numbers of bases that are complementary to MG aptamer (Bridge 6-6, 7-6, 8-6, 9-6 and 10-6. See Figure 3.4 for the sequences).

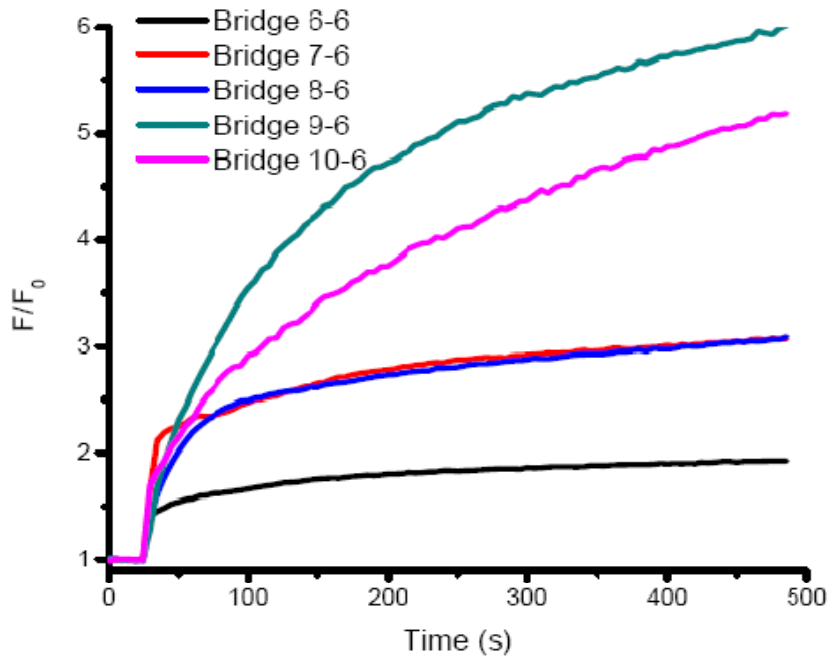

Figure 3.6 Sequence optimization of the bridge strands. 9-6 has the highest fluorescence increase.

During the optimization procedure, we tried to maximize the folds of the fluorescence increase upon the addition of 5 mM adenosine which was chosen as the signal output of the sensor. The kinetics of the reaction was monitored. We ensured that the equilibrium can be reached in less than 30 min. Upon addition of adenosine to the sensor solution, The folds of the fluorescence increase (F/F_0) increases when the number of bridging strand base complementary to MG aptamer (M) increases from 6 to 9, and then deceases when the number is 10 (Figure 3.6). Based on these results we conclude Bridge 9-6 is the optimal for the sensing application.

3.4.3 Sensor condition optimization

After the optimization of the bridging strand, 6-fold fluorescence increase was observed if the optimized sequence was used. However, because of the complexity of the system, there are more parameters that can be optimized. This section will discuss the

optimization of the buffer conditions and the concentrations of the three nucleic acid strands.

Buffer conditions optimization Since there are two aptamers in the design, each with its own optimal buffer condition for performance, a common condition suitable for both aptamer functions should be found first. Although adenosine aptamer was *in vitro* selected in a 20 mM Tris-acetate buffer with pH 7.6, it has been reported that adenosine aptamer-based biosensors are effective in a range of pH between 7.4 and 8.3. In addition, the Na^+ and Mg^{2+} concentrations can be varied from 100 mM to 300 mM and from 0 to 5 mM, respectively. Encouraged by these facts, we used the system developed by Li and co-workers to test the performance of adenosine aptamer in different buffers, and found that the sensing performance is similar at pH between 7.4 and 8.4 and concentrations of NaCl between 150 mM and 300 mM and $MgCl_2$ between 2 mM and 5 mM.

After confirming the workable range of buffer conditions for adenosine aptamer, we next explored a common buffer condition that is also effective for MG aptamer. Since MG aptamer was selected in 10 mM Na-HEPES buffer at pH 7.4, together with 100 mM KCl and 5 mM NaCl, we decided to use 20 mM Tris (pH 7.4), 145 mM NaCl and 5 mM $MgCl_2$ as a compromise between buffers for adenosine and MG aptamers.

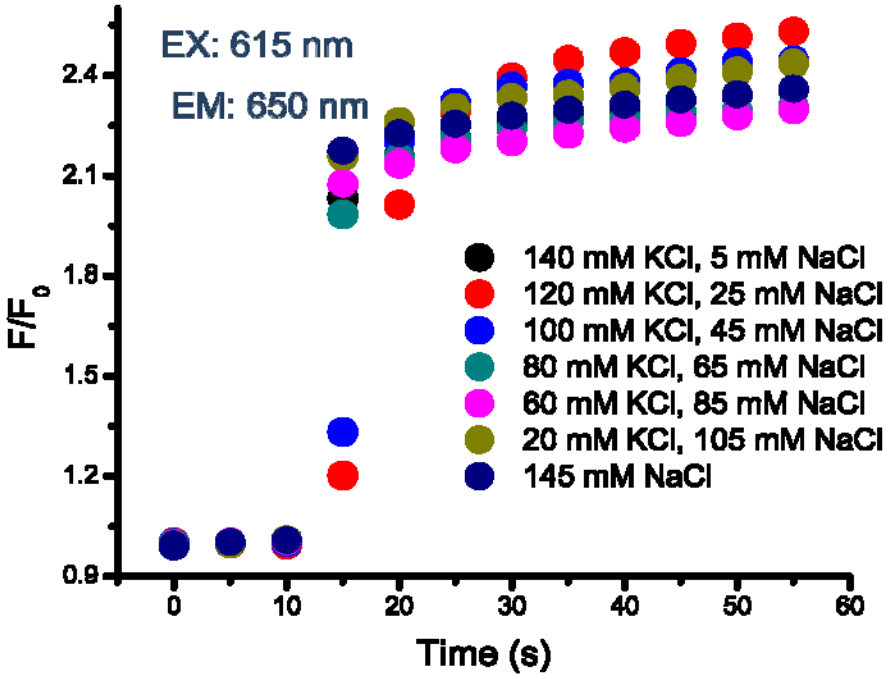

Figure 3.7 Performance of the sensor with varied potassium concentration in the buffer. 1 µM aptamer strand, bridge 6-5 and MG were used as the sensor. Besides KCl and NaCl, 5 mM MgCl2 and 20 mM Tris (pH 7.4) were also present in buffer. 5 mM adenosine was added at t = 10 s and fluorescence versus time was recorded and plotted.

Since the MG aptamer was selected in buffer containing potassium, we investigated whether replacing NaCl with KCl in the buffer may help to increase the performance of the sensor. The sensor performance was tested using Bridge 6-5 (Figure 3.4) in buffers containing 20 mM Tris (pH 7.4), 5 mM $MgCl_2$ and 145 mM of total monovalent metal ions, but with different ratios of Na^+ and K^+. Our results showed that variation of potassium concentration did not change the signal significantly (by around 10%, Figure 3.7). Monovalent metal ions are necessary for the MG aptamer affinity because the DNA strand has to fold, during which the negative charge on the DNA backbone has to be neutralized. As K^+ and Na^+ has the similar ability to help DNA fold, variation of K^+ concentration did not affect the sensor performance significantly. We

decided to use 20 mM Tris (pH 7.4), 5 mM $MgCl_2$, 140 mM KCl and 5 mM NaCl as the optimized buffer to make it as close as possible to the buffer in which MG aptamer was selected. It is worthwhile to point that since two aptamers are used in this label-free system, each with its own optimized condition, the range of optimal conditions is much narrower than that of the labeled systems.

Optimizations of the concentrations of the nucleic acid strands Since there are three DNA species (the aptamer and bridging strands and MG) in the system, it offers a chance to optimize the ratio of the three species separately to increase the performance of the sensor. First, both DNA strands were kept 1 μM and MG concentration was varied. As presented in Figure 3.8A, MG = 0.6 μM has the best performance. We then kept the aptamer strand and MG concentrations to be 1 μM and 0.6 μM respectively and varied the concentration of the bridging strand (bridge 9-6). Based on the data in Figure 3.8B, 1.0 μM and 1.4 μM of Bridge 9-6 have similar fluorescence fold increase in the presence of 5 mM adenosine (around 10% difference). We decided to choose 1.4 μM of Bridge 9-6 to ensure the complete hybridization of the aptamer strand to the bridge strand. Therefore the optimal sensor design is for 1.4 μM Bridge 9-6 to be complementary to 1 μM aptamer strand while in the presence of 0.6 μM MG.

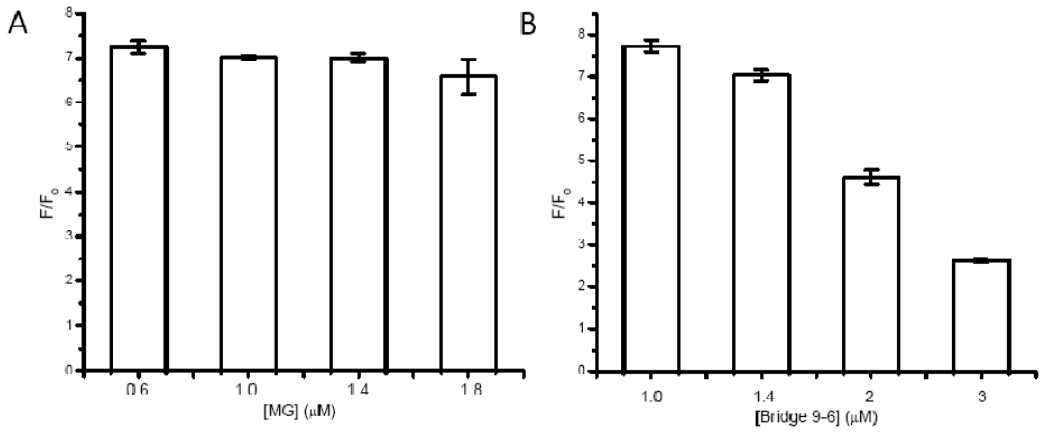

Figure 3.8 Optimization of the concentrations of MG (A) and the bridge strand 9-6 (B)

3.4.4 Sensor response at the optimized conditions

Under the optimal sensor design and buffer conditions, minimal fluorescence was observed in the absence of adenosine (black trace in Figure 3.9A). Upon addition of 5 mM adenosine, however, a 12 fold increase in fluorescence was observed (red trace in Figure 3.9A), indicating that the binding of adenosine by the adenosine aptamer caused the release of the bridging strand, recovering the affinity of the MG aptamer, which then binds MG, resulting in a fluorescence increase.

To quantify concentrations of adenosine based on the increase in MG fluorescence, we measured the saturated fluorescence upon addition of different concentrations of adenosine. The sensor solution concentration was diluted by 20% to what was described in the previous section in order to reduce the use of the materials. The results shown in Figure 3.9B indicate that the fluorescence of MG increases with an increasing concentration of adenosine, reaching ~12 fold fluorescence increase around 5 mM adenosine. The inset of Figure 3.9B shows the region between 0 and 1 mM adenosine where a linear relationship was observed between adenosine concentration and

MG fluorescence. A detection limit of 20 μM at 90% confidence level was calculated, which is comparable with other adenosine aptamer-based sensors.

3.4.5 Selectivity of the sensor

To test the selectivity of the sensor, 5 mM cytidine or uridine, the highest concentration tested for adenosine, was added to the sensor solution and no fluorescence increase was observed (see Figure 3.9C). Our results suggest that the sensor is specific to adenosine. Guanidine was not used due to poor solubility. The extraordinary selectivity of the sensor is not surprising; the fluorescence increase is initiated by the binding of adenosine to the aptamer strand. Previous studies have shown that the adenosine aptamer used in this study is not responsive to cytidine or uridine; thus no fluorescence can be observed. It also proved that the fluorescence increase of MG is from adenosine instead of any other changes of the physical properties of the solution introduced by the addition of adenosine.

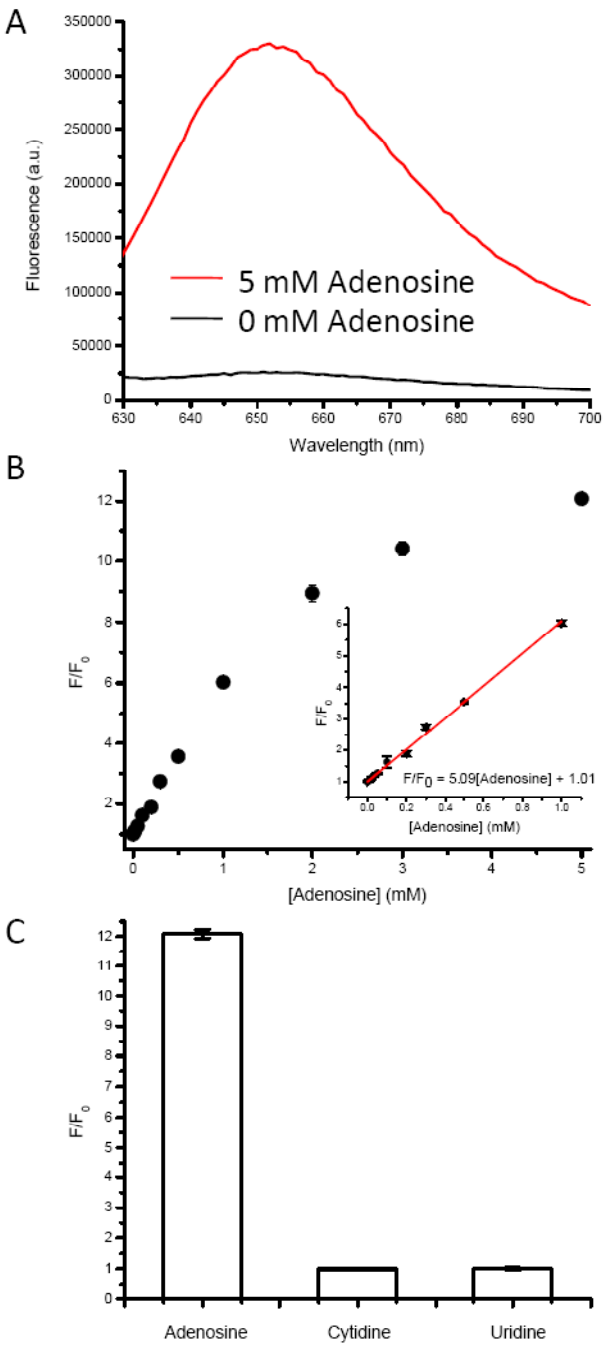

Figure 3.9 (A) Fluorescence enhancement of the optimized sensor upon the addition of adenosine; (B) the saturated fluorescence of malachite green with various concentrations of adenosine. The inset shows the fluorescence response at low concentrations of adenosine, and the red line shows a linear fitting of the data; (C) selectivity of the sensor toward other nucleosides. Cytidine and uridine did not increase the fluorescence of MG.

3.5 Conclusion, perspectives and future direction

We have demonstrated coupling of adenosine aptamer strand with MG aptamer strand through a bridging strand in which the fluorescence of malachite green can be regulated by the presence of adenosine. This system has sensitivity and selectivity comparable to other adenosine sensor systems, with the benefit that labeling of the DNA with fluorophores is not required. More importantly, the design is based purely on DNA hybridizations and therefore can be more generally applied to other aptamers for the sensing of a broad range of analytes.

There are two directions that the research can be further investigated. First of all, DNAzymes have been used to detect metal cations such Pb^{2+} and UO_2^{2+}. The label-free sensor design can be adapted so that it can be used for metal cation sensing. This research will provide evidence for the generality of the design. Second, the RNA aptamer is not as stable as DNA. Thus, minimizing the RNA bases of the MG aptamer is important. Although the DNA strand with the same sequence as the MG aptamer does not bind to MG, mutation of the bases which are far away from the binding sites can significantly increase the stability of the aptamer strand without affecting the sensor performance. Or DNA aptamer selection can be carried on to evolve a new aptamer.

3.6 References

(1) Tyagi, S. *Nat. Methods* **2009**, *6*, 331-338.

(2) White, C. E.; Argauer, R. J. *Fluorescence Analysis; a Practical Approach*; Marcel Dekker: New York, 1970.

(3) Babendure, J. R.; Adams, S. R.; Tsien, R. Y. *J. Am. Chem. Soc.* **2003**, *125*, 14716-14717.

(4) Grate, D.; Wilson, C. *Proc. Natl. Acad. Sci. U.S.A.* **1999**, *96*, 6131-6136.

(5) Grate, D.; Wilson, C. *Bioorg. Med. Chem.* **2001**, *9*, 2565-2570.

(6) Ellington, A. D.; Szostak, J. W. *Nature* **1990**, *346*, 818-822.

(7) Tuerk, C.; Gold, L. *Science* **1990**, *249*, 505-510.

(8) Liu, J.; Cao, Z.; Lu, Y. *Chem. Rev.* **2009**, *109*, 1948-1998.

(9) Shamah, S. M.; Healy, J. M.; Cload, S. T. *Acc. Chem. Res.* **2008**, *41*, 130-138.

(10) Famulok, M.; Hartig, J. S.; Mayer, G. *Chem. Rev.* **2007**, *107*, 3715-3743.

(11) Manimala, J. C.; Rajendran, M.; Ellington, A. D. *Recent Dev. Nucleic Acids Res.* **2004**, *1*, 207-231.

(12) Famulok, M.; Mayer, G.; Blind, M. *Acc. Chem. Res.* **2000**, *33*, 591-599.

(13) Hesselberth, J.; Robertson, M. P.; Jhaveri, S.; Ellington, A. D. *Rev. Mol. Biotechnol.* **2000**, *74*, 15-25.

(14) Wilson, D. S.; Szostak, J. W. *Annu. Rev. Biochem* **1999**, *68*, 611-647.

(15) Morris, K. N.; Jensen, K. B.; Julin, C. M.; Weil, M.; Gold, L. *Proc. Natl. Acad. Sci. U.S.A.* **1998**, *95*, 2902-2907.

(16) Flinders, J.; DeFina, S. C.; Brackett, D. M.; Baugh, C.; Wilson, C.; Dieckmann, T. *ChemBioChem* **2004**, *5*, 62-72.

(17) Nguyen, D. H.; Dieckmann, T.; Colvin, M. E.; Fink, W. H. *J. Phys. Chem. B* **2004**, *108*, 1279-1286.

(18) Li, Y.; Lu, Y. *Functional Nucleic Acids for Sensing and Other Analytical Applications*; Springer: New York, 2009.

(19) Fowler, C. C.; Li, Y. *Chem. Biol.* **2007**, *14*, 736-738.

(20) Lu, Y.; Liu, J. *Curr. Opin. Biotechnol.* **2006**, *17*, 580-588.

(21) Navani, N. K.; Li, Y. *Curr. Opin. Chem. Biol.* **2006**, *10*, 272-281.

(22) Potyrailo, R. A.; Conrad, R. C.; Ellington, A. D.; Hieftje, G. M. *Anal.Chem.* **1998**, *70*, 3419-3425.

(23) Mok, W.; Li, Y. *Sensors* **2008**, *8*, 7050-7084.

(24) Tan, L.; Li, Y.; Drake, T. J.; Moroz, L.; Wang, K.; Li, J.; Munteanu, A.; Yang, C. J.; Martinez, K.; Tan, W. *Analyst* **2005**, *130*, 1002-1005.

(25) Barrick, J. E.; Breaker, R. R. *Sci. Am.* **2006**, *296*, 50-57.

(26) O'Sullivan, C. K. *Anal. Bioanal. Chem.* **2002**, *372*, 44-48.

(27) Pei, R.; Rothman, J.; Xie, Y.; Stojanovic, M. N. *Nucleic Acids Res.* **2009**, *37*, e59/51-e59/56.

(28) Huang, C.-C.; Chang, H.-T. *Chem. Commun.* **2008**, 1461-1463.

(29) Tang, Z.; Mallikaratchy, P.; Yang, R.; Kim, Y.; Zhu, Z.; Wang, H.; Tan, W. *J. Am. Chem. Soc.* **2008**, *130*, 11268-11269.

(30) Shlyahovsky, B.; Li, D.; Weizmann, Y.; Nowarski, R.; Kotler, M.; Willner, I. *J. Am. Chem. Soc.* **2007**, *129*, 3814-3815.

(31) Cao, Z.; Suljak, S. W.; Tan, W. *Curr. Proteomics* **2005**, *2*, 31-40.

(32) Nutiu, R.; Li, Y. *J. Am. Chem. Soc.* **2003**, *125*, 4771-4778.

(33) Nutiu, R.; Li, Y. *Angew. Chem., Int. Ed.* **2005**, *44*, 1061-1065.

(34) Nutiu, R.; Li, Y. *Methods* **2005**, *37*, 16-25.

(35) Merino, E. J.; Weeks, K. M. *J. Am. Chem. Soc.* **2003**, *125*, 12370-12371.

(36) Li, B.; Qin, C.; Li, T.; Wang, L.; Dong, S. *Anal. Chem.* **2009**, *81*, 3544-3550.

(37) Wang, Y.; Liu, B. *Analyst* **2008**, *133*, 1593-1598.

(38) Wang, M.; Zhang, D.; Zhang, G.; Tang, Y.; Wang, S.; Zhu, D. *Anal. Chem.* **2008**, *80*, 6443-6448.

(39) Wang, J.; Liu, B. *Chem. Commun.* **2008**, 4759-4761.

(40) Li, B.; Wei, H.; Dong, S. *Chem. Commun.* **2007**, 73-75.

(41) Stojanovic, M. N.; Kolpashchikov, D. M. *J. Am. Chem. Soc.* **2004**, *126*, 9266-9270.

(42) Stojanovic, M. N. *J. Serb. Chem. Soc.* **2004**, *69*, 871-875.

(43) Kolpashchikov, D. M. *J. Am. Chem. Soc.* **2005**, *127*, 12442-12443.

(44) Xu, W.; Lu, Y. *Anal. Chem.* **2010**, *82*, 574-578.

(45) Huizenga, D. E.; Szostak, J. W. *Biochemistry* **1995**, *34*, 656-665.

(46) Xiang, Y.; Tong, A.; Lu, Y. *J. Am. Chem. Soc.* **2009**, *131*, 15352-15357.

Chapter 4 Characterization of the interaction of Cu^{2+}-dependent DNAzyme and Cu^{2+}

This chapter focuses on the specific interaction between Cu sensitive DNAzyme, called Cuzyme, and Cu^{2+}. Techniques including electron paramagnetic resonance (EPR), UV-Vis and circular dichroism were used in the characterization of this interaction.

4.1 Introduction

4.1.1 DNAzyme with Cu^{2+} as cofactor

Among the nuclease-like DNAzymes, the Cu-dependent DNAzyme is unique.[1-3] Most DNAzymes with nuclease activity catalyze the cleavage of DNA/RNA chimeric strands,[4-12] the cleavage site being an RNA base, such as 8-17[5] and 39E.[11,12] The Cu-dependent DNAzyme is the only DNAse-like DNAzyme that can cleave DNA.[1-3] The substrate strand does not contain RNA bases. This DNAzyme was evolved and truncated by Breaker and co-workers in 1996.[1-3]

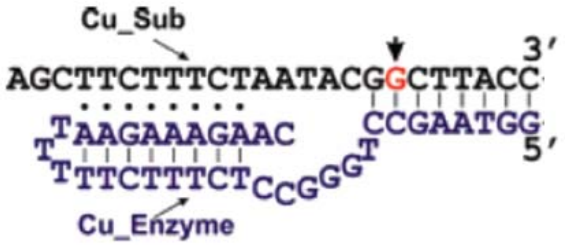

Figure 4.1 Secondary structure of the DNAzyme (in blue) that can cleave another DNA strand (in black). The thick black arrow indicates the cleavage site.

During the selection, the DNA library was incubated with both Cu^{2+} and ascorbate at varying concentrations.[1] The pool after seven rounds of selection showed robust nuclease activity and the pool after 8 rounds of selection was sequenced. Two classes of the Cu-dependent DNAzymes were selected in the original *in vitro* selection procedure carried out by the Breaker group, one of which required ascorbic acid even in the presence of Cu^{2+} (Class I). The other class (Class II) had activity even with the absence of ascorbate. More studies were conducted on Class II because of its relatively simple secondary structure and its ability to be truncated.

This chapter focuses on studies of the truncated Class II DNAzyme. The secondary structure of the optimized Class II DNAzyme is shown in Figure 4.1. The enzyme strand (named Cuzyme herein) is blue, the substrate strand (named Cusub) is black and the cleavage site is red. There are three stems on the Cuzyme-Cusub complex. The 5' end stem forms a duplex with the 3' end of Cusub (stem I); the 3' end self folds and forms a triplex with the 5' end of Cusub (stem II). The stem in the middle is believed to be the binding position for Cu^{2+} (stem III).

4.1.2 Progress on the characterization of the Cu^{2+}-DNAzyme interaction

There are limited reports on the characterization of the Cu^{2+}-dependent DNAzyme, most of which is focused on biochemical methods of characterization.[3] Mutational studies led to a proposed secondary structure of the DNAzyme.[2] The original Class II DNAzyme was reduced to a 46mer without significant loss of activity. For example, it was discovered that the cytosine base at the 3' terminus of the 46mer was important to essential to activity. The triplex stem was proposed based on the result (Figure 4.1). Other mutational studies included varying the number of base pairings present in stem I

and mutating stem II. Maximum activity was achieved when stem I formed a duplex and stem II formed a triplex. The mutation studies provided solid evidence of the proposed secondary structure shown in Figure 4.1.

Although the copper-dependent DNAzyme was selected in buffer at neutral pH in the presence of 1 M monovalent metal (K^+ + Na^+) and Cu^{2+} at varying concentrations, the DNAzyme showed some tolerance to changes in acidity and ion strength of the buffer. For instance, activity assays showed that the DNAzyme retained activity when the concentration of NaCl varied between 300 mM to 1 M. However, the DNAzyme is more sensitive to pH. Only ~50% activity was retained when the pH of the buffer varied from 7 by 1 unit. Moreover, excessive Cu^{2+} can result in loss of DNAzyme activity. A significant drop in activity was reported when Cu^{2+} concentration was increased 100 μM Cu^{2+} and complete loss of activity occurred at 1 mM Cu^{2+}.

Previous mutational studies were helpful in elucidating the properties of the DNAzyme. However, the chemistry behind the catalysis has not yet been revealed by these studies. For example, the binding site and binding geometry of Cu^{2+} to the DNAzyme were still unknown. DNA has multiple binding sites for metal cations, such as the phosphate groups and bases. The number of Cu^{2+} ions capable of binding to each DNAzyme has not been reported either. Therefore, previous studies have opened the door for a deeper understanding of the interaction between the Cu^{2+}-dependent DNAzyme and its metal cation cofactor, properties of which we address in our studies presented here.

4.1.3 Cu sensor based on the Cuzyme

Before the selection of Cuzyme, very few Cu sensors were available with high sensitivity[13-24] and selectivity. Cu^{2+} is known to quench the fluorescence of dyes, leading

to low sensitivity. The selection of Cuzyme provided the opportunity to sense copper in solution.

In 2007, Cuzyme was developed into a sensor for Cu^{2+} detection.[25] The sensor is based on the Cuzyme-Cusub presented in Figure 4.1. The sensor design scheme was presented in Chapter 1. Under optimized conditions, a detection limit of 35 nM was reported.

Ascorbate was added to accelerate the cleavage of Cusub so that the detection time can be shortened without loss of sensitivity. Although DNAzyme activity does not require the presence of ascorbate, the catalysis efficiency was significantly enhanced by its presence.

It was well known that ascorbate can reduce Cu^{2+} to Cu^{+}. Thus, it was suspected that the DNAzyme was sensitive to Cu^{+} too. It was discovered that the Cu^{2+} sensor also responded to Cu^{+}, which indicated that Cu^{+} could also be detected. If ascorbate was not present, the signal of the sensor to Cu^{+} was higher than that of Cu^{2+} at the same concentration. This result indicated that the DNAzyme was more sensitive to Cu^{+} than Cu^{2+}.[25] However, the enzymatic activity of the DNAzyme with Cu^{+} has not been systematically studied. More mechanistic and structural information of the DNAzyme can be revealed by the study.

4.1.4 Spectroscopic studies of the mechanism of the catalysis by DNAzymes

It is possible to obtain important information of the interaction between DNAzymes and metal cations such as binding affinity through biochemical studies.[26-30] Mutational studies isolated the residue important for the copper binding. However, the majority of the detailed information of interactions cannot be revealed by biochemical

assays only, such as the ligands essential for metal cation binding, the metal binding geometry and the structure-related catalysis mechanism.

Before the DNAzyme crystal structure was solved, spectroscopy was used to probe interactions that could not be determined by biochemical assays alone. For example, Fröster Resonance Energy Transfer (FRET) was used to study metal cation dependent folding of the DNAzyme.[31-35] UV-Vis was used to directly observe binding of metal cations to the DNAzyme.[36] Circular dichroism was used to probe global changes to DNA conformation.[37-42] If the nucleic acids are spin-labeled, EPR is a powerful tool to study conformational changes as well.[43-45] XAFS, although useful in characterizing metal-DNAzyme interactions, has not been widely applied because of the cost and difficulty of data interpretation.[46]

Unfortunately, the majority of the divalent metal cations that are known to activate DNAzyme activity are spectroscopically silent, (e.g., Pb^{2+}, Zn^{2+} and UO_2^{2+}). In other words, these cations cannot be probed directly by spectroscopic means. Cu^{2+} is known to have EPR and UV-Vis signal. Thus, we aim at studying the Cu^{2+}-DNAzyme interaction by spectroscopes.

4.2 Experimental

4.2.1 EPR spectra acquisition

DNA (0.5 mM, sequences in Figure 4.1) was dissolved in 50 mM HEPES (pH 7.0) buffer containing 1.5 M NaCl and 6% glycerin. $CuSO_4$ was added to the solution at various concentrations, followed by flash freezing of the solution in liquid nitrogen. The samples were kept in liquid nitrogen until EPR spectra acquisition.

EPR spectra were acquired on a Varian E-line Century Series X-band CW EPR spectrometer at 30 K. The EPR parameters are summarized in Table 4.1.

Table 4.1 Parameters of the EPR spectra acquisition

Center (Gauss)	Scan range (Gauss)	Frequency (GHz)	Scan number	Power (mW)	Modulation
2800	2000	9	20	0.5	5

4.2.2 Titrations by UV-Vis

DNA (0.5 mM) was dissolved in 50 mM HEPES (pH 7.0) buffer containing 1.5 M NaCl. Cu^{2+} was added slowly with stirring for at least 10 minutes, followed by the acquisition of the UV-Vis spectrum.

UV-Vis spectra (400 nm-1400 nm) were acquired on a Varian 500 UV-Vis spectrometer with a scan rate of 300 nm per minute.

4.2.3 Circular dichroism (CD)

DNA (2.5 μM) was dissolved in 50 mM HEPES (pH 7.0) buffer containing 1.5 M NaCl. Metal cations were added slowly with stirring for at least 10 minutes, followed by spectrum acquisition.

Buffer was used as the background. The samples were scanned from 220 nm to 320 nm and each sample was averaged over 10 acquisitions.

4.3 Results and discussion

4.3.1 EPR spectra interpretation

To probe copper-dependent DNAzyme metal binding interactions, 1 equivalent of Cu^{2+} was added to 0.5 mM nucleic acids with varied sequences as well as the monomer of DNA – dNTP in buffer (50 mM HEPES, pH 7.0, 1.5 M NaCl). The nucleic acid sequences included the Cuzyme-Cusub complex, the 39E-39S complex (cis-form), the 17E-17S complex (cis-form) and a mixture of dNTP (i.e., dATP, dCTP, dGTP and dTTP). The solutions were flash-frozen and subjected to EPR spectra acquisition.

The normalized EPR spectra of the samples are plotted in Figure 4.2A. The spectra have similar shape and g values. This is different from what was expected. It was hypothesized that the interaction between Cu^{2+} and the Cuzyme-Cusub complex was specific; this spectrum should be different from those of Cu^{2+} and the control nucleic acids (17E and 39E systems and dNTP). Here, preliminary analysis through Peisach-Blumberg plot indicates that Cu^{2+} binds to DNA molecules through their phosphate groups. Supporting evidence of this interaction comes from the observation that Cu^{2+} has strong affinity to phosphates.

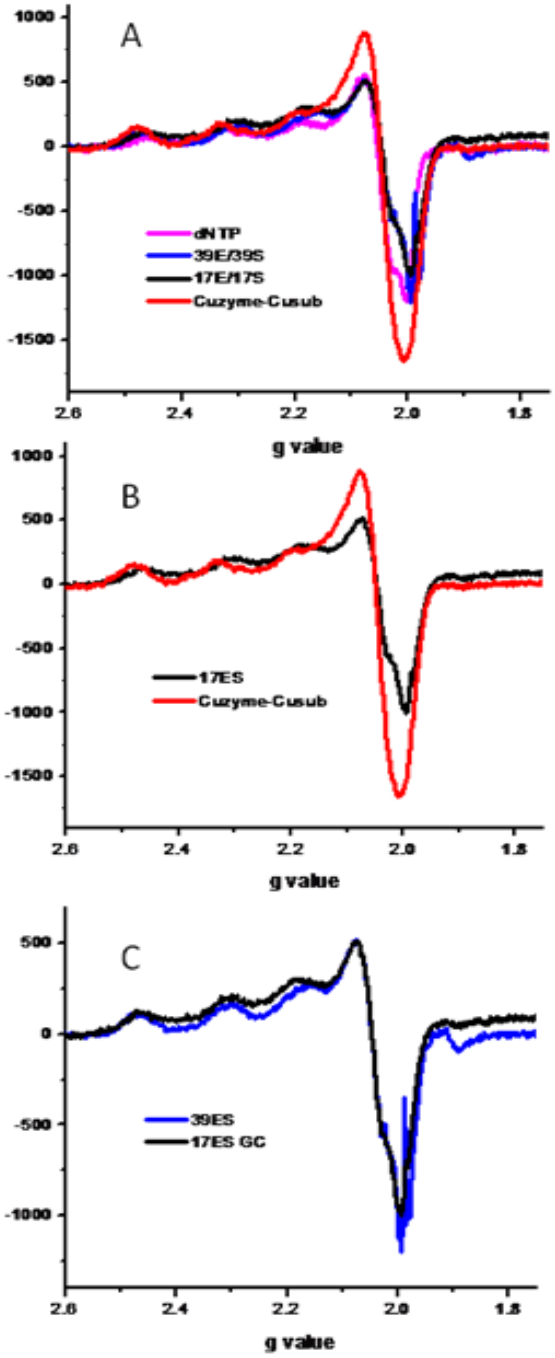

Figure 4.2 Overlaid EPR spectra of Cu^{2+} with dNTP, 39E, 17E or Cuzyme (A); and a comparison of the EPR spectra of Cu^{2+} with 17E or Cuzyme (B) and 17E and 39E (C)

However, several points are worth noting. First, the normalized signal strength of Cu^{2+} in Cuzyme-Cusub solution is stronger than the other control samples. As the

concentrations of Cu^{2+} in all samples were the same (0.5 mM), the signal difference can only be explained by the broadening of the signal. The EPR signal is broadened when the binding of Cu^{2+} to the ligand is flexible, which is common for Cu^{2+} in biological buffers such as Tris and HEPES. Signal broadening leads to a drop in the EPR signal intensity. Thus, the increased signal intensity of the Cuzyme-Cusub sample indicates that Cu^{2+} binds to Cuzyme-Cusub more strongly than the control DNA sequences and dNTP. The higher metal binding affinity can be from the specific interaction between the cofactor and the copper dependent DNAzyme.

Slight shape differences of the EPR spectra were also observed. Figure 4.2B shows the overlay of the EPR spectra of Cu^{2+} in Cuzyme-Cusub solution with that of Cu^{2+} in 17E-17S solution. The three peaks, with g values at 2.5, 2.3 and 2.1, did not perfectly overlap. More significantly, a shoulder was observed at g=2.05 in the Cu^{2+}-17E /17S sample. The shoulder was not significant in the Cuzyme-Cusub system. It is difficult to conclude that the binding modes of Cu^{2+} to DNA with different sequences are different since only a small difference in signal intensity indicated that the binding of Cu^{2+} to the Cuzyme-Cusub complex could be unique. It is noted that the spectra of Cu^{2+} with 17E/17S and 39E/39S were almost identical in both shape and signal intensity (Figure 4.2C), which can be interpreted as non-specific Cu^{2+} binding to DNA.

4.3.2 EPR: Cu^{2+} Titration

Since the EPR studies above did not give strong evidence of specific Cu^{2+} binding to the DNAzyme, a titration of Cu^{2+} into 0.5 mM Cuzyme-Cusub was performed. The purpose was to measure the binding affinity of the interaction and to determine the number of Cu^{2+} cations bound to each Cuzyme-Cusub complex.

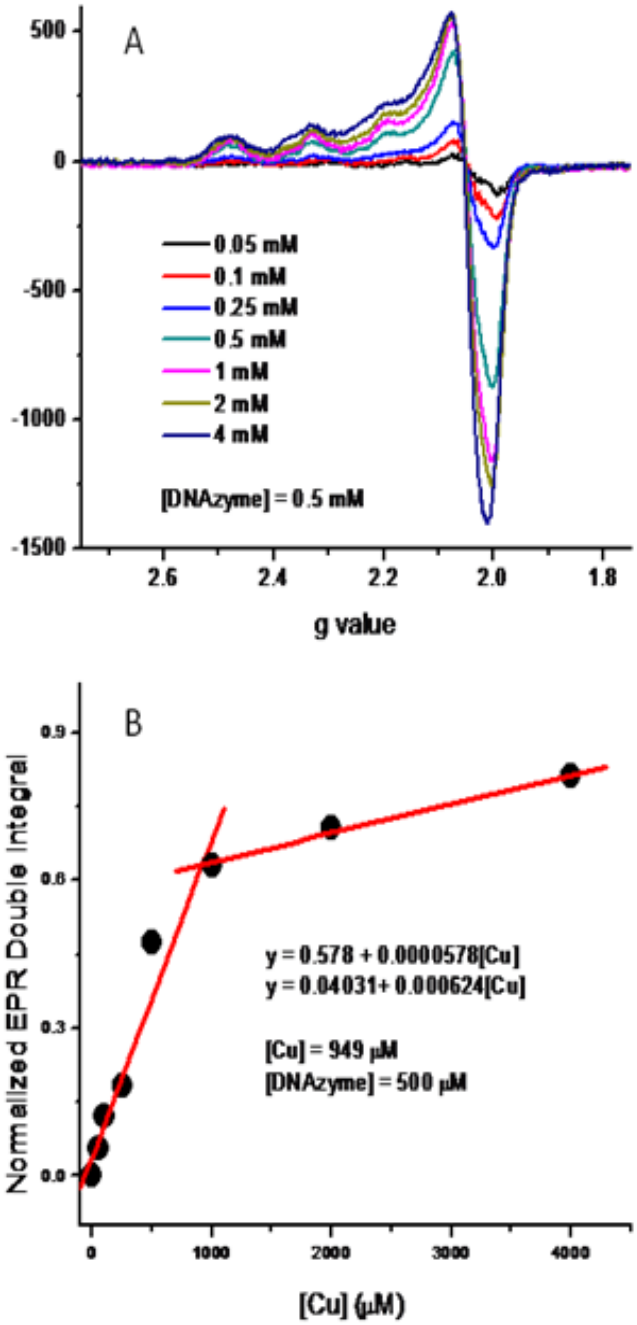

Figure 4.3 EPR spectra of varying concentrations of Cu^{2+} in solution containing 0.5 mM Cuzyme (A); and the plot of the integrated EPR signals versus Cu^{2+} concentration (B)

The EPR spectra of varying Cu^{2+} concentrations in solution with Cuzyme are presented in Figure 4.3A. No significant changes in spectral lineshape were observed with increasing concentrations of Cu^{2+}. Although signal intensity increased with increasing Cu^{2+} concentrations, the changes were not linear. In order to present the trend more clearly, the double integral of the EPR signal versus the concentration of Cu^{2+} is plotted in Figure 4.3B.

From Figure 4.3B, a linear relation was observed when the concentration of Cu^{2+} was between 0 and 1 mM; when the Cu^{2+} concentration exceeded 1 mM, the signal increase was not linear. The signal saturation is interesting because it indicated that there were two binding modes. When the Cu^{2+} concentration is lower than 1 mM, Cu^{2+} binds to DNA in mode 1. Due to a limited number of the binding sites in this mode, when the concentration of Cu^{2+} exceeds 1 mM, Cu^{2+} binds to the DNAzyme in an alternative mode, leading to signal saturation.

It is possible to calculate the number of binding sites for mode 1. The red traces in Figure 4.3B are the linear fitting of data points at Cu^{2+} concentrations lower than and higher than ~1 mM. The two fits intersect at 0.95 mM, indicating that ~2 equivalents of Cu^{2+} can bind to the DNAzyme (0.5 mM) in mode 1. This number provides evidence that mode 1 binding of Cu^{2+} is specific and that this may be the species responsible for enzymatic activity.

4.3.3 Circular dichroism (CD) characterization of the metal-DNAzyme interaction

EPR studies showed that the modes of specific and non-specific metal binding may involve similar ligands and binding geometry. Although these modes are

distinguishable, no other information can be acquired without advanced EPR techniques such as 2D-EPR. Thus, other spectroscopic techniques including CD were used to characterize the interaction between the copper sensitive Cuzyme and Cu^{2+}.

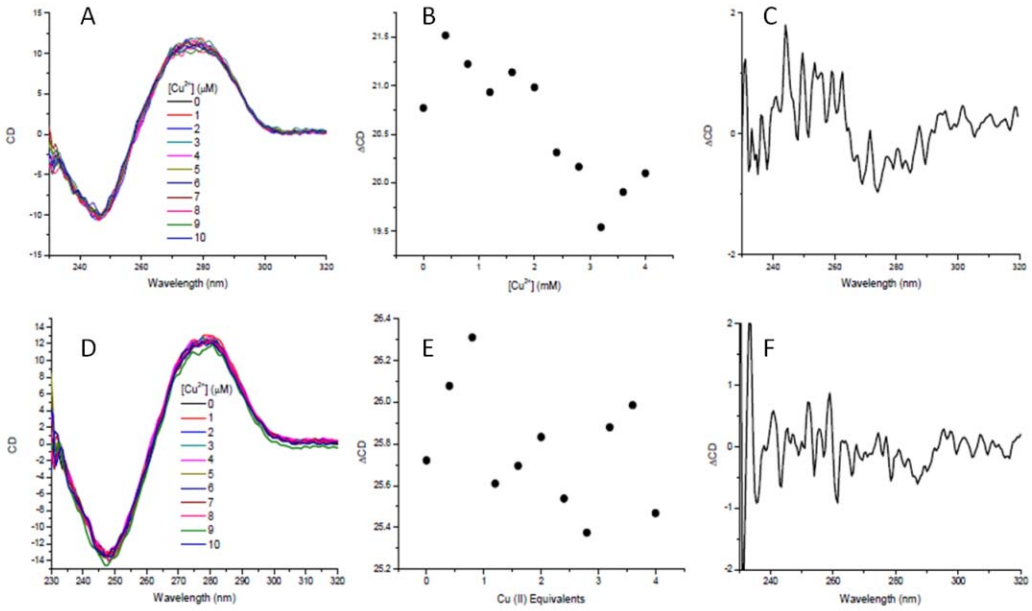

Figure 4.4 Circular dichroism spectra of Cuzyme (A, B, C) and control samples of double stranded DNA (see details in texts; D, E, F) with various concentrations of Cu^{2+}. Intensities of the spectra versus Cu^{2+} concentrations were plotted in B and E. The difference of the spectra in the presence or absence of 4 equivalents Cu^{2+} were plotted in C and F.

Circular dichroism was used to characterize the secondary structure change of the DNAzyme induced by Cu^{2+} binding. Cuzyme-Cusub and Cusub-Antisub (antisub refers to the antisense sequence of Cusub) were dissolved in buffer (2.5 μM) in the absence or presence of Cu^{2+}. The spectra were plotted in Figure 4.4A (Cuzyme-Cusub system) and Figure 4.4D (Cusub-Antisub system). There was no significant change in the shape of the spectra. It is not surprising because CD monitors the conformation of DNA; DNA folding

was not affected significantly by the introduction of the metal cations, as indicated by only subtle changes in the EPR spectra upon metal binding.

However, a slight signal decrease was observed. The difference of the peaks at 275 nm and 245 nm was plotted in Figure 4.4B. A 10% decrease in signal intensity was observed when 4 equivalents of Cu^{2+} were present. However, this trend was not observed for the control double stranded DNA system (Figure 4.4E); the peak difference scatters between 25.3-26.5 mdeg. The signal differences between 4 equivalents and 0 equivalents of Cu^{2+} in both systems are plotted in Figures 4.4C and 4.4F, respectively. Although the spectra are noisy, the trend can be observed.

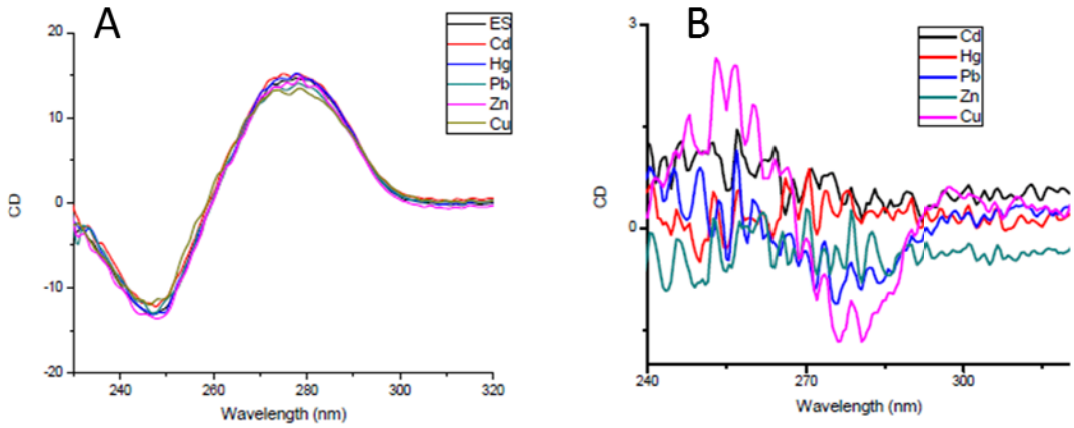

Figure 4.5 CD spectra of 0.5 mM Cuzyme with 2 mM divalent metal cations (A) and their corresponding difference spectra in the presence or absence of metal cations (B)

The signal decrease in the CD spectrum upon Cu^{2+} addition to the DNAzyme system is surprising. The introduction of a metal cation is expected to improve DNA folding, leading to a signal with the same or even increased intensity. However, Cu^{2+} appears to denature the copper dependent DNAzyme-substrate complex, which can be

important to enzymatic activity. This denaturing is unique, which was not observed in the control system.

Further investigation was carried out by addition of 4 equivalents of various metal cations into a solution of Cuzyme-Cusub. The CD spectra was acquired and plotted in Figure 4.5A. Slight intensity change was only observed when Cu^{2+} was added. The corresponding difference CD spectra are plotted in Figure 4.6B. It can be observed that Zn^{2+}, Cd^{2+} and Hg^{2+} did not introduce any signal change. Pb^{2+} led to changes in CD intensity which was only half of the change observed by introduction of Cu^{2+}. The result emphasizes the specificity that Cuzyme has for Cu^{2+}.

4.3.4 Proposed mechanism

The metalloenzyme model suggests that the metal cation is the active site for catalysis, and that the protein/DNA ligand provides the necessary binding mode for activity. However, It has been discovered that folding plays an important role in the reaction catalyzed by DNAzymes. For example, both FRET and single molecule FRET indicated that the cleavage reaction catalyzed by 8-17 with the presence of Zn^{2+} includes two steps, the conformational change resulting from the addition of Zn^{2+} (folding) and that during cleavage. In addition to folding, the activity of the DNAzymes, such as 10-23 and 8-17, can be activated by monovalent metal cations.[38] Based on these discoveries, it was proposed that the DNAzyme catalyzed reaction is conformation-change-based. The most specific metal cation cofactor has the highest folding efficiency (and thus highest activity), which explains the selectivity of the DNAzyme.

The Cu-dependent DNAzyme is hypothesized to be conformation sensitive. Cuzyme can switch to the active conformation upon binding Cu^{2+}, as Cu^{2+} can induce

DNAzyme folding through binding to the DNA phosphates. This may be the reason why EPR did not show very different spectral differences upon Cu^{2+} addition to Cuzyme in comparison to the control DNA. Different from the control DNA, Cuzyme takes a specific conformational change, which accounts for the catalytic activity. This conformational change was probed by CD as the "denaturing" of the enzyme-substrate complex.

4.3.5 UV-Vis Cu^{2+} titration

As Cu (II) has UV-Vis-NIR absorption, we hoped to use UV-Vis spectroscopy to study the interaction between the Cuzyme and Cu^{2+}. UV-Vis has been widely used to study the binding of Cu^{2+} to biomolecule ligands. Binding affinities can also be measured through titration. Thus, we titrated $CuSO_4$ into the Cuzyme system and used dsDNA (double stranded DNA) as a control system. As shown in Figure 4.6, we observed very similar Vis-NIR spectra. There are three major peaks on the spectra at 700 nm, 950 nm and 1150 nm. The peak at 1150 nm is in the IR region, which is close to the water absorption band. This peak is relatively weak, and of the same intensity as background peaks so we did not use it for analysis.

Signal saturation was not observed in our studies, indicating that there was only one mode of binding, or the binding modes cannot be distinguished by this technique. The lack of binding saturation did not allow for the calculation of a binding affinity. The origins of the peaks are not clear. It is probably due to the binding of Cu^{2+} to the phosphates. It solidifies the mechanism proposed above that Cu binds to phosphate groups on the DNAzyme, leading to a conformational change that accounts for the cleavage of the substrate strand.

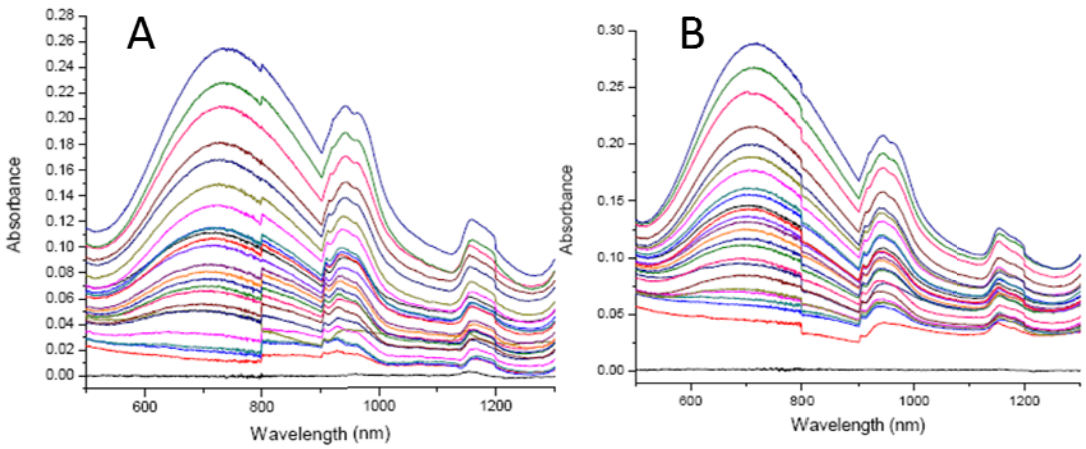

Figure 4.6 UV-Vis titrations of Cu^{2+} into 0.5 mM Cuzyme (A) and double strand DNA (B)

4.4 Conclusion, perspectives and future direction

In this chapter, we used spectroscopic techniques to characterize the interaction between a Cu-dependent DNAzyme, Cuzyme, and its metal cofactor, Cu^{2+}. EPR studies provides evidence that Cu^{2+} binds to the DNAzyme and control dsDNA in the same mode, resulting in similar EPR spectra characteristics. Further EPR analysis suggested that there are two binding modes between Cu^{2+} and the DNAzyme, one of which is likely responsible for enzymatic activity. EPR titration experiments also helped determine that one DNAzyme molecule can bind to two Cu^{2+} cations. In order to further probe the mechanism, circular dichroism was used. It was discovered that Cu^{2+} can lead to decreases in CD signal intensity or denaturing of the Cu-dependent DNAzyme structure, and that this weakening is specific to Cu^{2+}. Based on the spectroscopic studies, it was hypothesized that Cu^{2+} leads to a conformational change of the Cuzyme and that this specific conformation is responsible for catalytic activity.

A more rigorous way to probe conformational changes is to use FRET. It is predicted that if a DNAzyme is internally labeled with a fluorescent donor and acceptor, the FRET efficiency would correlate to Cu^{2+} concentration. Single molecule FRET experiments can even reveal more information on the hypothesized conformation change induced by Cu^{2+}. Another direction that can be considered is that 2D-EPR. Thus it is possible to obtain more specific information about the binding mode. Moreover, if the DNAzyme is spin labeled, it is even possible to know the residue that responsible for Cu^{2+} binding.

Perhaps the most complete information of the Cu^{2+}-Cuzyme interaction will be achieved by solving either the NMR or crystal structure of the complex. Spectroscopy is a powerful tool, but it is difficult to obtain a complete image of the metal-DNAzyme interaction through the use of any one spectroscopic technique. This problem can potentially be solved by the acquisition of a three dimensional structure of the copper bound Cuzyme system, which may also shed light on other metal dependent DNAzyme systems.

4.5 References

(1) Carmi, N.; Shultz, L. A.; Breaker, R. R. *Chem. Biol.* **1996**, *3*, 1039-1046.

(2) Carmi, N.; Balkhi, H. R.; Breaker, R. R. *Proc. Natl. Acad. Sci. U.S.A.* **1998**, *95*, 2233-2237.

(3) Carmi, N.; Breaker, R. R. *Bioorg. Med. Chem.* **2001**, *9*, 2589-2600.

(4) Gast, F. U.; Amiri, K. M. A.; Hagerman, P. J. *Biochemistry* **1994**, *33*, 1788-1796.

(5) Li, J.; Zheng, W.; Kwon, A. H.; Lu, Y. *Nucleic Acids Res.* **2000**, *28*, 481-488.

(6) Cairns, M. J.; Hopkins, T. M.; Witherington, C.; Wang, L.; Sun, L.-Q. *Nat.Biotechnol.* **1999**, *17*, 480-486.

(7) Joyce, G. F. *Methods Enzymol.* **2001**, *341*, 503-517.

(8) Nelson, K. E.; Bruesehoff, P. J.; Lu, Y. *J. Mol. Evol.* **2005**, *61*, 216-225.

(9) Bruesehoff, P. J.; Li, J.; Augustine, A. J.; Lu, Y. *Combin. Chem. High Throughput Screen.* **2002**, *5*, 327-335.

(10) Sugimoto, N.; Ohmichi, T. *FEBS Lett.* **1996**, *393*, 97-100.

(11) Liu, J.; Brown, A. K.; Meng, X.; Cropek, D. M.; Istok, J. D.; Watson, D. B.; Lu, Y. *Proc. Natl. Acad. Sci. U.S.A.* **2007**, *104*, 2056-2061.

(12) Brown, A. K.; Liu, J.; He, Y.; Lu, Y. *ChemBioChem* **2009**, *10*, 486-492.

(13) Sasaki, D. Y.; Shnek, D. R.; Pack, D. W.; Arnold, F. H. *Angew. Chem., Int. Ed.* **1995**, *34*, 905-907.

(14) Torrado, A.; Walkup, G. K.; Imperiali, B. *J. Am. Chem. Soc.* **1998**, *120*, 609-610.

(15) Bolletta, F.; Costa, I.; Fabbrizzi, L.; Licchelli, M.; Montalti, M.; Pallavicini, P.; Prodi, L.; Zaccheroni, N. *J. Chem. Soc., Dalton Trans.* **1999**, 1381-1386.

(16) Grandini, P.; Mancin, F.; Tecilla, P.; Scrimin, P.; Tonellato, U. *Angew. Chem., Int. Ed.* **1999**, *38*, 3061-3064.

(17) Klein, G.; Kaufmann, D.; Schurch, S.; Reymond, J.-L. *Chem. Commun.* **2001**, 561-562.

(18) Zheng, Y.; Huo, Q.; Kele, P.; Andreopoulos, F. M.; Pham, S. M.; Leblanc, R. M. *Org. Lett.* **2001**, *3*, 3277-3280.

(19) Boiocchi, M.; Fabbrizzi, L.; Licchelli, M.; Sacchi, D.; Vazquez, M.; Zampa, C. *Chem. Commun.* **2003**, 1812-1813.

(20) Zheng, Y.; Orbulescu, J.; Ji, X.; Andreopoulos, F. M.; Pham, S. M.; Leblanc, R. M. *J. Am. Chem. Soc.* **2003**, *125*, 2680-2686.

(21) Dujols, V.; Ford, F.; Czarnik, A. W. *J. Am. Chem. Soc.* **1997**, *119*, 7386-7387.

(22) Kaur, S.; Kumar, S. *Chem. Commun.* **2002**, 2840-2841.

(23) Wu, Q.; Anslyn, E. V. *J. Am. Chem. Soc.* **2004**, *126*, 14682-14683.

(24) Royzen, M.; Dai, Z.; Canary, J. W. *J. Am. Chem. Soc.* **2005**, *127*, 1612-1613.

(25) Liu, J.; Lu, Y. *J. Am. Chem. Soc.* **2007**, *129*, 9838-9839.

(26) Lu, Y. *Chem. Eur. J.* **2002**, *8*, 4588-4596.

(27) DeRose, V. J. *Curr. Opin. Struct. Biol.* **2003**, *13*, 317-324.

(28) Brown, A. K.; Li, J.; Pavot, C. M. B.; Lu, Y. *Biochemistry* **2003**, *42*, 7152-7161.

(29) Takagi, Y.; Warashina, M.; Stec, W. J.; Yoshinari, K.; Taira, K. *Nucleic Acids Res.* **2001**, *29*, 1815-1834.

(30) Liu, Z.; Mei, S. H. J.; Brennan, J. D.; Li, Y. *J. Am. Chem. Soc.* **2003**, *125*, 7539-7545.

(31) Ha, T. *Methods* **2001**, *25*, 78-86.

(32) Liu, J.; Lu, Y. *J. Am. Chem. Soc.* **2002**, *124*, 15208-15216.

(33) Kim, H.-K.; Liu, J.; Li, J.; Nagraj, N.; Li, M.; Pavot, C. M. B.; Lu, Y. *J. Am. Chem. Soc.* **2007**, *129*, 6896-6902.

(34) Kim, H.-K.; Rasnik, I.; Liu, J.; Ha, T.; Lu, Y. *Nat. Chem. Biol.* **2007**, *3*, 763-768.

(35) Liu, J.; Lu, Y. *Protocol* **2006**, *335*, 257-271.

(36) Cunningham, L. A.; Li, J.; Lu, Y. *J. Am. Chem. Soc.* **1998**, *120*, 4518-4519.

(37) Pohl, F. M.; Jovin, T. M. *J. Mol. Biol.* **1972**, *67*, 375-396.

(38) Mazumdar, D.; Nagraj, N.; Kim, H.-K.; Meng, X.; Brown, A. K.; Sun, Q.; Li, W.; Lu, Y. *J. Am. Chem. Soc.* **2009**, *131*, 5506-5515.

(39) Germann, M. W.; Schoenwaelder, K. H.; Van de Sande, J. H. *Biochemistry* **1985**, *24*, 5698-5702.

(40) Thamann, T. J.; Lord, R. C.; Wang, A. H.; Rich, A. *Nucleic Acids Res.* **1981**, *9*, 5443-5457.

(41) Chattopadhyaya, R.; Ikuta, S.; Grzeskowiak, K.; Dickerson, R. E. *Nature* **1988**, *334*, 175-179.

(42) Benight, A. S.; Wang, Y.; Amaratunga, M.; Chattopadhyaya, R.; Henderson, J.; Hanlon, S.; Ikuta, S. *Biochemistry* **1989**, *28*, 3323-3332.

(43) Glasfeld, A.; Guedon, E.; Helmann, J. D.; Brennan, R. G. *Nat. Struct. Biol.* **2003**, *10*, 652-657.

(44) Hunsicker-Wang, L.; Vogt, M.; DeRose, V. J. *Methods Enzymol.* **2009**, *468*, 335-367.

(45) Schiemann, O. *Methods Enzymol.* **2009**, *469*, 329-351.

(46) B.Ravel; Slimmer, S. C.; Meng, X.; Wong, G. C. L.; Y.Lu *Radiat. Phys. Chem.* **2009**, *78*, S75-S79.

Chapter 5 Cooperativity of the 8-17 DNAzyme

In this chapter, the responses of a fluorescent sensor based on the 8-17 DNAzyme in the presence of two metal cations are discussed. During the course of data analysis, information about the interaction between the 8-17 DNAzyme and metal cations was revealed.

5.1 Introduction

5.1.1 8-17 DNAzymes

The specific interaction of metal cations and nucleic acids has been of interest to researchers for decades.[1-8] This field has experienced an increased interest after the discovery of ribozymes[9-11] and DNAzymes,[12] the corresponding RNA and DNA catalytic nucleic acids that require metal cations for their enzymatic activity.[13-25] It has been hypothesized and accepted that the metal cations bind to ribozymes or DNAzymes in the same way as metalloproteins.[6] However, the binding mode of metals in metalloproteins can be probed by physical techniques. Very few cases of the biophysical studies of the DNAzyme/ribozyme-metal interaction have been reported.

The '8-17' DNAzymes are a class of catalytic DNA molecules that catalyze the cleavage of chimeric DNA/RNA substrates, and have been isolated in multiple research groups under differing selection conditions.[26-33] The DNAzyme-substrate complex contains three parts – two double stranded "arms" and a loop (Figure 1.2). The loop is

believed to be the binding site of the metal cofactor; however, direct evidence for the hypothesis has not been reported.

The catalytic activity of 8-17 requires the divalent metal ions as the cofactor. The activity of the cofactor follows the order: Pb^{2+}>> Zn^{2+}>>Cd^{2+}>Mg^{2+}≈ Ca^{2+}.[34] Because the 8-17 DNAzyme has much higher activity in the presence of Pb^{2+} than any other metal ions, it was converted to biosensors for highly selective detection of Pb^{2+}. 17E DNAzyme falls into the 8-17 category and it has been converted into various biosensors for Pb^{2+} detection with high sensitivity and specificity. However, a systematic study of the sensor response to Pb^{2+} in the presence of other metal cations has not been reported thus far.

5.1.2 Model for the kinetics of the 8-17 catalyzed reactions

Both biochemical and biophysical characterizations supported the hypothesis that the 8-17 DNAzyme is a metalloenzyme.[34] Similar to other metalloenzymes, the catalytic kinetics follows the Michaelis-Menton equation. The fluorescent resonance energy transfer (FRET) studies show that the catalysis is a one-step or two-step procedure. Pb^{2+} does not change the conformation of the DNAzyme-substrate complex and the cleavage happens upon binding of Pb^{2+}. However, other metal ions, such as Zn^{2+}, change the confirmation of the DNA complex, followed by the cleavage of the substrate.[35-37] Single molecular FRET studies were consistent with this observation.[38] Besides divalent metal ions, monovalent metal ions such as Li^{+} and NH_4^{+} were able to fold DNAzyme-substrate complex, followed by cleavage of the substrate. During the folding process, Z-DNA formation at the hypothesized metal binding region was even observed.[39] Because of the diversity of the metal cation cofactors and their different folding effect, it is difficult to

hypothesize that the binding sites and binding geometries are the same for all the cations because of the diversity of the cation co-factors that can activate the DNAzyme.

5.1.3 8-17-based fluorescent sensors

17E DNAzyme which belongs to the 8-17 DNAzymes has been developed into biosensors for Pb^{2+} detection.[40,41] As the catalytic activity of 17E is much more sensitive to Pb^{2+} than other divalent metal cations, the sensors were reported to have high selectivity. The sensitivity of the sensors varies with the signal transduction technologies. The fluorescence based on 17E has sensitivity as low as 10 nM, which is 50 times lower than the EPA defined lead toxic level.

The recovery of the fluorescence includes two steps – the substrate cleavage and the dissociation of the product. The first step is believed to be the rate-limiting step. Although the sensor is usually used for Pb^{2+} detection, it is a powerful tool to study the kinetics of the DNAzyme because of less time consumption compared to kinetic assays based on gel electrophoresis. In this chapter, 8-17-based Pb^{2+} sensor was used to study the kinetics of the 8-17 DNAzyme in the presence of both Pb^{2+} and another metal cation, namely Zn^{2+}, Cd^{2+} or Mg^{2+}.

5.2 Experimental

5.2.1 DNA and chemicals

Nucleic acids were purchased from Integrated DNA Technologies, Inc. (Coralville, IA) with HPLC purification. Other chemicals were purchased from Sigma-Aldrich. Buffers were prepared in Millipore water.

The sequences of the DNAs are presented in Table 5.1

Table 5.1 DNA sequences of the 8-17-based sensor

17S	5′-FAM-ACTCACTAT rA GGAAGAGATG-dabcyl
17E	5′-CATCTCTTCTCCGAGCCGGTCGAAATAGTGAGT-BHQ1

5.2.2 Fluorescence measurement and data analysis

Both 17E and 17S were dissolved in buffer of 50 mM HEPES-Na (pH 7.0) with a concentration of 30 nM. The sensor solution was heated to 80 °C and cooled to ambient temperature in one hour to ensure complete hybridization.

Fluorescence experiments were carried out on a Fluromax-2 fluorimeter (HORIBA Jobin Yvon inc., Edison, NJ). Kinetics mode was used in the data acquisition. The fluorophore was excited at 495 nm and the reslting emission at 520 nm was recorded. After the addition of metal cations, the emission was recorded for six times with various time intervals based on which the initial fluorescence rate was calculated. The fluorescence versus time was plotted and linearly fitted. The slope is defined as the initial rate (dF/dt). The time intervals were between 1 s and 10 s to ensure 1) the fluorescence is not saturated and 2) noise is minimized. All the measurements were performed 3 times and their average was plotted.

5.3 Results and discussions

8-17-based sensors were developed for detection of Pb^{2+} in drinking water and paint, when Zn^{2+} interference was observed during detection (unpublished data). As reported before,[41] the 8-17-based sensor is around a hundred times more sensitive to Pb^{2+} than to Zn^{2+}. It was reported that if the concentration of Zn^{2+} is close or lower than Pb^{2+}, the false positive signal would be around 1%. However, practically, a much higher false positive signal than what was expected was observed when both Pb^{2+} and Zn^{2+} were present (unpublished data, and the systematic results are shown in the next section). It was realized that this phenomenon was not only practically important, but also of scientific interest. Thus, we aimed at performing a systematic study of the response of the 8-17-based sensors towards the co-existence of Pb^{2+} and other divalent metal cations. Zn^{2+}, Cd^{2+} and Mg^{2+} were chosen for this study because their range of responses towards the 8-17 varied considerably in terms of absolute concentrations for activity of the DNAzyme..

5.3.1 Fluorescence responses of the 8-17-based sensor towards the coexistence of Pb and Zn

First, we measured the fluorescence increase with various concentrations of the metal cations. As shown in Figure 5.1A, the sensor has linear response versus the Pb^{2+} concentration when it is between 0-4 μM. The overall signal however is not linear, and when the concentration is higher than 8 μM, saturation of the response is observed. Figure 5.1B shows that the linear range of the sensor towards the presence of Zn^{2+} is 0 to 150 μM. The signal reaches saturation when the concentration of Zn^{2+} is higher than 300 μM. To fully characterize the performance of the sensor with co-existence of Pb^{2+} and

Zn^{2+}, we chose the Pb^{2+} and Zn^{2+} concentrations to be 0.4, 2, 5, 10 μM and 20, 100, 200, 400 μM, respectively. Four concentrations were chosen so as to represent the lower linear range, higher linear range, non-linear range and saturation range. Thus, our first trial was to measure the sensor response towards the presence of both Zn^{2+} and Pb^{2+} with the combinations of the concentrations mentioned above; the results are presented in Figure 5.1C. It was observed that presence of Zn^{2+} enhanced the signal from 0.4 or 2 μM Pb^{2+}. This is not surprising because it was reported that Zn^{2+} responds to the 8-17-based sensor.[41] However, it may also be noticed that at high concentration of Pb^{2+} and Zn^{2+} (for instance, the Pb^{2+} and Zn^{2+} concentrations are 10 and 400 μM respectively), Zn^{2+} did not interfere the Pb^{2+} sensing. This is due to the saturation of the signal.

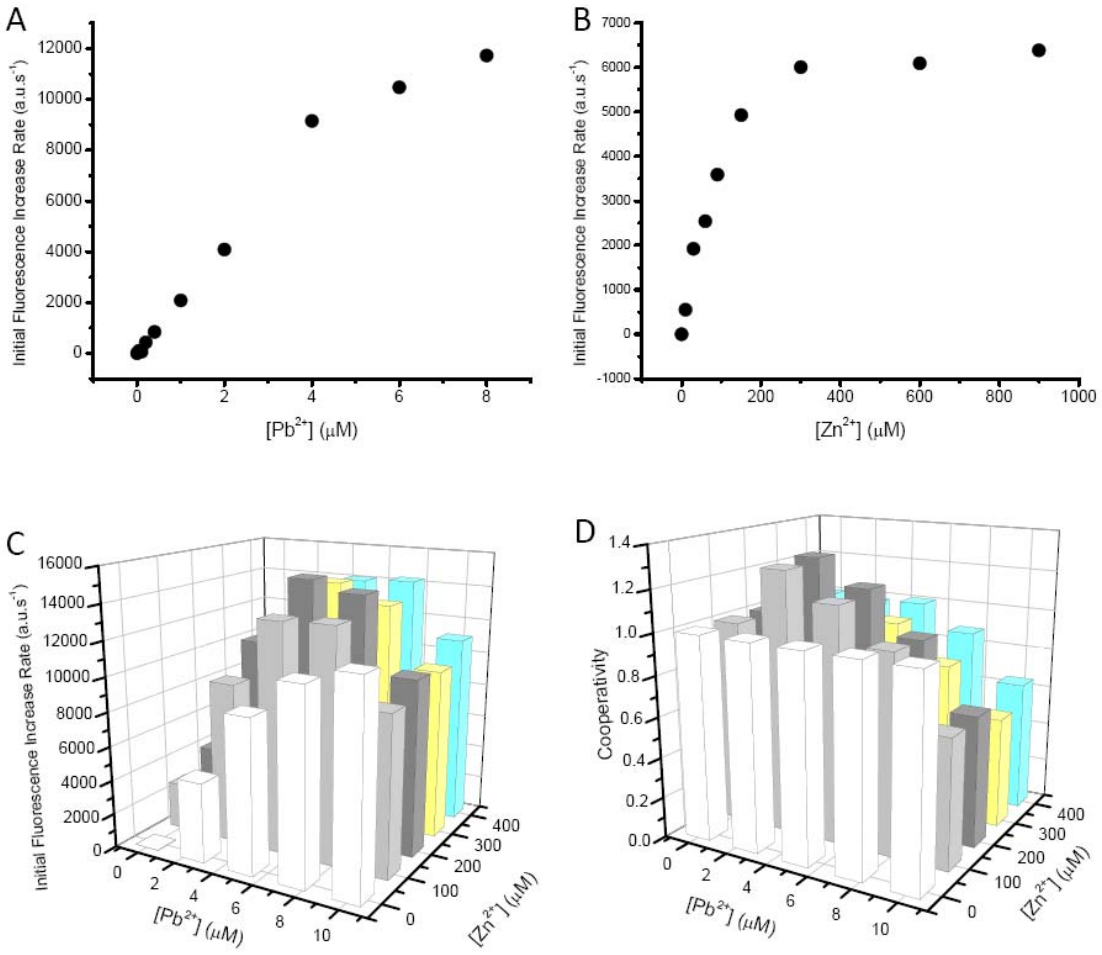

Figure 5.1 Initial rates of the fluorescence increase of the 8-17 sensor in the presence of Pb^{2+} (A), Zn^{2+} (B) and both (C). Calculated cooperativity was plotted in (D).

In order to better understand and analyze the data, we define:

Cooperativity = S (Pb^{2+}+Zn^{2+})/[S(Pb^{2+})+S(Zn^{2+})] where S(Pb^{2+}+Zn^{2+}), S(Pb^{2+})and S(Zn^{2+}) mean the initial fluorescence increase rates of the 8-17-based sensor in the presence of both Pb^{2+} and Zn^{2+}, Pb^{2+} and Zn^{2+} only, respectively.

If the sensor has linear response towards different metal ions, we expect the cooperativity to be 1. Cooperativity versus concentrations of metal cations is plotted in Figure 5.1D. Consistent with what we observed before, when both Pb^{2+} and Zn^{2+}

concentrations fall in the linear range, we observed a cooperativity effect wherein, the combined signal was higher than 1, which suggested that the sensor exhibited non-linear performance upon coexistence of two metal cations. However, this phenomenon was not observed when the Pb^{2+} concentrations were higher than 4 μM, which was ascribed to the signal saturation. In order to investigate the cooperativity (>1) exhibited at the lower linear range concentrations of both metal ions, we decided to lower their concentrations further.

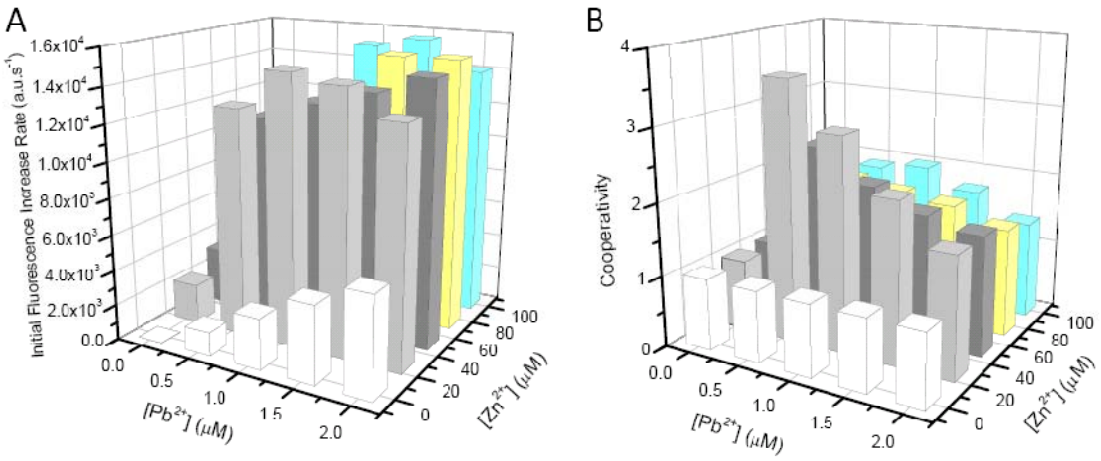

Figure 5.2 Initial rate of fluorescence increase of the 8-17 sensor (A) and calculated cooperativity (B) with both Pb^{2+} and Zn^{2+}.

We chose concentrations at the lower linear range from 0.2, 0.5, 1, 2 μM and 10, 20, 50, 100 μM for Pb^{2+} and Zn^{2+} respectively. The signal responses of the 8-17-based sensor towards the presence of the mixture of Pb^{2+} and Zn^{2+} with various concentrations are plotted in Figure 5.2A. We observed that the signal increased significantly in the presence of Zn^{2+} saturated the sensor signal when the Pb^{2+} concentration was kept at a constant value. Cooperativity was calculated and plotted in Figure 5.2B. We observed the cooperativity reached as high as 3.6 when Pb^{2+} and Zn^{2+} concentrations were 0.2 and 20

μM. The cooperativity decreased with the increase of the concentrations of both metal cations. From Figure 5.2A, we conclude this decrease is still due to signal saturation.

5.3.2 Fluorescence responses of the 8-17-based sensor towards the coexistence of Pb and other metal cations

Since this phenomenon was both interesting and encouraging, we also wondered about the generality in the presence of other metal ions. Thus, we measured the 8-17 sensor response towards the co-existences of Pb^{2+}/Cd^{2+} and Pb^{2+}/Mg^{2+}. Cd^{2+} was chosen because it has the similar electronic structure with Zn^{2+}. Mg^{2+} was chosen due to its high abundance in water. As Cd^{2+} has similar properties as Zn^{2+}, but with lower 8-17 activity, we chose the concentrations to be 50, 100, 200 and 500 μM. We chose the concentrations of Mg^{2+} close to the environmental level (up to mM level), which were 0.5, 1, 2 and 5 mM. The signal and cooperativity of the sensor to the metal cations mixture are plotted in Figure 5.3.

Interestingly, the cooperativity studies with Cd^{2+} indicated that it inhibited the combined signal. When the concentration of Pb^{2+} was constant, the signal decreased with the increase of Cd^{2+}. The signal increased with an increased concentration of Pb^{2+} when the Cd^{2+} concentration is constant. We also observed a decreased cooperativity with increased concentrations of both cations. The interference of Mg^{2+} to Pb^{2+} sensing is more complicated. With 0.5 mM Mg^{2+}, the Pb^{2+} signal was enhanced and the cooperativity was higher than 1. At this concentration, Mg^{2+} performed like Zn^{2+}. With higher concentration, Mg^{2+} inhibits the 17E activity, with cooperativity lower than 1. Mg^{2+} shares similarity to Cd^{2+} at high concentrations (higher than 1 mM).

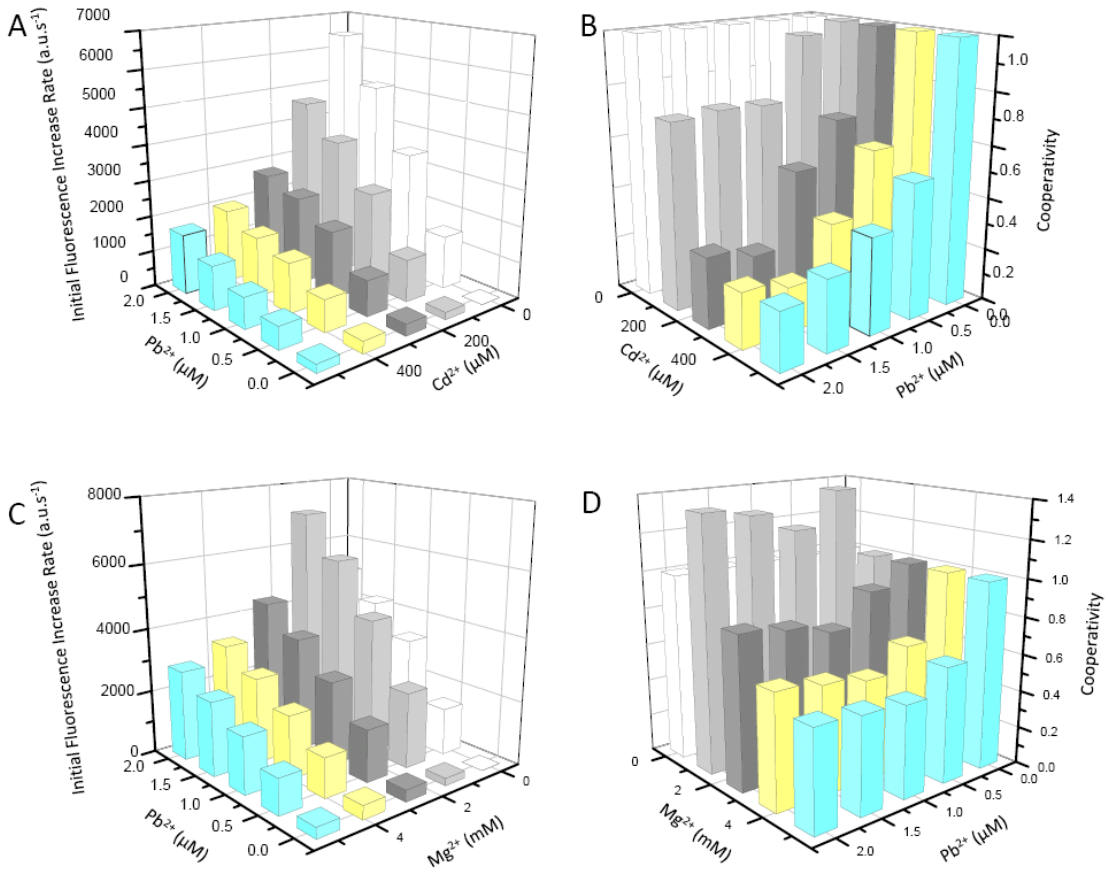

Figure 5.3 Initial rate of fluorescence increase of the 8-17 sensor (A and C) and calculated cooperativity (B and D) with Pb^{2+}/Cd^{2+} (A and B) and Pb^{2+}/Mg^{2+} (C and D)

5.3.3 Theoretical investigation

We believe that cooperativities other than '1' are of scientific interest because it sheds light on the cation-DNAzyme interaction. Based on the idea that 8-17 is a metalloenzyme as our starting point and considering the simplest case wherein, the responses of the 8-17 toward Zn^{2+} and Pb^{2+} are independent, we assume that:

(1) DNAzyme-substrate complex (ES) binds metal cation cofactor (M). The ES-M complex accounts for the cleavage of the substrate

(2) Steady-state assumption is valid and used to simplify the mathematics

(3) The DNAzyme individually binds to each of the metal cation; the interaction of the DNAzyme two-metal species is ignored.

Thus, we have the processes described in Figure 5.4.

$$ES + Pb^{2+} \underset{k_{-1}}{\overset{k_1}{\rightleftarrows}} [ES\text{-}Pb] \xrightarrow{k_2} Product$$

$$ES + Zn^{2+} \underset{k'_{-1}}{\overset{k'_1}{\rightleftarrows}} [ES\text{-}Zn] \xrightarrow{k'_2} Product$$

Figure 5.4 Kinetic model of the 8-17 catalyzed cleavage of the substrate strand

Steady-state assumption is also utilized herein to simplify the calculation. The metal-DNA complexes thus have the constant concentrations. We thus have the following equations.

$$\frac{d[ES-Pb]}{dt} = k_1[ES][Pb^{2+}] - k_{-1}[ES-Pb] - k_2[ES-Pb] = 0 \quad (5.1)$$

$$\frac{d[ES-Zn]}{dt} = k_1'[ES][Zn^{2+}] - k_{-1}'[ES-Zn] - k_2'[ES-Zn] = 0 \quad (5.2)$$

At the initial stage, we ignore the cleaved product, thus we have the following equation

$$E_0 = [ES] + [ES-Pb] + [ES-Zn] \quad (5.3)$$

Through equations 5.1-5.3, we can calculate the concentrations of both ES-Pb and ES-Zn complexes, which are presented in equations 5.4-5.5.

$$[ES-Pb] = \frac{E_0[Pb^{2+}]k'_M}{k_M k'_M + k_M[Zn^{2+}] + k'_M[Pb^{2+}]} \quad (5.4)$$

$$[ES-Zn] = \frac{E_0[Zn^{2+}]k_M}{k_M k'_M + k_M[Zn^{2+}] + k'_M[Pb^{2+}]} \quad (5.5)$$

In the equations, k_M and k'_M are the apparent dissociation constants of DNA-metal complex. They are defined by equation 5.6.

$$k_M = \frac{k_{-1}+k_2}{k_1} \quad (5.6)$$

Thus, we can calculate the initial reaction rate.

$$v_0 = \frac{d[Product]}{dt} = k_2[ES-Pb] + k'_2[ES-Zn] = \frac{E_0(5.[Pb^{2+}]k'_M k_2 + E_0[Zn^{2+}]k_M k'_2)}{k_M k'_M + k_M[Zn^{2+}] + k'_M[Pb^{2+}]} \quad (5.7)$$

With the same assumption, we can calculate the initial rate for the cleavage of the substrate catalyzed by the DNAzyme strand and Pb^{2+} or Zn^{2+} only. They are presented in Equations 5.8-5.9.

$$v_0(Pb) = \frac{E_0[Pb^{2+}]k_2}{k_M+[Pb^{2+}]} \quad (5.8)$$

$$v_0(Zn) = \frac{E_0[Zn^{2+}]k'_2}{k'_M+[Zn^{2+}]} \quad (5.9)$$

Mathematically, v_0(Pb) or v_0(Zn) < v_0 < v_0(Pb) + v_0(Zn), or the cooperativity is lower than 1. This is not what we observed, which evidences that our assumptions are incorrect. As assumptions 1 and 2 have been widely accepted, we believe that the inconsistency between our observation and derivation is because assumption 3 is wrong.

5.3.4 Proposal of the new binding model

To interpret the data, we propose a new intermediate [DNAzyme-Zn-Pb]. This species has faster reaction rate and accounts for the cooperativity higher than 1. Our previous studies indicated that Zn^{2+} introduced a global folding of the DNAzyme-substrate complex while Pb^{2+} does not introduce an observable folding by FRET. The result evidenced that Pb^{2+} and Zn^{2+} have different binding mode and binding site. Thus, it is possible for both of them to bind the DNA complex and have a higher reaction rate. Our proposal is presented in Figure 5.5.

The inhibition of cleavage reaction by Cd^{2+} can be due to two possible reasons. Cd^{2+} or Mg^{2+} has the same binding site as Pb^{2+}, and [DNAzyme-Cd] complex is not as

reactive as [DNAzyme-Pb] intermediate. Another possibility is that both the metal species bind to the DNAzyme complex. The inhibition is because of the low reactivity of [DNAzyme-Pb-M] intermediate. We believe the latter is closer to the reality. If the former was true, there would be two intermediates present, [DNAzyme-Cd] and [DNAzyme-Pb]. Thus, the reaction rate should be between the rates with the presence of only Pb^{2+} and Cd^{2+}. This was not observed, making us believe the existence of [DNAzyme-Pb-Cd] intermediate. Mg^{2+} accelerates cleavage with low concentration and inhibits the reaction at high concentration. We hypothesize that the folding of the DNA complex is different with different concentrations, which makes the reactivity of [DNAzyme-Pb-Mg] different.

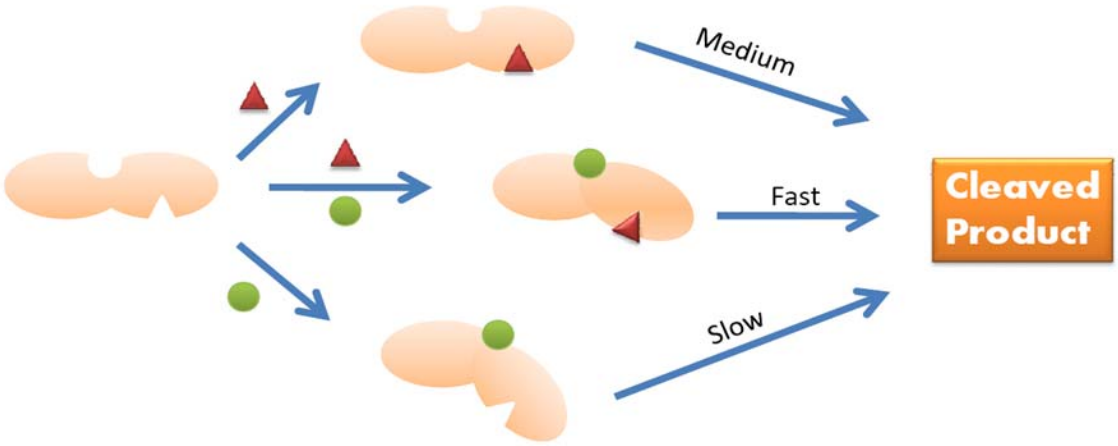

Figure 5.5 Proposed interaction of the metal cations and 8-17 DNAzyme. Red triangle stands for Pb^{2+} and green ball stands for Zn^{2+}.

5.4 Conclusion, perspectives and future direction

We systematically studied the signal responses of the 8-17-based sensor towards the co-existence of Pb^{2+} and other divalent metal cations. It was observed that Zn^{2+} accelerates the cleavage reaction and Cd^{2+} inhibits the reaction. Mg^{2+} accelerates the

reaction at low concentration and inhibits the reaction at high concentration. We initially assumed that the DNAzyme-substrate complex bound to each to metal ion and formed to distinct DNAzyme-metal ion intermediates; however, this assumption was different from our observations.

We therefore propose a new intermediate [DNAzyme-Pb-M], which accounts for the acceleration or inhibition of the reaction. The hypothesis can be proved by careful FRET experiments. The study on the one hand presents challenges for application of the 8-17-based sensor in diverse metal ion environments, and on the other hand presents a direction for interpretation of obtained results.

5.5 References

(1) Lippard, S. J. *Acc. Chem. Res.* **1978**, *11*, 211-217.

(2) Barton, J. K.; Lippard, S. J. *Metal Ions Biol.* **1980**, *1*, 31-113.

(3) Lippert, B.; Leng, M. *Top. Biol. Inorg. Chem.* **1999**, *1*, 117-142.

(4) Guo, Z.; Sadler, P. J. *Angew. Chem., Int. Ed.* **1999**, *38*, 1512-1531.

(5) Erkkila, K. E.; Odom, D. T.; Barton, J. K. *Chem. Rev.* **1999**, *99*, 2777-2795.

(6) Lu, Y. *Chem. Eur. J.* **2002**, *8*, 4588-4596.

(7) DeRose, V. J. *Curr. Opin. Struct. Biol.* **2003**, *13*, 317-324.

(8) Sigel, R. K. O.; Pyle, A. M. *Chem. Rev.* **2007**, *107*, 97-113.

(9) Grabowski, P. J.; Zaug, A. J.; Cech, T. R. *Cell* **1981**, *23*, 467-476.

(10) Guerrier-Takada, C.; Gardiner, K.; Marsh, T.; Pace, N.; Altman, S. *Cell* **1983**, *35*, 849-857.

(11) Cech, T. R. *Proc. Natl. Acad. Sci. U.S.A.* **1986**, *83*, 4360-4363.

(12) Breaker, R. R.; Joyce, G. F. *Chem. Biol.* **1994**, *1*, 223-229.

(13) Weinstein, L. B.; Jones, B. C. N. M.; Cosstick, R.; Cech, T. R. *Nature* **1997**, *388*, 805-808.

(14) Piccirilli, J. A.; Vyle, J. S.; Caruthers, M. H.; Cech, T. R. *Nature* **1993**, *361*, 85-88.

(15) Pan, T.; Long, D. M.; Uhlenbeck, O. C.; Gesteland, R. F.; Atkins, J. F. In *The RNA World*; Cold Spring Harbor Laboratory Press: Cold Spring Harbor, New York, 1993, p 271-302.

(16) Bassi, G. S.; Murchie, A. I. H.; Walter, F.; Clegg, R. M.; Lilley, D. M. J. *EMBO J.* **1997**, *16*, 7481-7489.

(17) Faulhammer, D.; Famulok, M. *J. Mol. Biol.* **1997**, *269*, 188-202.

(18) Takagi, Y.; Warashina, M.; Stec, W. J.; Yoshinari, K.; Taira, K. *Nucleic Acids Res.* **2001**, *29*, 1815-1834.

(19) Liu, Z.; Mei, S. H. J.; Brennan, J. D.; Li, Y. *J. Am. Chem. Soc.* **2003**, *125*, 7539-7545.

(20) Zivarts, M.; Liu, Y.; Breaker, R. R. *Nucleic Acids Res.* **2005**, *33*, 622-631.

(21) Woodson, S. A. *Curr. Opin. Chem. Biol.* **2005**, *9*, 104-109.

(22) Roychowdhury-Saha, M.; Burke, D. H. *RNA* **2006**, *12*, 1846-1852.

(23) Stahley, M. R.; Strobel, S. A. *Curr. Opin. Struct. Biol.* **2006**, *16*, 319-326.

(24) Freisinger, E.; Sigel, R. K. O. *Coord. Chem. Rev.* **2007**, *251*, 1834-1851.

(25) Hollenstein, M.; Hipolito, C.; Lam, C.; Dietrich, D.; Perrin, D. M. *Angew. Chem., Int. Ed.* **2008**, *47*, 4346-50.

(26) Faulhammer, D.; Famulok, M. *Angew. Chem., Int. Ed.* **1996**, *35*, 2837-2841.

(27) Santoro, S. W.; Joyce, G. F. *Proc. Natl. Acad. Sci. U.S.A.* **1997**, *94*, 4262-4266.

(28) Li, J.; Zheng, W.; Kwon, A. H.; Lu, Y. *Nucleic Acids Res.* **2000**, *28*, 481-488.

(29) Peracchi, A. *J. Biol. Chem.* **2000**, *275*, 11693-11697.

(30) Cruz, R. P. G.; Withers, J. B.; Li, Y. *Chem. Biol.* **2004**, *11*, 57-67.

(31) Peracchi, A.; Bonaccio, M.; Clerici, M. *J. Mol. Biol.* **2005**, *352*, 783-794.

(32) Schlosser, K.; Gu, J.; Sule, L.; Li, Y. *Nucleic Acids Res.* **2008**, *36*, 1472-1481.

(33) Liu, Y.; Sen, D. *J. Mol. Biol.* **2008**, *381*, 845-859.

(34) Brown, A. K.; Li, J.; Pavot, C. M. B.; Lu, Y. *Biochemistry* **2003**, *42*, 7152-7161.

(35) Liu, J.; Lu, Y. *J. Am. Chem. Soc.* **2002**, *124*, 15208-15216.

(36) Kim, H.-K.; Liu, J.; Li, J.; Nagraj, N.; Li, M.; Pavot, C. M. B.; Lu, Y. *J. Am. Chem. Soc.* **2007**, *129*, 6896-6902.

(37) Lee, N. K.; Koh, H. R.; Han, K. Y.; Kim, S. K. *J. Am. Chem. Soc.* **2007**, *129*, 15526-15534.

(38) Kim, H.-K.; Rasnik, I.; Liu, J.; Ha, T.; Lu, Y. *Nat. Chem. Biol.* **2007**, *3*, 763-768.

(39) Mazumdar, D.; Nagraj, N.; Kim, H.-K.; Meng, X.; Brown, A. K.; Sun, Q.; Li, W.; Lu, Y. *J. Am. Chem. Soc.* **2009**, *131*, 5506-5515.

(40) Li, J.; Lu, Y. *J. Am. Chem. Soc.* **2000**, *122*, 10466-10467.

(41) Liu, J.; Lu, Y. *Anal. Chem.* **2003**, *75*, 6666-6672.

Chapter 6 Aptamer functionalized liposomes for targeted drug delivery

This work has been published in *Angewandte Chemie*. (Cao, Z.; Tong, R.; Mishra, A.; Xu, W.; Wong, G. C. L.; Cheng, J.; Lu, Y. *Angew. Chem. Int. Ed.* 2009, **48**, 6494-6498).

6.1 Introduction

6.1.1 Brief introduction to liposomes

A liposome is a construct that mimics cell membranes. The word liposme comes from the Greek “lipo” meaning “fat” and “soma” meaning “body.” Today, the term liposome refers to an artificial vesicle composed of a phospholipid bilayer. A typical liposome is shown in Figure 6.1.

As shown in Figure 6.1, liposome is a hollow spherical structure composed of a phospholipid bilayer. The phospholipid bilayer assembles through hydrophobic interactions. The alkyl chains of the lipids are hydrophobic and thus in an aqueous environment are energetically driven to associate with one another inside the bilayer while the hydrophilic phosphates expose themselves to direct contact with the aqueous solution.

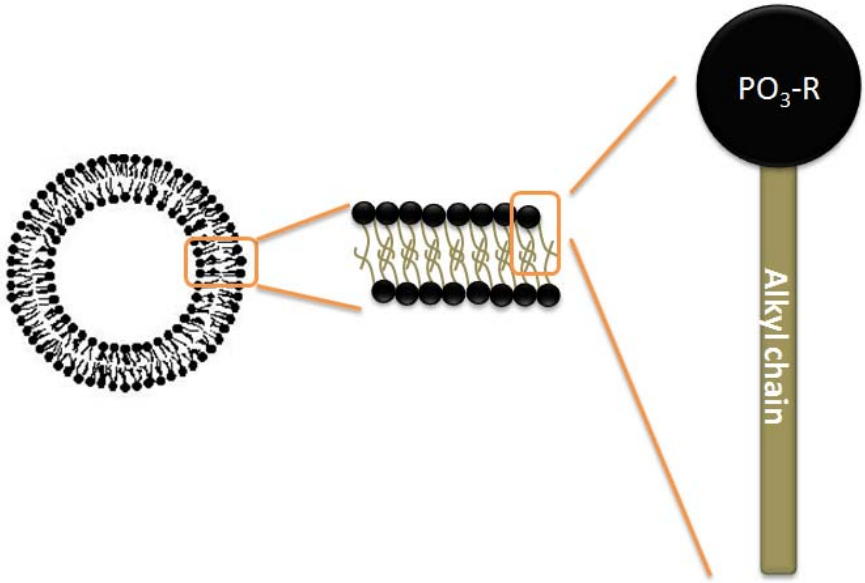

Figure 6.1 Liposome structure. Liposomes have hollow spherical construct composed of phospholipids. The phospholipids have hydrophilic phosphate and hydrophobic carbon chains.

Liposomes are not stable. They are sensitive to heat, osmotic pressure, and solution density changes. For example, if the osmotic pressure inside and outside the liposome is not balanced, this can cause the liposome's components to rearrange, leading to the leakage of the species encapsulated inside, or even destroy the liposome's structure. Density changes lead to the ascendance or subsidence of the liposomes, which significantly destabilize the liposomes. Moreover, liposomes are sensitive to chemicals that interact with lipids. For instance, it was discovered that phospholipid 1,2-dioleoyl-sn-glycero-3-phosphoethanolamine (DOPE) binds mercury. The liposomes composed of DOPE can be destroyed by Hg^{2+} because of the surface energy change induced by the

binding event. The binding leads to the reassembly of the bilayer structure to reach the lowest energy.[1,2]

6.1.2 Liposomes in drug delivery

Liposomes are of interest to biologists and physicians because they have been widely used in the delivery and controlled release of drugs. Liposomes can encapsulate drug solutions and effectively protect the encapsulated drug from hazardous conditions such as the presence of acid and enzymes encountered during the drug delivery process.

Liposomes are expected to release the drug into cells. There are three mechanisms by which unfunctionalized liposomes release encapsulated drugs. First, because of the amphipathic nature of the phospholipids which compose both liposomes and cell membranes, these structures can fuse with cells and deliver the encapsulated drugs. Second, when the phospholipids of the liposomes fuse with a cell membrane, the liposome becomes part of the cell, releasing the drug into the cell. Finally, if some portion of the liposome survives intact inside the cell, organelles such as lysosomes can open them, releasing their encapsulated drug.[3]

After forty years of development,[4] liposomes have been approved by the U.S. Food and Drug Administration for clinical applications.[5] However, targeted drug delivery using liposomes has not yet been widely applied, and there is room for improvement in liposome technology. The strategy to increase the efficacy of liposome-based delivery focuses on enhancing their permeation and retention (EPR),[6,7] which is a passive strategy. The most important challenge in this field is side effects due to non-targeted drug delivery.[8,9] Previous studies have shown that cisplatin,[10,11] an inorganic anti-tumor drug with significant cytotoxicity,[12] when encapsulated in liposomes, had poor-to-moderate

efficacy.[13,14] The problem can only be solved by functionalizing the liposome to bring about targeted drug delivery.[15]

Antibodies dominate the field of targeted drug delivery.[12,16-19] They are of practical significance in the delivery of drugs that have severe side effects. As mentioned above, cisplatin is a platinum-based complex. It was discovered that cisplatin reacts with DNA in cells, leading to the dysfunction of genomic material.[10,11] Its function is nonspecific, being equally toxic to cancerous and non-cancerous cells. Therefore, to specifically target cisplatin to cancerous cells, it has been functionalized by antibodies[17-19] which recognize the receptors on the surface of tumor cells, to enhance the uptake of the medicine by the tumor and to minimize the side effects. However, challenges exist.[20] First, antibodies are difficult to control; they have poor site specificity and varied affinity. Second, antibodies are immunogenic,[21] which requires extra steps before the drug delivery. And finally, antibodies are produced in biological systems, which cause cost issues when the system is scaled up.

6.1.3 Aptamers that target tumor cells

One alternative to antibodies is aptamers. Aptamers[22-26] have promising applications in cancer biology, since aptamers that recognize cancer-related proteins including PDGF, VEGF, HER3, NFkB, and PMSA have been found.[27] Although they have not yet been applied in clinics, the aptamers could perform important roles in the treatment of cancer.[28-43]

Aptamers can find more applications in cancer biology because of a method developed by Tan and co-workers called cell-SELEX,[27] a SELEX process that uses cells as the selection target. During the selection process, the aptamers are selected to bind to one of

the components of the cell membrane, typically a membrane receptor. Those winners are amplified for the next round of selection. It is noted that the targets for the selection is unknown during the selection; it is verified after the sequence of the aptamer is obtained.

Cell-SELEX[27] significantly enlarged the library of aptamers that bind to cells. It has the potential to select aptamers that bind to unknown cells because the selection method does not require detailed information about the cells. If tumor cells are used as the targets, numerous aptamers that recognize the tumor cells can be selected; novel therapies can be developed based on the aptamers.

6.1.4 Liposomes in sensing

Besides liposome's wide applications in drug delivery, it has been reported that liposomes can be used to detect mercury by encapsulating a high concentration of fluorescein in liposomes. Because of the self-quenching of this dye, the liposome solution has a relatively low fluorescent background. The lipids that compose the liposomes have been found to have specific interactions with the mercury cations. When Hg^{2+} binds to the lipids, the liposomes are destabilized and the fluorescent dye is released from the lipsomes; the localized fluorescein molecules are released evenly in the solution, leading to the decrease of the self-quenching effect. As a result, a fluorescence increase is detected. The sensing system has high selectivity and specificity. It does not appreciably respond to any other divalent metal cations, but Hg^{2+} concentrations as low as 10 nM lead to a detectable fluorescence change.

Although the system responds to Hg^{2+}, it is not a sensor. The concentration of liposome varies from batch to batch, making it difficult to normalize the fluorescence response.

However, it is a good platform for the sensing of mercury, and it proves liposomes' potential in heavy metal detection.

6.1.5 Aptamer functionalized liposome for cisplatin delivery

Efforts were made to combine the advantages of both liposome and aptamer. Nucleotin was chosen as the target. Nucleotin is a bcl-2 mRNA binding protein involved in cell proliferation. It is over-expressed in human breast cancer cells such as MCF-7.[44-48] Liposomes were functionalized by AS1411,[49] a 26-mer DNA aptamer that recognizes nucleotin.[44] Once functionalized with AS1411, the lipsomes recognize the breast tumor cells. When the liposomes interact with the cells, they fuse, delivering the cisplatin encapsulated in the lipsomes to the cells. This leads to cellular death. Because of the high specificity of AS1411 for nucleotin and the fact that nucleotin is unique to breast cancer cells, this drug delivery system is more cytotoxic to breast cancer cells than other cells.

6.2 Experimental

6.2.1 Liposome preparation, functionalization and purification

Liposome preparation:[50,51] Stock solutions of HSPC[52] (1.25 mg), cholesterol, and mPEG2000–DSPE in chloroform were mixed with a 2:1:0.16 molar ratio in a scintillation vial. This mixture was blown dry with N_2 and further dried under vacuum for at least 6 h. The buffer for the liposome preparation contained 25 mM 2-[4-(2-hydroxyethyl)-1-piperazinyl]-ethanesulfonic acid (HEPES, pH 7.6), 150 mM NaCl, 5 mM KCl, 1 mM $MgCl_2$, and 1 mM $CaCl_2$. This buffer solution (100 mL) containing 3 nmol cholesterol-tagged DNA (sequence: 5'-GGT GGT GGT GGT TGT GGT GGT GGT GGT TTT TTT

TTT TT-cholesterol-3') was added to the dry lipids. After the mixture had been incubated for 6 h at 37 ˚C, liposome-preparation buffer (400 mL) containing 4 mM cisplatin or 50 mM fluorescein was added. This solution was gently stirred and kept at 37 ˚C for 3 h.

After that, the solution was stirred and then quickly frozen and thawed for at least five cycles. The final solution was incubated at 37 ˚C overnight. The lipid mixture was then extruded to form liposomes of approximately 200 nm in diameter by following the instructions from Avanti Polar Lipids, Inc. The liposomes were purified on a column packed with Sephadex G-100 medium to remove free cisplatin or calcein.

6.2.2 Fluorecein and cisplatin delivery

A cell-specific uptake study was done by confocal fluorescence microscopy. The MCF-7 and LNCaP cells, cultured as recommended by the American Type Culture Collection (ATCC) in Dulbecco's modified Eagle's medium (DMEM) and Ham's F-12K medium, respectively, were incubated in chamber slides in the medium to allow 70% confluence in 12-24 h. The cell medium was removed. The cells were washed with prewarmed PBS (1 × 100 $mLwell^{-1}$) and incubated with prewarmed Opti-MEM medium (phenol red reduced) for 30 min before the addition of the liposome solution. Cells were further incubated for 5 h or 10 h at 37 ˚C. At the prescheduled times, the cells were washed with prewarmed PBS (3 × 100 $mLwell^{-1}$) and fixed with 4% paraformaldehyde solution for 10 min. The cells were washed again with PBS (1 × 100 mL well) and analyzed with a confocal fluorescence microscopy.

6.3 Results and discussion

Fluorescein was used in order to evaluate the delivery of the material encapsulated in the liposomes to the cells, As shown in Figure 6.2, after the incubation with the liposome solution, the dye was successfully delivered into the MCF-7 cells. As a comparison, the liposome system cannot deliver dyes to the LNCaP cells. This is because the latter do not overepxress nucleotin in their cell membranes. Because the concentrations of liposome and cells were low, the interaction between liposomes and LNCaP cells are very difficult.

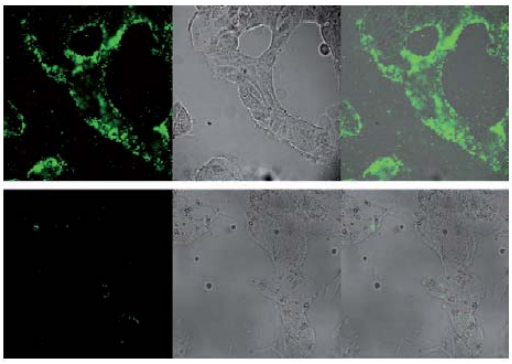

Figure 6.2 Confocal images of MCF-7 (top) and LNCaP (bottom) cells treated with NCL-aptamer-functionalized liposomes containing calcein. From left to right: fluorescence image, transmission image, and overlay.

Encouraged by the success of the dye delivery, the dye was replaced by the anti-tumor drug cisplatin. Its cytotoxicity was evaluated by measuring the viability of the cells. As presented in Figure 6.3, the viability of the MCF-7 cells decreased by 20% and 60% 2 and 4 days after the application of the cisplatin-encapsulated liposomes, respectively. No significant viability change was observed if the liposome functionalized by DNA molecules without affinity for nucleotin was used, which showed that the binding affinity

of the aptamer was essential. The cells that were exposed to liposomes not encapsulating cisplatin saw excellent survival rates, indicating that the cytotoxicity of the system was from cisplatin, not the DNA aptamer or the liposome. Finally, the system did not affect the viability of LNCaP cells. This is consistent with the dye delivery experiment. As the material inside the liposomes cannot be delivered into the LNCaP cells, the viability was not affected.

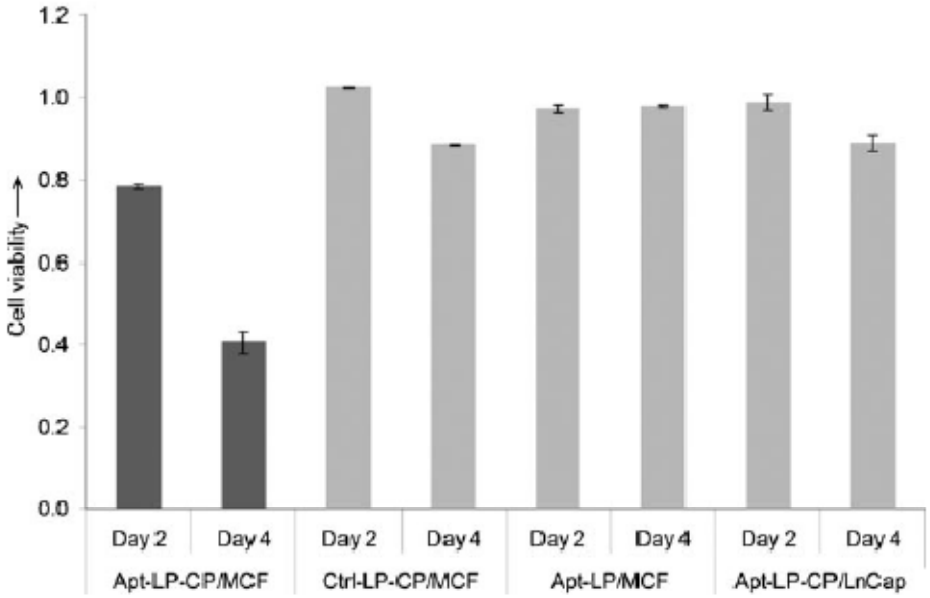

Figure 6.3 Cell viability assays for different liposome/cell combinations. Viability measurements were taken at day 2 and day 4 of the liposome/cell incubation. Columns 1 and 2: MCF-7 cells treated with NCL-aptamer-functionalized liposomes loaded with cisplatin; columns 3 and 4: MCF-7 cells treated with a control group of DNA-functionalized liposomes loaded with cisplatin; columns 5 and 6: MCF-7 cells treated with NCL-aptamer-functionalized liposomes with no cisplatin; columns 7 and 8: LNCaP cells treated with NCL-aptamer-functionalized liposomes loaded with cisplatin.

DNA can be programmed because the interaction of DNA molecules is much more predictable than protein interactions. One of the advantages of this drug delivery system over the antibody-based system is that the rate of drug delivery can be controlled by introducing the antisense sequence of the aptamer strand. This is useful in the case of

over-dosing. In most cases, the dosing of a new medicine is difficult to decide and over-dosing is common and dangerous. However, if over-dosing happens when using this system, the anti-aptamer can be applied. This will decrease the affinity of the aptamer for the tumor cells, which will in turn decrease the drug delivery efficiency and minimize any side effects from over-dosing.

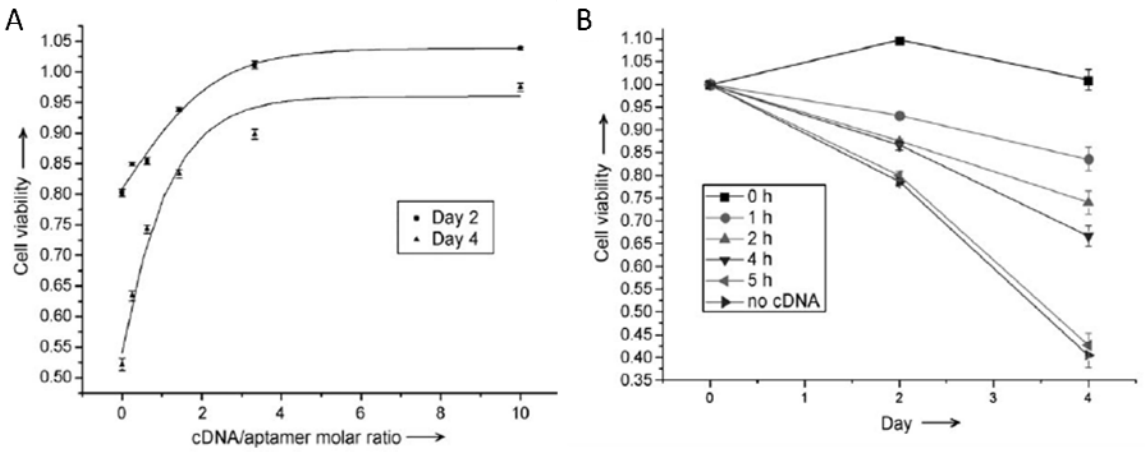

Figure 6.4 (A) Effect of the concentration of the anti-aptamer on the viability of MCF-7 cells treated with the functional liposomes. (B) Time-dependent effect of the anti-aptamer on the viability of MCF-7 cells treated with the functional liposomes.

Figure 6.4A presents the cell viability after the cisplatin-encapsulated liposomes and anti-aptamer have been applied with various concentrations. If more than four equivalents of anti-aptamer were applied, the cytotoxicity of the cisplatin could be minimized ("rescue effect"). Figure 6.4B indicated that the "rescue" effect of anti-aptamer is time-dependent. If the anti-aptamer was applied immediately after the application of the cisplatin-containing liposomes, almost all the cells could be "rescued." However, there was almost no "rescue" effect if there was a 5-h interval between the applications of the liposomes and the anti-aptamer.

6.4 Conclusion and perspective

The liposome was successfully functionalized by the DNA aptamer AS1141, which binds to nucleotin, a protein that is over-expressed in human breast cancer cells. The liposomes can specifically deliver fluorescent dye to the cells. If cisplatin was encapsulated, MCF-7 cells could be specifically killed without affecting the viability of LNCaP cells which lack nucleotin in the cell membrane. Control experiments indicated that the drug delivery effect was due to the specific interaction between the aptamer and breast cancer cells.

An anti-aptamer sequence was applied as a "rescue" in case of over dosing. If more than four equivalents of the anti-aptamer were applied, only trivial cytotoxicity was observed. However, the time of the application of the anti-aptamer is critical. An interval of less than 5 hours between the applications of the liposomes and anti-aptamers is required to produce the "rescue" effect.

Although this drug delivery system successful delivered cisplatin to breast cancer cells, more research must be performed before it can be used in clinical practice. First, the retention time of DNA molecules is typically several minutes. If this system is used *in vivo* in its current form, the DNA aptamer will be degraded before it reaches the tumor region. This problem can be solved by PEGylating or methylating the DNA aptamer, or using L-DNA. Another problem is cost. Cholesterol-conjugated DNA is costly, which induces a concern for *in vivo* applications. Despite the difficulties, the system presented in this chapter provided a promising approach to realize targeted drug delivery by liposomes.

6.5 References

(1) Girault, L.; Lemaire, P.; Boudou, A.; Debouzy, J.-C.; Dufourc, E. J. *Eur. Biophys. J.* **1996**, *24*, 413-421.

(2) Yigit, M. V.; Mishra, A.; Tong, R.; Cheng, J.; Wong, G. C. L.; Lu, Y. *Chem. Biol.* **2009**, *16*, 937-942.

(3) Samad, A.; Sultana, Y.; Aqil, M. *Curr. Drug Delivery* **2007**, *4*, 297-305.

(4) Kaneda, Y. *Adv. Durg Delivery Rev.* **2000**, *43*, 197-205.

(5) Wagner, A.; Platzgummer, M.; Kreismayr, G.; Quendler, H.; Stiegler, G.; Ferko, B.; Vecera, G.; Vorauer-Uhl, K.; Katinger, H. *J. Liposome Res.* **2006**, *16*, 311-319.

(6) Matsumura, Y.; Maeda, H. *Cancer Res.* **1986**, *46*, 6387-6392.

(7) Maeda, H.; Wu, J.; Sawa, T.; Matsumura, Y.; Hori, K. *J. Controlled Release* **2000**, *65*, 271-284.

(8) Woo, J.; Chiu, G. N. C.; Karlsson, G.; Wasan, E.; Ickenstein, L.; Edwards, K.; Bally, M. B. *Int. J. Pharm.* **2008**, *349*, 38-46.

(9) Mamot, C.; Drummond, D. C.; Greiser, U.; Hong, K.; Kirpotin, D. B.; Marks, J. D.; Park, J. W. *Cancer Res.* **2003**, *63*, 3154-3161.

(10) Kelland, L. *Nat. Rev. Cancer* **2007**, *7*, 573-584.

(11) Jamieson, E. R.; Lippard, S. J. *Chem. Rev.* **1999**, *99*, 2467-2498.

(12) Bednarski, P. J.; Grunert, R.; Zielzki, M.; Wellner, A.; Mackay, F. S.; Sadler, P. J. *Chem. Biol.* **2006**, *13*, 61-67.

(13) Meerum Terwogt, J. M.; Groenewegen, G.; Pluim, D.; Maliepaard, M.; Tibben, M. M.; Huisman, A.; ten Bokkel Huinink, W. W.; Schot, M.; Welbank, H.; Voest, E. E.; Beijnen, J. H.; Schellens, J. H. M. *Cancer Chemother. Pharmacol.* **2002**, *49*, 201-210.

(14) White, S. C.; Lorigan, P.; Margison, G. P.; Margison, J. M.; Martin, F.; Thatcher, N.; Anderson, H.; Ranson, M. *J. Cancer* **2006**, *95*, 822-828.

(15) Noble, C. O.; Kirpotin, D. B.; Hayes, M. E.; Mamot, C.; Hong, K.; Park, J. W.; Benz, C. C.; Marks, J. D.; Drummond, D. C. *Expert Opin. Ther. Targets* **2004**, *8*, 335-353.

(16) Dhar, S.; Liu, Z.; Thomale, J.; Dai, H.; Lippard, S. J. *J. Am. Chem. Soc.* **2008**, *130*, 11467-11476.

(17) Park, J. W.; Kirpotin, D. B.; Hong, K.; Shalaby, R.; Shao, Y.; Nielsen, U. B.; Marks, J. D.; Papahadjopoulos, D.; Benz, C. C. *J. Controlled Release* **2001**, *74*, 95-113.

(18) Sapra, P.; Allen, T. M. *Cancer Res.* **2002**, *62*, 7190-7194.

(19) Elbayoumi, T. A.; Torchilin, V. P. *Eur. J. Pharm. Sci.* **2007**, *32*, 159-168.

(20) Sapra, P.; Allen, T. M. *Prog. Lipid Res.* **2003**, *42*, 439-462.

(21) Kirpotin, D. B.; Drummond, D. C.; Shao, Y.; Shalaby, M. R.; Hong, K.; Nielsen, U. B.; Marks, J. D.; Benz, C. C.; Park, J. W. *Cancer Res.* **2006**, *66*, 6732-6740.

(22) Bock, L. C.; Griffin, L. C.; Latham, J. A.; Vermaas, E. H.; Toole, J. J. *Nature* **1992**, *355*, 564-566.

(23) Burgstaller, P.; Famulok, M. *Angew. Chem., Int. Ed.* **1994**, *33*, 1084-1087.

(24) Kim, M.; Jeoung, Y.-H.; Lee, S. J.; Choi, I.; Pyun, K.-H.; Lee, Y. *Mol. Cells* **1995**, *5*, 555-562.

(25) Tuerk, C.; Gold, L. *Science* **1990**, *249*, 505-510.

(26) Ellington, A. D.; Szostak, J. W. *Nature* **1990**, *346*, 818-822.

(27) Fang, X.; Tan, W. *Acc. Chem. Res.* **2010**, *43*, 48-57.

(28) Blank, M.; Weinschenk, T.; Priemer, M.; Schluesener, H. *J. Biol. Chem.* **2001**, *276*, 16464-16468.

(29) Wang, C.; Zhang, M.; Yang, G.; Zhang, D.; Ding, H.; Wang, H.; Fan, M.; Shen, B.; Shao, N. *J. Biotechnol.* **2003**, *102*, 15-22.

(30) Daniels, D. A.; Chen, H.; Hicke, B. J.; Swiderek, K. M.; Gold, L. *Proc. Natl. Acad. Sci. U.S.A.* **2003**, *100*, 15416-15421.

(31) Cerchia, L.; Duconge, F.; Pestourie, C.; Boulay, J.; Aissouni, Y.; Gombert, K.; Tavitian, B.; de, F. V.; Libri, D. *PLoS Biol.* **2005**, *3*, e123.

(32) Hicke, B. J.; Marion, C.; Chang, Y.-F.; Gould, T.; Lynott, C. K.; Parma, D.; Schmidt, P. G.; Warren, S. *J. Biol. Chem.* **2001**, *276*, 48644-48654.

(33) Ohuchi, S. P.; Ohtsu, T.; Nakamura, Y. *Biochimie* **2006**, *88*, 897-904.

(34) Shangguan, D.; Li, Y.; Tang, Z.; Cao, Z. C.; Chen, H. W.; Mallikaratchy, P.; Sefah, K.; Yang, C. J.; Tan, W. *Proc. Natl. Acad. Sci. U.S.A.* **2006**, *103*, 11838-11843.

(35) Guo, K.-T.; Schaefer, R.; Paul, A.; Gerber, A.; Ziemer, G.; Wendel, H. P. *Stem Cells* **2006**, *24*, 2220-2231.

(36) Tang, Z.; Shangguan, D.; Wang, K.; Shi, H.; Sefah, K.; Mallikratchy, P.; Chen, H. W.; Li, Y.; Tan, W. *Anal. Chem.* **2007**, *79*, 4900-4907.

(37) Shangguan, D.; Meng, L.; Cao, Z. C.; Xiao, Z.; Fang, X.; Li, Y.; Cardona, D.; Witek, R. P.; Liu, C.; Tan, W. *Anal. Chem.* **2008**, *80*, 721-728.

(38) Chen, H. W.; Medley, C. D.; Sefah, K.; Shangguan, D.; Tang, Z.; Meng, L.; Smith, J. E.; Tan, W. *ChemMedChem* **2008**, *3*, 991-1001.

(39) Farokhzad, O. C.; Cheng, J.; Teply, B. A.; Sherifi, I.; Jon, S.; Kantoff, P. W.; Richie, J. P.; Langer, R. *Proc. Natl. Acad. Sci. U.S.A.* **2006**, *103*, 6315-6320.

(40) Cheng, J.; Teply, B. A.; Sherifi, I.; Sung, J.; Luther, G.; Gu, F. X.; Levy-Nissenbaum, E.; Radovic-Moreno, A. F.; Langer, R.; Farokhzad, O. C. *Biomaterials* **2007**, *28*, 869-876.

(41) Bagalkot, V.; Zhang, L.; Levy-Nissenbaum, E.; Jon, S.; Kantoff, P. W.; Langer, R.; Farokhzad, O. C. *Nano Lett.* **2007**, *7*, 3065-3070.

(42) Gu, F.; Zhang, L.; Teply, B. A.; Mann, N.; Wang, A.; Radovic-Moren, A. F.; Langer, R.; Farkokhzad, O. *Proc. Natl. Acad. Sci. U.S.A.* **2008**, *105*, 2586-2591.

(43) Dhar, S.; Gu, F. X.; Langer, R.; Farokhzad, O. C.; Lippard, S. J. *Proc. Natl. Acad. Sci. U.S.A.* **2008**, *105*, 17356-17361.

(44) Bates, P. J.; Kahlon, J. B.; Thomas, S. D.; Trent, J. O.; Miller, D. M. *J. Biol. Chem.* **1999**, *274*, 26369-26377.

(45) Srivastava, M.; Pollard, H. B. *FASEB J.* **1999**, *13*, 1911-1922.

(46) Derenzini, M.; Sirri, V.; Trere, D.; Ochs, R. L. *Lab. Invest.* **1995**, *73*, 497-502.

(47) Otake, Y.; Soundararajan, S.; Sengupta, T. K.; Kio, E. A.; Smith, J. C.; Pineda-Roman, M.; Stuart, R. K.; Spicer, E. K.; Fernandes, D. J. *Blood* **2007**, *109*, 3069-3075.

(48) Xu, K.; Luduena, R. F. *Cell Motil. Cytoskeleton* **2002**, *53*, 39-52.

(49) Soundararajan, S.; Chen, W.; Spicer, E. K.; Courtenay-Luck, N.; Fernandes, D. J. *Cancer Res.* **2008**, *68*, 2358-2365.

(50) Kirpotin, D.; Park, J. W.; Hong, K.; Zalipsky, S.; Li, W.-L.; Carter, P.; Benz, C. C.; Papahadjopoulos, D. *Biochemistry* **1997**, *36*, 66-75.

(51) Park, J. W.; Hong, K.; Carter, P.; Asgari, H.; Guo, L. Y.; Keller, G. A.; Wirth, C.; Shalaby, R.; Kotts, C.; et al. *Proc. Natl. Acad. Sci. U.S.A.* **1995**, *92*, 1327-1331.

(52) Park, J. W.; Hong, K.; Kirpotin, D. B.; Colbern, G.; Shalaby, R.; Baselga, J.; Shao, Y.; Nielsen, U. B.; Marks, J. D.; Moore, D.; Papahadjopoulos, D.; Benz, C. C. *Cancer Res.* **2002**, *8*, 1172-1181.